ELECTRICALLY DRIVEN ION SEPARATIONS AND NANOFILTRATION THROUGH MEMBRANES COATED WITH POLYELECTROLYTE MULTILAYERS

By

Nicholas White

A DISSERTATION

Submitted to
Michigan State University
in partial fulfillment of the requirements
for the degree of

Chemistry – Doctor of Philosophy

2015

ABSTRACT

ELECTRICALLY DRIVEN ION SEPARATIONS AND NANOFILTRATION THROUGH MEMBRANES COATED WITH POLYELECTROLYTE MULTILAYERS

By

Nicholas White

Polyelectrolyte multilayer (PEM) films deposited using the layer-by-layer (LBL) method are attractive for their simple deposition, tailorable nature, scalability, and charge or size-based selectivity for solutes. This dissertation explores ion separations in electrodialysis (ED) and solute removal through nanofiltration with PEMs deposited on polymer membranes.

ED membranes typically exhibit modest selectivities between monovalent and divalent ions. In contrast, this work shows that K^+/Mg^{2+} ED selectivities reach values >1000 when using Nafion 115 cation-exchange membranes coated with multilayer poly(4-styrenesulfonate) (PSS)/protonated poly(allylamine) (PAH) films. For comparison, the corresponding K^+/Mg^{2+} selectivity of bare Nafion 115 is <2. However, water-splitting at strongly overlimiting current densities may lead to a local pH increase close to the membrane surface and alter film permeability or allow passage of $Mg(OH)_x$ species to decrease selectivity. When the source phase contains high salt concentrations, the K^+ transference number approaches unity and the K^+/Mg^{2+} selectivity is >20,000, presumably because the applied current is below the limiting value for K^+ and H^+ transport is negligible at this high K^+ concentration. The high selectivities of these membranes may enable

electrodialysis applications such as purification of salts that contain divalent or trivalent ions.

The high ED selectivities of $(PAH/PSS)_5PAH$-coated Nafion membranes translate to separations with Li^+/Co^{2+} and K^+/La^{3+}. Even with adsorption of only 3 polyelectrolyte layers, Nafion membranes exhibit a Li^+/Co^{2+} selectivity >23. However, the resistance to monovalent-ion passage does not decrease significantly with fewer polyelectrolyte layers. At overlimiting currents, hydroxides from water splitting form insoluble metal hydroxides to foul the membrane. With 0.1 M source-phase salt concentrations, transference numbers for monovalent cations approach unity and selectivities are >5000 because the diffusion-limited K^+ or Li^+ currents exceed the applied current. However, ED selectivities gradually decline with time. Thus, future research should aim to increase membrane stability and limiting currents to fully exploit the remarkable selectivity of these membranes.

PEMs deposited on commercial ultrafiltration (UF) membranes also show high rejections of organic dyes. Coating the surface of polyethersulfone (PES) membranes imparts a selective barrier to dye molecules used in textile production. These films achieve dye rejections >98% and may be useful for wastewater treatment and dye recovery. Other studies in microfluidic channels exploit ion transport phenomena in the vicinity of ion-selective junctions, such as cation-exchange membranes. These studies suggest that ion concentration polarization (ICP) could remove charged species from feed streams.

To Mum and Dad

A little nonsense now and then is relished by the wisest men

-Roald Dahl

ACKNOWLEDGEMENTS

Though this dissertation appears to be an individual work, the reality is that I owe its completion to many people who helped me reach this point. First, I would like to thank my advisor, Dr. Merlin Bruening, for his leadership, patience, and integrity throughout my time in the group. I am fortunate to have a mentor who is heavily vested in my success as a writer and researcher but also one I can talk to freely about current events or somewhere new to travel. I would like to thank my committee members, Dr. Vlad Tarabara, Dr. Dana Spence, and Dr. Gary Blanchard, for their invaluable instruction in the classroom and guidance and direction outside of it.

I am grateful to my fellow group members for our discussions about research, the welcome distractions about other matters, and particularly for their support and fellowship throughout my time in the lab. In addition, I appreciate the diligent work of two undergraduate students, Maria Misovich and Elena Alemayehu, who contributed extensively to the electrodialysis work.

The completion of this degree would have been impossible without a solid foundation. I am enormously grateful to Mary Fredell, my high school chemistry teacher, for challenging me from the start and pushing me to excel. Similarly, my life as a graduate student would have been much more difficult without the help of numerous chemistry department personnel – especially Dr. Kathy Severin, Paul Reed, Dr. Tom Carter, Glenn Wesley, Marvey Olsen, Scott Bankroff, and Bob Rasico.

On a more personal level, I am indebted to my family and friends for their unwavering support throughout this effort. To my close friends near and far – you know who you are – thank you for supporting me at every turn and being there when it mattered most. To Mum, Dad, Tom, Steph, and all my family abroad – your steadfast belief and encouragement means more to me than I can express in words. Graduate school is a difficult journey made easier by the support of those around you, and I've been extraordinarily fortunate to have such devoted family and friends.

TABLE OF CONTENTS

LIST OF TABLES

LIST OF FIGURES

KEY TO ABBREVIATIONS

AEM	Anion-exchange membrane
AM-MAPTAC	[3-(2-methylpropionamido) propyl] trimethyl ammonium chloride
CAD	Computer-aided design
CEM	Cation-exchange membrane
Da	Daltons
ED	Electrodialysis
EDS	Energy dispersive spectroscopy
HDACS	Hexamethylene-1,6-di(aminocarboxysulfonate)
ICP	Ion concentration polarization
ICP-OES	Inductively coupled plasma – optical emission spectroscopy
KOAc	Potassium acetate
LBL	Layer-by-layer
M_w	Molecular weight
MWCO	Molecular weight cutoff
NF	Nanofiltration
PAA	Poly(acrylic acid)
PAH	Poly(allylamine hydrochloride)
PAMAM	Poly(amidoamine) dendrimer
PCBS	Poly(1-[p-(3′-carboxy-4′-hydroxyphenylazo)benzenesulfonamido]-1,2-ethandiyl)

PCTE	Polycarbonate track-etch
PDADMAC	Poly(diallyl dimethyl ammonium chloride)
PDMAEMA	Poly[2-(dimethylamino) ethyl methacrylate]
PDMS	Polydimethyl siloxane
PEI	Polyethyleneimine
PEM	Polyelectrolyte multilayer
PES	Polyethersulfone
PHEMA-g-PAA	Poly(2-hydroxyethyl methacrylate)-graft-poly-(acrylic acid)
PSS	Poly(4-sodium styrene sulfonate)
RO	Reverse osmosis
SEM	Scanning electron microscope
sPEEK	Sulfonated polyether ether ketone
sPPBP	Poly(4-phenoxybenzoyl-1,4-phenylene)
XPS	X-ray photoelectron spectroscopy

CHAPTER 1

Introduction and Background

This dissertation investigates electrically driven ion transport through membranes modified with polyelectrolyte multilayers (PEMs) formed through layer-by-layer (LBL) adsorption. Remarkably, deposition of PEMs on membranes leads to electrodialysis selectivities >1000 in the transport of monovalent over multivalent cations.[1] LBL adsorption of PEMs yields relatively dense films that prevent passage of multivalent cations as well as larger molecules. Moreover, electromigration transport imbalances between the film and substrate membrane strongly influence cation transport. Strong electric fields near and inside the membrane cause secondary mass transport effects that reduce electrical efficiency and may also degrade the PEM.

This chapter provides background for this work and initially discusses ion-exchange as a method to separate and purify ions. Secondly, I present membrane-based technologies that separate charged species in solution, with emphasis on commercial techniques and particularly electrodialysis, an electrically-driven process that uses ion-exchange membranes. This section describes mass transport and membrane materials in commercially viable membrane configurations and applications of electrodialysis. Subsequent sections discuss the general utility of polymer thin films, LBL assembly of PEMs, and an outline of this dissertation.

1.1 Ion-exchange

Ion-exchange is a reversible chemical process whereby ions interchange between two electrolytes. In most applications, ions in solution exchange with similarly charged ions adsorbed to an oppositely charged species affixed to an immobile solid phase.[2] While ion-exchange has served as a method for demineralizing aqueous solutions since at least the 1930s and 40s,[3] newer ion-exchange applications focus on the food & beverage industry,[4,5] water softening,[6,7] industrial wastewater reclamation,[8] nitrate removal,[9] and purification of salts.[10,11] This section discusses ion chromatography as a primary method for separating and purifying ions.

1.1.1 Ion Chromatography

Ion chromatography separates ions based on coulombic interactions with a stationary phase and is the most popular method for separating proteins.[12] As equation 1.1 shows, cation-exchange materials retain positively charged species because of negatively charged functional groups within the exchanger. Anion-exchange groups retain anions because of positively-charged functional groups as shown in equation 1.2,[13]

$$R - X^- C^+ \; + \; M^+ B^- \; \rightleftharpoons \; R - X^- M^+ \; + \; C^+ \; + \; B^- \qquad (1.1)$$

$$R - X^+ A^- \; + \; M^+ B^- \; \rightleftharpoons \; R - X^+ B^- \; + \; M^+ \; + \; A^- \qquad (1.2)$$

where $R-X^-$ and $R-X^+$ represent negatively and positively charged functional groups on the stationary phase, respectively, C^+ and M^+ are cations, and A^- and B^- are anions.[14]

In its early development, crystalline zirconium phosphate ion-exchangers provided minimal ion selectivity, but later development of hexacyanoferrate exchangers provided selectivity for cesium over rubidium and potassium.[15] Ultimately, simple resinous exchangers comprised of iminodiacetate groups on a polystyrene backbone were developed to effectively remove trace concentrations of multivalent-metal cations from aqueous waste streams.[15] Current column packings for ion-chromatography employ thin coatings of acid- or base-functionalized polystyrene deposited on porous microparticles.[13,16]

Ion chromatography enables effective purification of aqueous ions. Cassidy *et al.* successfully separated mixtures of common metal cations using sulfonate and sulfate cation exchangers and low-concentration (2.5-50 mg L^{-1}) solutions.[17] The authors also separated mixtures of lanthanide cations via ion chromatography, but the separation again required low (~10 mg L^{-1}) concentrations.[18] Larger-scale separations in the mining or recycling industries require much higher throughput, and sensitive chromatographic separation techniques are ill-suited for this application. Nevertheless, ion-exchange remains a leading purification technique in these industries, but it produces large waste eluent streams during resin regeneration.[19]

1.2 Membrane-based Ion Separations

This work aims to develop new membranes for ion separations. Membranes provide an ideal, scalable separation platform because their molecular level structure is easily fabricated across large surface areas. Variation of membrane composition affords control over the permeation of various chemical species and makes membranes desirable for many processes.[20] Membrane technologies are central in nanofiltration (NF),[21-24] gas separations,[25-27] protein capture and digestion,[28,29] reverse osmosis (RO),[23,30-32] electrodialysis,[1,33-35] forward osmosis,[36,37] facilitated-transport dialysis,[38-40] and membrane distillation.[41,42]

RO is the primary method for large-scale desalination of seawater, whereas water softening and treatment of effluent waste streams often employ NF. Gas separation membranes are already used extensively for nitrogen production from air and for removing carbon dioxide from methane in natural gas.[20] Forward osmosis and membrane distillation are relatively new technologies with potential applications in power generation,[43] desalination[44] and food processing,[45,46] whereas facilitated-transport dialysis exhibits high selectivity but technical challenges hinder its adoption.[47] In contrast, electrodialysis facilitates a wide variety of commercial processes, and research continues to expand these applications. This section focuses on common membrane processes for removing charged species from feed streams. Because reverse osmosis is so prevalent, I

first discuss its principles and limitations before focusing on the methods studied in this dissertation – nanofiltration and, particularly, electrodialysis.

1.2.1 Reverse Osmosis

RO is a pressure-driven filtration through membranes that are permeable to water but nearly impermeable to salts and other dissolved species. This technique requires large hydrostatic pressures to overcome natural osmotic pressure such that the resulting positive pressure creates a positive chemical potential gradient across the membrane. This gradient drives the liquid against the normal direction of osmosis while retaining salts and other molecules in the feed stream.[30] Liquid flux through RO membranes, J_i, is proportional to the permeability, A, of the membrane to the liquid and the difference between the applied pressure, Δp, and the osmotic pressure differential across the membrane, $\Delta\pi$, (equation 1.3).

$$J_i = A(\Delta p - \Delta\pi) \quad (1.3)$$

Equation 1.4 describes the osmotic pressure for an ideal thermodynamic solution,

$$\pi = CRT \quad (1.4)$$

where C is the molar ion concentration, R is the gas constant, and T is the process temperature. The osmotic pressure of seawater is typically 22-26 atm, so large trans-membrane pressures drive the separation.[48]

The solution-diffusion model effectively describes the performance of RO membranes. In this model, which applies to dense, non-porous membranes, ions permeate through the membrane due to chemical potential gradients. Figure **1**.**1**a

shows osmosis when a semi-permeable membrane separates a salt solution from pure water. Pressure is the same on both sides of the membrane, and a continuous increase in the water chemical potential from the salt-solution side to the pure-water side originates from decreasing salt concentration. Solvent activity is higher on the pure-water side so water flows through the membrane toward the salt-solution. Application of pressure to the salt-solution side of the membrane causes a water chemical potential gradient from the salt-solution toward the pure-water permeate (See Figure **1**.**1**b), and water flows from the salt solution to the water side as a result.[49] Although RO effectively removes most dissolved species from solution, the low permeability of RO membranes to virtually all dissolved species makes them ineffective for solute separations.[50,51]

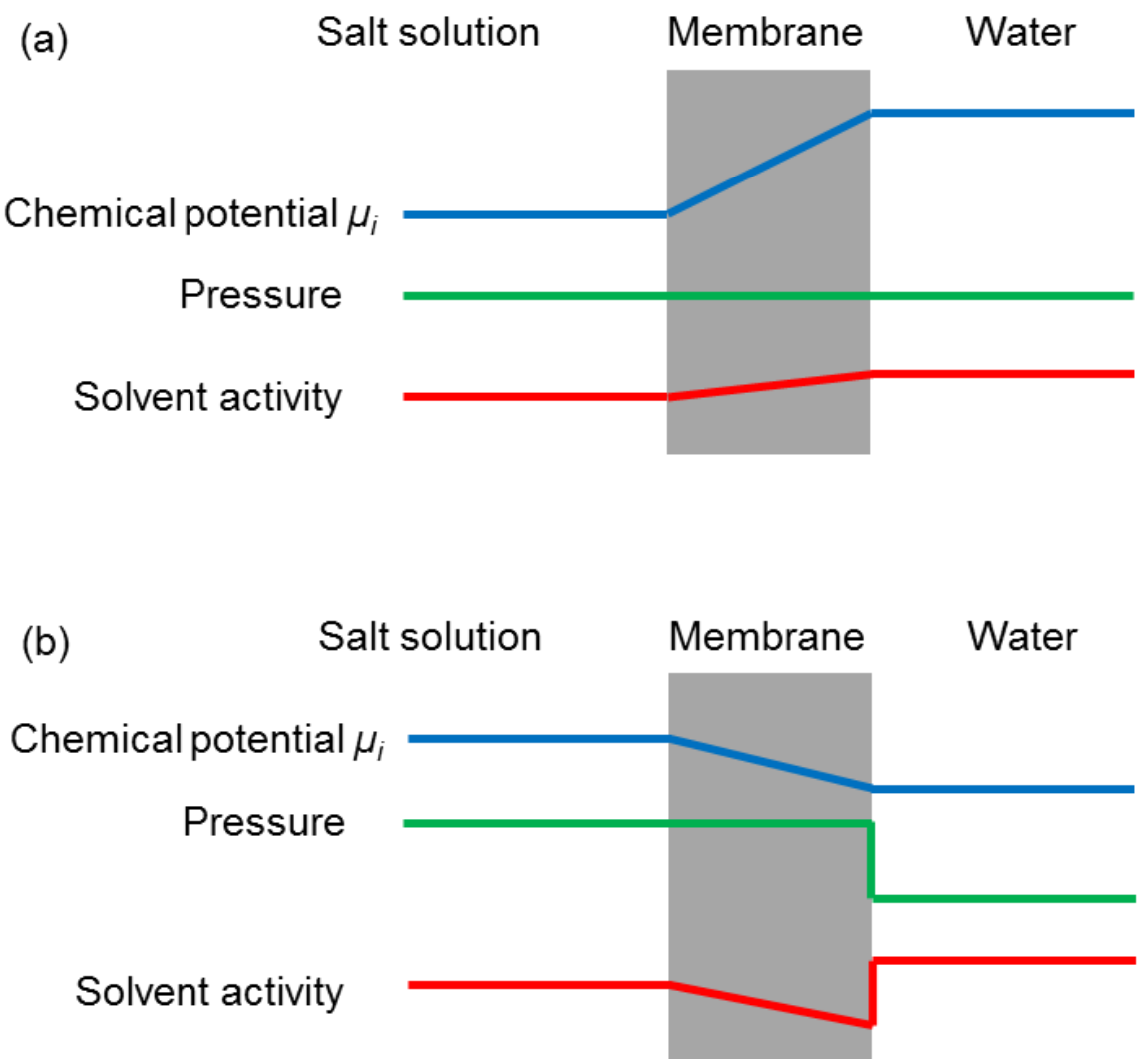

Figure 1.1**.** Comparison of chemical potential, pressure, and solvent activity profiles for normal osmosis conditions (a) and reverse osmosis (b). Water follows the chemical potential gradient and flows from the salt-solution side to the pure-water side in reverse osmosis. (Redrawn from *J. Membr. Sci.* 1995, *107*, 1-21)

1.2.2 Nanofiltration

NF employs nano-porous membranes to selectively remove specific solutes. Selective exclusion is primarily based on size for larger molecules, but membrane surface charge becomes significant when the hydrated radius of the ions approaches the pore diameter.[52,53] Driven by pressure, NF is similar to RO but requires lower transmembrane pressures and provides lower monovalent ion rejection.

The solution-diffusion model often describes NF performance when membranes have very small pores and behave in a non-porous manner to most solution components.[54,55] Equation 1.5 shows the salt flux, J_j, through a membrane where c_{j_f} and c_{j_p} are the salt concentrations on the feed and permeate sides, respectively, and B is the the salt permeability constant.

$$J_j = B(c_{j_f} - c_{j_p}) \tag{1.5}$$

The water flux depends on the osmotic pressure and the pressure applied across the membrane (see equation 1.3). Membrane performance is usually evaluated in terms of salt removal; reported as rejection, R, as defined in equation 1.6.

$$R = \left(1 - \frac{c_{j_f}}{c_{j_p}}\right) x\ 100\% \tag{1.6}$$

Equation 1.7 describes the membrane selectivity, α, for solute 1 over solute 2, where the numerical subscripts refer to the species. One can also describe the selectivity in terms of $R_1$and R_2, the rejections of solute 1 and 2, respectively.[56]

$$\alpha = \frac{c_{1_p}/c_{1_f}}{c_{2_p}/c_{2_f}} = \frac{100 - R_1}{100 - R_2} \quad (1.7)$$

Charged NF membranes rely on both Donnan and size exclusion to reject small, charged solutes. In Donnan exclusion, the charged membrane creates a potential that excludes solutes with the same charge. The potential forms due to unequal permeabilities of cations and anions in the membranes and is particularly effective for multivalent ions. Schaep *et al.* found that for both negatively-charged (NF40) and positively-charge (UTC 20) membranes with similarly-small pore radii near 0.4 nm, rejections of Na_2SO_4, $MgCl_2$, and NaCl are similar, and the ion rejections are inversely proportional to their diffusion coefficients. This suggests that for very small pores, charge is not the primary factor for rejection. However, for NTR 7450 membranes with larger pore radii around 0.8 nm, two studies suggest that Donnan exclusion is the primary determinant in salt rejection.[52,57]

By changing the pH of an electrolyte solution, Childress and coworkers found that NaCl rejection increases from <20% when protonated-NF55 membranes are predominantly positively charged, to nearly 90% at pH 8. The authors attribute the unusual result to changes in pore size as a function of pH and low Donnan exclusion at low pH because of relatively-high proton concentrations.[58] Increasing the magnitude of positive surface charge allowed Ouyang *et al.* to achieve Na^+/Mg^{2+} selectivities of 22 along with a solution flux of 0.85 $m^3\ m^{-2}\ day^{-1}$ (4.8 bar transmembrane pressure) for membranes consisting of five-bilayer poly(styrene sulfonate) (PSS)/protonated poly(allylamine hydrochloride) (PAH) films on alumina supports.[59] In addition, Stanton *et al.*

demonstrated Cl^-/SO_4^{2-} selectivities as high as 35 with $(PSS/PAH)_4PSS$ films deposited on alumina supports.[60] Malaisamy *et al.* reported Cl^-/SO_4^{2-} selectivities of up to 27 with PSS/poly(diallyl dimethyl ammonium chloride) (PDADMAC) films deposited on commercial ultrafiltration membranes.[61]

NF is a versatile technique with varied applications including softening water,[62,63] removing heavy metal ions,[64,65] removing organic contaminants from wastewater,[66,67] and recovering monovalent ions.[68] Chapter 4 in part examines removal of charged organic dyes from an industrial effluent using nanofiltration membranes modified with thin films. The high flux through ultrafiltration membranes combined with high rejections from nanofiltration films may prove useful in treating high-volume waste streams.[69]

1.2.3 Electrodialysis

In electrodialysis (ED) ions move across a membrane from a feed stream to a receiving stream due to an electric field, and the quantity of ions moving across the membrane varies with the applied current. Typical ED processes utilize alternating anion and cation-exchange membranes to control ion transport in a configuration known as an ED stack (Figure 1.2). Pairs of ion-exchange membranes, referred to as cell pairs that can number as many as 50 in commercial stacks, isolate salt solutions from separate receiving solutions. Positively-charged cations migrate toward the cathode while anions migrate toward the anode. Cations pass through cation-exchange membranes but are

retained by anion-exchange membranes, and, likewise, anions are retained by cation-exchange membranes. This process desalts alternating cells while enriching adjacent cells with ions (Figure 1.2).[20]

Manegold and Kalauch first proposed the use of selective anion and cation-exchange membranes to separate ions from water,[70] but Meyer and Strauss first described ED with such membranes in a multicellular arrangement between electrodes.[71] Because of the harsh conditions that result from electric fields, electrodialysis was impractical until researchers at Ionics Membranes developed stable membranes.[72,73] Subsequent installations focused on concentrating seawater for salt production in Japan[74] or desalination in the United States.[20] However, these systems suffered from scale formation until the development of electrodialysis polarity reversal in the 1970s,[75] which limited the need for anti-scaling chemicals by reversing the flow of colloidal particles and preventing them from forming a film on the membrane.[76] This section discusses ion-exchange membranes for electrodialysis, mass transport during these separations, and lastly, the extensive applications of the technology.

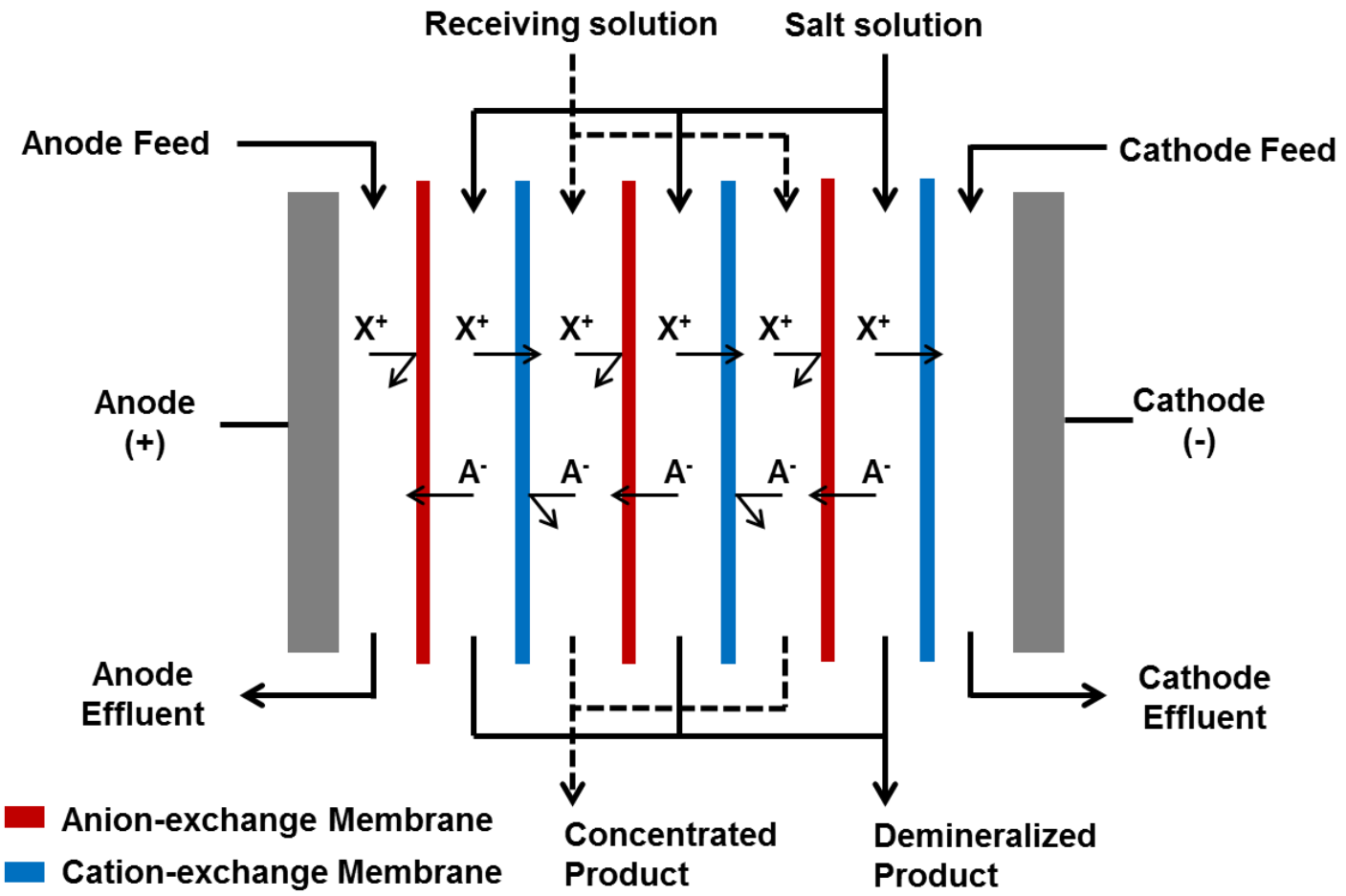

Figure 1.2. Schematic diagram of an electrodialysis stack. Anion and cation-exchange membranes prevent passage of cations (X^+) and anions (A^-), respectively. (Redrawn from *Desalination* 2007, *205*, 38-46)[77]

1.2.3.1 Ion-exchange Membranes

Ion-exchange membranes contain high concentrations of fixed ionic groups and accordingly show many of the properties of ion-exchange resins. When exposed to aqueous environments, the ionic groups absorb water and the materials swell, sometimes dramatically, in part because of charge repulsion.[78,79] Consequently, ion-exchange membranes often contain cross-links to limit swelling. However, a high cross-linking density may make polymers brittle so membranes are stored and handled water, which plasticizes the membrane.[20,80] Broadly, ion-exchange materials may be either heterogeneous or homogenous.

1.2.3.1.1 Heterogeneous Ion-exchange Membranes

Heterogeneous membranes consist of finely dispersed cation- or anion-exchange particles in a polymeric support.[81] The support material serves as a strong mechanical substrate whereas the resin imparts desirable ion-exchange properties. However, although heterogeneous membranes are durable, their electrochemical performance is often relatively poor.[82] Choi and coworkers reported that heterogeneity decreases membrane conductivity, an essential characteristic for ED processes.[83] Vyas *et al.* found that the resin-particle size distribution and loading in the membrane affect electrochemical and mechanical properties, but an optimized composition yields membranes comparable to the best-performing commercial products.[84]

ED stacks supply uniform current during electrically-driven separations. However, heterogeneous membranes with non-conducting regions cause an uneven distribution of current densities across the surface (Figure 1.3), and locally high current densities increase concentration polarization at the membrane-solution interface.[85] Thus, heterogeneous membranes are used much less frequently than their homogeneous counterparts.

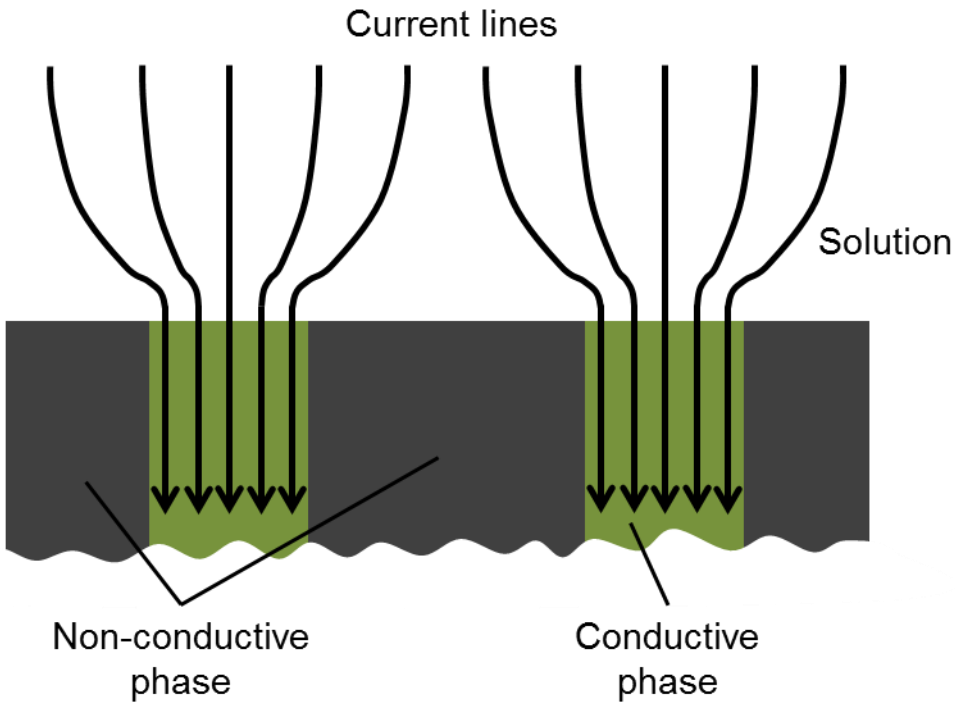

Figure 1.3. Schematic diagram of the current density distribution close to a heterogeneous membrane surface. Heterogeneous membranes experience locally high current densities because of non-conducting regions. (Redrawn from *Colloid Interface Sci.* 2005, *285*, 247-258)[85]

1.2.3.1.2 Homogeneous Ion-exchange Membranes

Many commercial ion-exchange membranes are single-phase, homogeneous polymers. In most cases, membrane preparation includes formation of a crosslinked base membrane and subsequent conversion to a charged form by post-treatment with trimethyl amine (anion-exchange membranes)[86] or sulfonation with concentrated sulfuric acid (cation-exchange membranes).[87] Crosslinking strongly enhances the mechanical strength of the membranes and reduces swelling in water. However, excessive crosslinking can reduce the overall permeability of the membrane and may decrease conductivity, though experiments by Mikhailenko *et al.* indicate such decreases to be minimal.[88]

The positive charge in anion-exchange membranes typically stems from quaternary ammonium, sulfonium, or phosphonium functional groups (Figure 1.4). Quaternary ammonium groups were initially believed to have higher thermal and chemical stability than phosphonium or sulfonium groups,[89] but more recent work by Gu and coworkers suggests that phosphonium is less vulnerable to nucleophilic attack than ammonium in alkaline conditions.[90] Amine-based anion-exchange membranes are particularly vulnerable at the α-C atom, and research has focused on steric protection of this position to increase durability.[91]

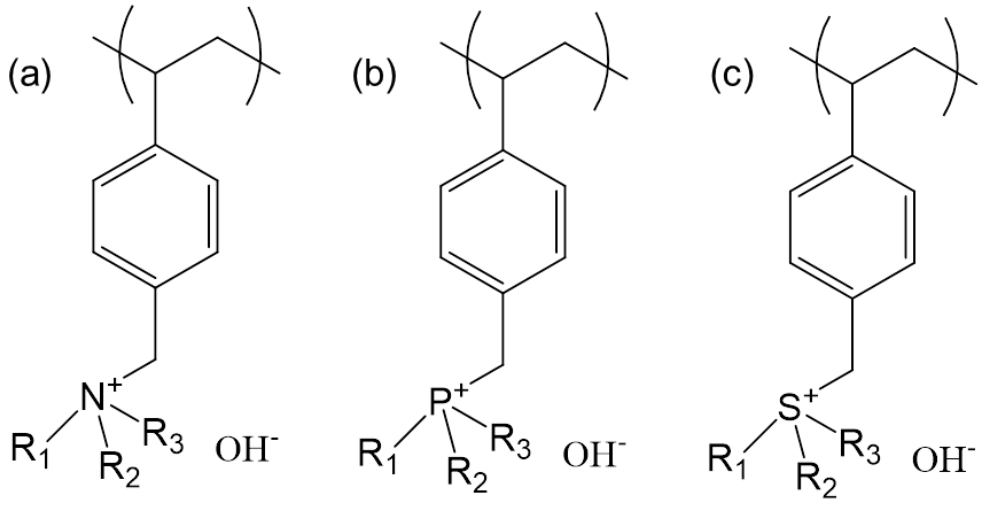

Figure 1.4. Chemical structures of (a) ammonium, (b) phosphonium, and (c) sulfonium functional groups commonly found in anion-exchange membranes. (Redrawn from *J. Membr. Sci.* 2011, *377*, 1-35)[89]

Sulfonate groups are the most common source of cation-exchange sites in negatively-charged membranes. Based on tetrafluoroethylene, Nafion is a perfluorinated block-copolymer with strong, terminal sulfonic acid groups (Figure 1.5a).[92] The extreme hydrophobicity of the backbone in this perfluoro polymer helps limit swelling in water, while the sulfonic acid groups are strongly polar. The large internal differences in hydrophobicity cause formation of water channels that support water permeability despite a relatively low water uptake.[93] However, Nafion's high cost and persistence in natural environments spurred research on hydrocarbon-based cation-exchange membrane materials such as those in Figure 1.5b and c. These materials mimic Nafion and perform satisfactorily when sulfonic

acid groups are spaced away from the hydrophobic backbone. However, durability remains a significant challenge.[94]

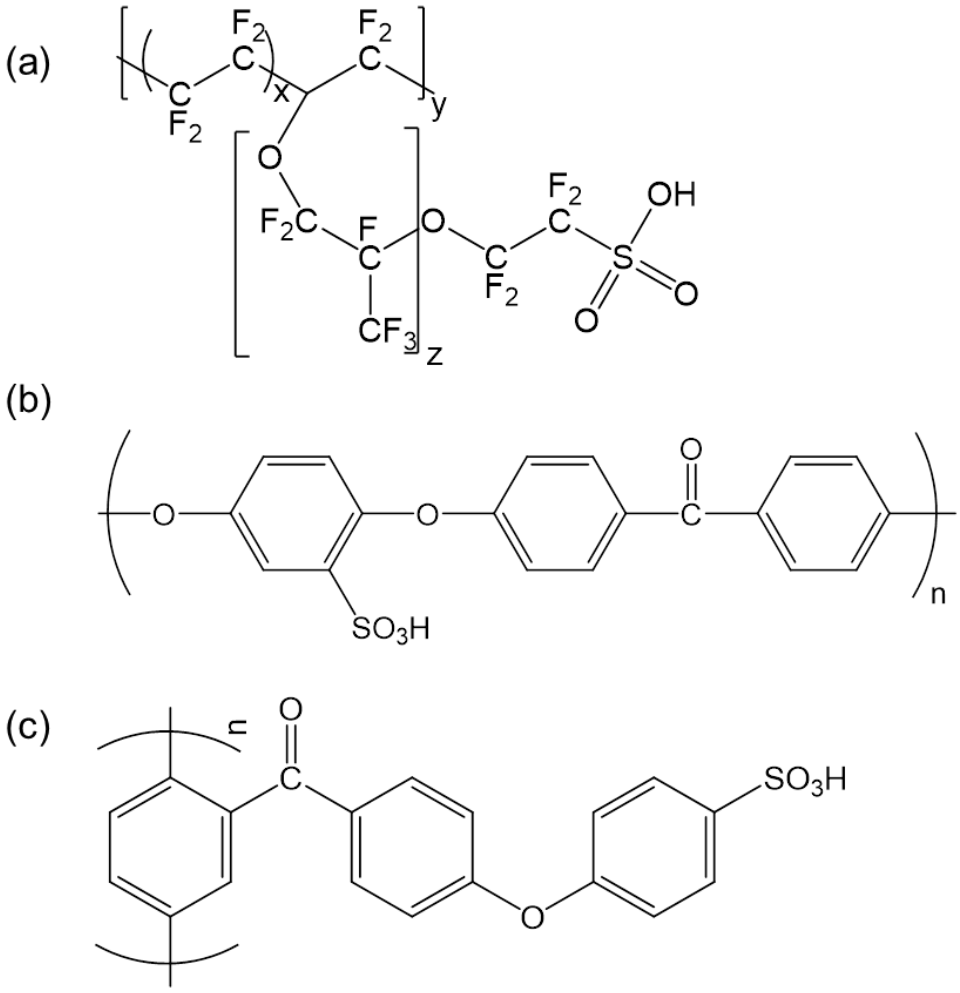

Figure 1.5. Cation-exchange polymers used in electrodialysis and fuel-cells. Nafion (a) is a perfluorinated block copolymer, whereas sulfonated polyether ether ketone (sPEEK) (b) and poly(4-phenoxybenzoyl-1,4-phenylene) (sPPBP) (c) have hydrocarbon backbones.[95] (redrawn from *Int. J. Hydrogen Energy* 2010, *35*, 9349-9384)[96]

1.2.3.2 Mass Transport

Figure 1.6 shows concentration and potential profiles during ion transport in ED cells, assuming all compartments are very well mixed. In the presence of an electric field, cations (X^+) and anions (A^-) are alternately concentrated and depleted between anion and cation-exchange membranes. The electrical potential profile assume that all electrical resistance originates from the membranes, which are uniformly conductive. Consequently, in the well-stirred ED system shown, the driving force (current) could increase indefinitely and result in infinite membrane productivity.[20]

Real ED systems experience relatively little resistance from the membranes, while substantial resistance occurs in the water-filled compartments between cell pairs. This is particularly true for ion-depleted regions in the dilute compartment where fewer ions are available to carry current.[97] These regions form next to the membrane and place an upper bound on the total current throughput.

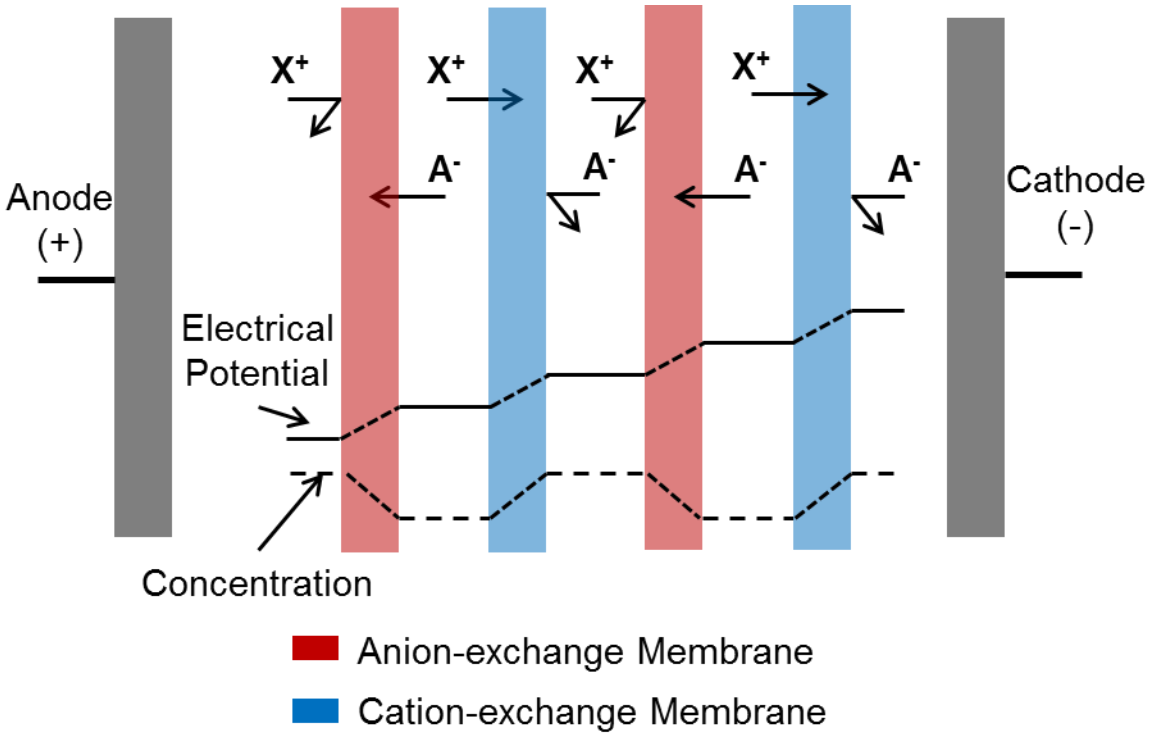

Figure 1.6. Schematic of the concentration and potential gradients in a well-stirred electrodialysis cell, where all of the electrical resistance occurs across the membrane. (Redrawn from *Membrane Technology and Applications*, 2nd ed.; J. Wiley: Chichester ; New York, 2004)[20]

Concentration polarization controls the overall performance in ED.[20,98] Because ion-exchange membranes are more permeable to some ions than others, the concentration of some ions near the membrane surface falls as compared to the bulk solution.[99] In the example shown in Figure 1.7, only cations carry current through the membrane, whereas both cations and anions carry current in the bulk solution. Assuming electrical mobilities for both ions are equal, cations become

depleted at the membrane interface because the supply of cations to this interface is approximately half the electromigratory transport of cations away from it. Similarly, an ion-enriched area forms on the receiving side of the membrane because the supply of cations from the membrane is greater than the migration away from it.[100] Similar concentration profiles appear for the anions, and these boundary layers greatly affect the local resistance of the aqueous solution.

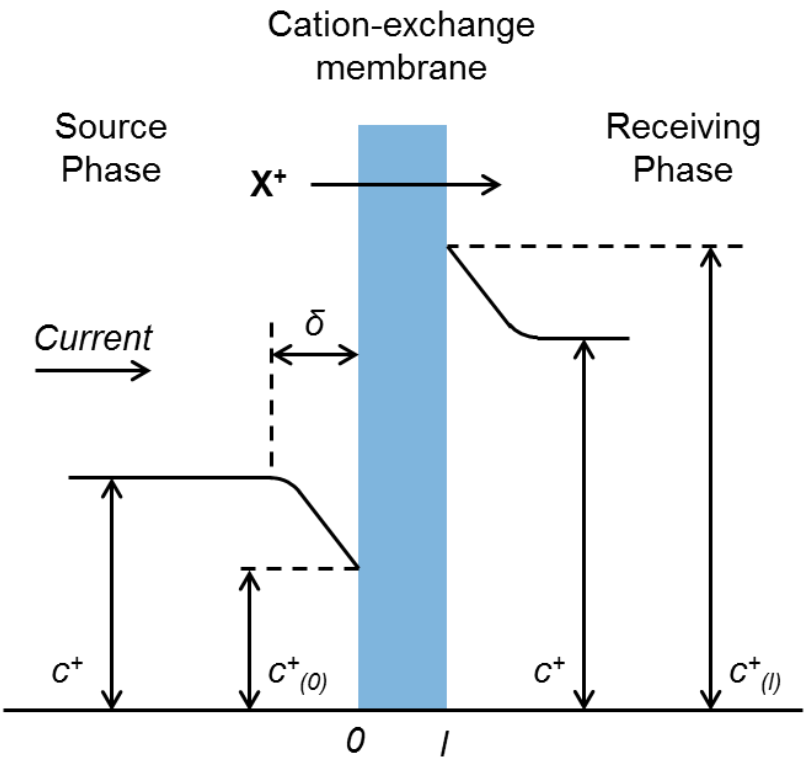

Figure 1.7. Schematic diagram of ion concentration gradients near a cation-exchange membrane during electrodialysis, showing the formation of the boundary layer in the presence of an applied current. (Redrawn from *Membrane Technology and Applications*, 2nd ed.; J. Wiley: Chichester ; New York, 2004)[20]

A number of studies modeled ion transport through electrodialysis membranes. [101-104] The boundary layer thickness, δ, in ED varies depending on the extent of turbulence, but the unstirred region is generally 20-50 μm thick.[105] The diffusive flux of cations, J_D^+, through the boundary layer should follow Fick's first law of diffusion, which for a linear concentration profile is given in equation 1.8:

$$J_D^+ = \frac{D^+(c^+ - c_{(0)}{}^+)}{\delta} \quad (1.8)$$

where D^+ is the diffusion coefficient of the cation in water, c^+ is the concentration of the cation in the bulk solution, and $c_{(0)}{}^+$ is the cation concentration at the membrane surface on the source-side. However, the total ion flux in the boundary layer also includes electromigration, so equation 1.9 gives the overall flux, J^+, which is the sum of the fluxes due to diffusion and electromigration (in the absence of convection):

$$J^+ = \frac{D^+(c^+ - c_{(0)}{}^+)}{\delta} + \frac{t^+ I}{F} \quad (1.9)$$

where I is the current through the membrane, F is the Faraday constant, and t^+ is the fraction of the total current carried by the cation, also known as the transference number.

Transport through the membrane depends on two factors: voltage drop across the membrane due to membrane resistance, and diffusion due to concentration differences on either side of the membrane. Total ion flux, J^+, through the membrane is given by equation 1.10:

$$J^+ = \frac{t_{(m)}{}^+ I}{F} + \frac{P^+\left(c_{(0)}{}^+ - c_{(l)}{}^+\right)}{l} \quad (1.10)$$

where P^+ is the cation-permeability of a membrane with thickness l,and $t_{(m)}{}^+$ is the cation transference number within the membrane. Typical ion-exchange membranes have low diffusive permeability to ions,[106] so the diffusive flux is very small compared to electromigration through the membrane, and the $\frac{P^+\left(c_{(0)}{}^+ - c_{(l)}{}^+\right)}{l}$ term is negligible. At steady state, the total cation flux in the boundary layer (equation 1.9) should equal the cation flux through the membrane (equation 1.10), to give equation 1.11 (neglecting $\frac{P^+\left(c_{(0)}{}^+ - c_{(l)}{}^+\right)}{l}$).

$$D^+ \frac{\left(c^+ - c_{(0)}{}^+\right)}{\delta} + \frac{t^+ I}{F} = \frac{t_{(m)}{}^+ I}{F} \quad (1.11)$$

In ideally-selective cation exchange membranes, $t_{(m)}{}^+ \approx 1$ and equation 1.11 can be simplified to yield equation 1.12.

$$I = \frac{F}{(1-t^+)} . \frac{D^+}{\delta}\left(c^+ - c_{(0)}{}^+\right) \quad (1.12)$$

If the boundary layer has a constant thickness, the equation reaches a limiting value when the cation is depleted completely at the membrane surface ($c_{(0)}{}^+ \approx 0$). Thus, the current reaches its maximum value when the cation concentration approaches 0, and the supply of cations to the interface is limited by their diffusion to the surface as shown in equation 1.13.

$$I_{lim} = \frac{D^+ F c^+}{\delta\left(1-t^+\right)} \quad (1.13)$$

Exceeding the limiting current will not increase transport of the cation through the membrane. Instead, anion electromigration, water splitting, and electroosmotic flow will provide the necessary current carriers.[107,108] All of these require electrical power but do not contributing to the separation and negatively impact ED efficiency.[20]

1.2.3.3 Efficiency

In ED, the energy (per mole) consumed to drive a separation is a primary measure of efficiency. Equation 1.14 shows the power as it relates to the current through the membrane, I, and the total resistance of the system, R.

$$P = I^2 R \tag{1.14}$$

The theoretical current, I_{theor}, required for a separation is directly proportional to the quantity of charge moved across the membrane as shown in equation 1.15:

$$I_{theor} = z\,\Delta C\,F\,Q \tag{1.15}$$

where z is the charge on the ion, ΔC is the difference in molar concentration from the source-side to the receiving-side of the membrane, F is the Faraday constant, and Q is the source-phase flow rate. Substituting equation 1.15 into equation 1.14, we obtain equation 1.16 for the theoretical power consumption for a given ED process.

$$E_{theor} = I\,R\,z\,\Delta C\,F\,Q \tag{1.16}$$

The energy consumed during ED is, of course, higher than the theoretical limit. As Figure 1.7 shows, the actual concentration difference across the membrane is larger than in the absence of polarization. Moreover, depletion regions lead to areas of high resistance. Generally, rapid flow across the membrane surface helps to mitigate concentration polarization, but this requires energy-consuming pumps so there is a energy tradeoff between pumping costs and reducing concentration polarization.[109] Additional energy losses occur from non-ideally selective ion-exchange membranes that permit passage of anions and cations and osmotic transport of water molecules that can change source and receiving-phase concentrations.[110] Nevertheless, concentration polarization remains the greatest efficiency challenge in ED separations.

1.2.3.4 Applications

The largest application of ED is the production of potable water from brackish water. Small-scale ED plants were first installed for specialized island-based desalination operations and were cheaper to run than distillation plants of the same size.[111] ED processes are competitive with RO for desalination when the total dissolved salts fall between 1000 and 5000 mg L^{-1} and also offer a number of advantages: very high water recovery, low membrane fouling potential, and high operating temperatures and lifetimes. However, ED membranes do not remove neutral species such as viruses and some bacteria, which is essential for water treatment.[112]

Amor and coworkers removed fluoride ions from brackish groundwater using 10-cell pairs of cationic-CMX and anionic-ACS Neosepta membranes in ED. Fluoride removal increased nearly three-fold when the flow rate through the ED stack increased from 50 L h^{-1} to 180 L h^{-1}, a direct result of reduced boundary-layer thickness at higher flow rates.[113] The authors further investigated fluoride reduction in a two-stage ED process where the first stage removed multivalent cations to limit scaling. ED decreased fluoride concentrations ~80% to within potable water limits. Moreover, experiments with chemical pretreatment steps proved unnecessary because ED effectively removes fluoride and divalent cations.[114]

Seawater contains high concentrations of sulfates and other ions that can precipitate on ion-exchange membranes in ED. Sata *et al.* deposited single cationic-polyelectrolyte layers on commercial cation-exchange membranes to exclude Ca^{2+} from the receiving solution. Unmodified cation-exchange membranes were essentially non-selective between Na^{+} and Ca^{2+}, but Na^{+}/Ca^{2+} selectivities increased to as much as 2.8 with adsorbed polyelectrolytes.[115]. Later work employed a single layer of anionic polyelectrolyte on the surface of Neosepta anion-exchange membranes. As Figure 1.8 illustrates, the dense charge of a polyelectrolyte film (PSS) on the positively charged anion-exchange membrane rejects most sulfate anions. In ED with 0.04 N sodium chloride and sodium sulfate, membranes modified with PSS show Cl^{-}/SO_4^{2-} selectivities as high as 10, and the rejection mechanism relies primarily on electrostatic repulsion between the

sulfonate groups in PSS and the multiply-charged anion. However, selectivity declines dramatically at higher concentrations and is essentially 1 for 0.5 N solutions.[116]

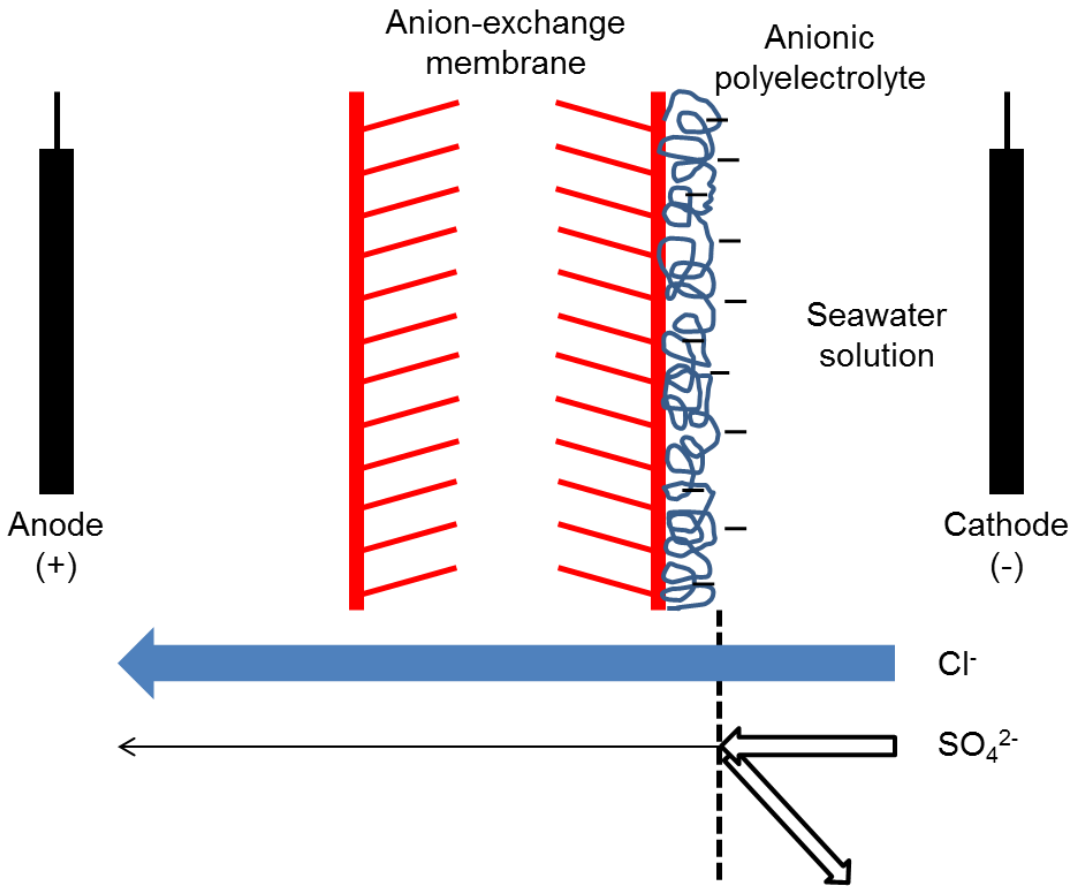

Figure 1.8. Anion-exchange membranes coated with single polyanion layers selectively reject multivalent sulfate ions while passing chloride. (Redrawn from *Membrane Technology and Applications*, 2nd ed.; J. Wiley: Chichester ; New York, 2004)[20]

1.2.3.5 Bipolar Membranes

Separation of charged species from non-electrolytes has spurred the development of bipolar membranes designed to split water. Bipolar membranes are a class of ion-exchange membranes in which an anion-exchange material is laminated to a cation-exchange material (Figure 1.9).[117] Under an electric field, salt ions migrate away from the interface, completely depleting the membranes interior of salt. At high salt depletion, protons and hydroxide from the dissociation of water are the only species carrying current, and the result is an alkaline solution on the anion-exchange side of the membrane and an acidic solution on the cation-exchange side.[118]

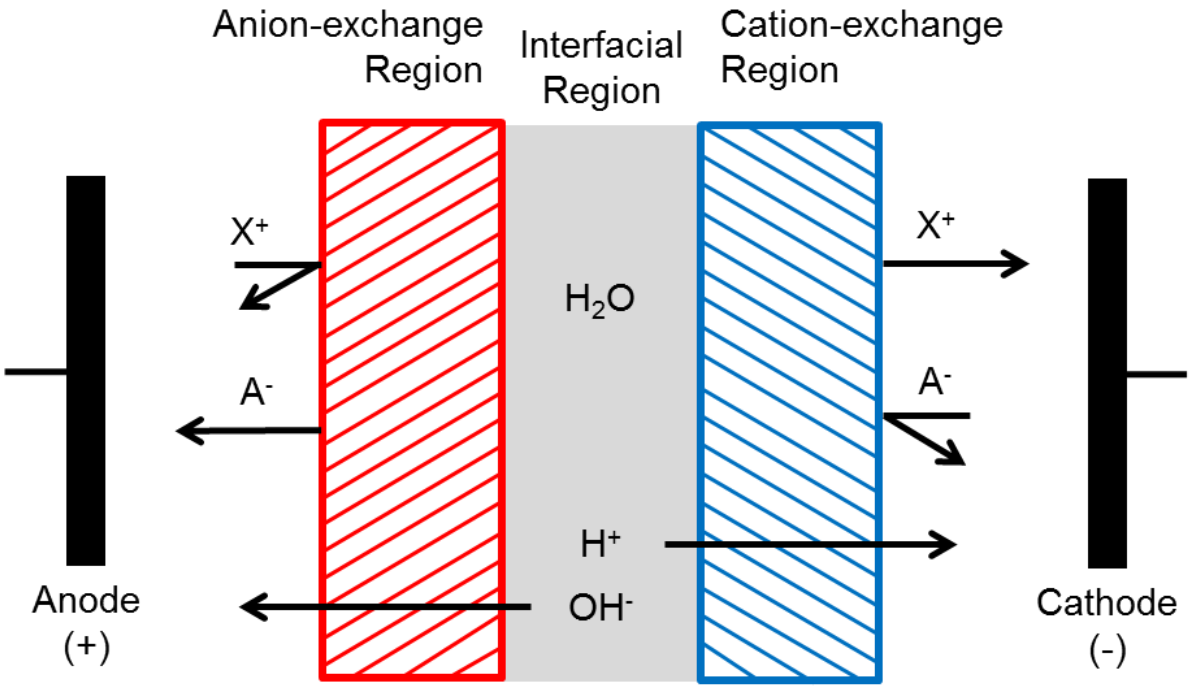

Figure 1.9. Schematic diagram of a single bipolar membrane that produces protons and hydroxide ions at the interface between anion- and cation-exchange regions. (Adapted from *J. Membr. Sci.* 1993, *78*, 13-23)[117]

Pairing bipolar membranes with additional cation and anion-exchange membranes in ED permits acid and base production from salts. Mazrou *et al.* produced high purity (>99%) sodium hydroxide and hydrochloric acid via water splitting induced with bipolar membranes. The authors reported current efficiencies as high as 90%, but this value declined to near 50% as the concentration of NaOH and HCl increased from 0.1 M to 1.5 M.[119] Later studies determined that the primary reason for the decrease in current efficiency was proton leakage through the anion-exchange membrane. Acid concentrations >1 M

reduced the selectivity of the anion-exchange membranes, and the ED efficiency declined as a result.[120] However, Gineste produced up to 6 M acid/base using an ED configuration that eliminates direct contact between the acid-production chamber and hydroxides produced at the cathode.[121] Thus, both configuration and selectivity are highly important to efficient ED processes.

ED of salts can also effectively produce organic acids. Beginning with sodium citrate, Xu and coworkers produced 0.15 M citric acid using bipolar membranes with sulfonic acid and quaternary ammonium groups. Unlike traditional production through fermentation, ED produces high-purity citric acid and very little waste.[122] Ferrer *et al.* used bipolar membranes to generate 7 M formic acid from sodium formate at 80% efficiency and a 50 mA cm^{-2} current density. The high ED efficiency required current densities below limiting values, which were determined experimentally by monitoring the cell voltage as a function of current density.[123] Other studies with bipolar membranes in ED demonstrated its utility for preparing acetic acid,[124] propionic acid,[125] lactic acid,[126-131] salicylic acid,[132] gluconic acid,[133] vitamin C,[134] and some amino acids.[135,136]

New ED processes have may find specialized uses in the food industry. After consumer preference shifted toward fresh-pressed, unclarified apple juices, growers needed to eliminate enzymatic browning that reduces apple juice shelf life and appeal. Apple pulp contains polyphenols which, catalyzed by polyphenol oxidase, form o-quinones that polymerize to produce color- and odor-altering pigments.[137] Though initially achieved through acid addition to inhibit the enzyme,

the resulting product was diluted and had a salty aftertaste.[138] Tronc *et al.* explored ED as a means to deactivate the enzyme through acidification ,[139,140] but subsequent studies required that the juice be kept at room temperature for 1 h to inhibit enzymes.[141] Quoc and coworkers employed bipolar membranes in ED to acidify juice to pH ~2 via water-splitting reactions before heating to 45 °C for 5 min to deactivate the enzyme. ED combined with heat treatment stabilized the juice without altering flavor or desirable color and clarity characteristics.[142] More recent studies sought to improve nutritional value with ED by either de-acidifying juices[143-146] or enriching antioxidants in cranberry juice.[147]

Other food-industry ED applications include demineralizing whey and producing soy proteins. Greiter and Fischer utilized ED to reduce ion concentrations in whey by 90%, and, when compared to conventional ion-exchange processes, found ED produces 70% less waste water and 80% less salt.[148] General Electric Corp. commercialized an ED stack and membranes specifically for desalting whey.[149]

Soya proteins are traditionally isolated in the food industry by isoelectric precipitation. In this method, the pH of dissolved proteins is lowered to the isoelectric point, ~4.5, with hydrochloric acid, and the solvated proteins readily precipitate. The product is rinsed with water and neutralized with sodium hydroxide to regenerate solubility in water.[150] However, this method subjects proteins to locally extreme pH levels that can cause denaturation,[151] and the addition of acids and bases increases mineral content.[152] Bazinet *et al.* developed

an ED process to decrease pH from 8 to the protein isoelectric point with bipolar membranes. The authors precipitated 95% of the protein with only ~0.5 kWh kg^{-1} of energy consumed. Furthermore, ED does not increase mineral content because counterion removal occurs when pH is restored via ED to its original level.[153,154]

1.3 Applications and uses of thin films

Polymer thin films are useful as anti-reflective coatings,[155-157] active interfaces in chemical and biological sensors,[158-161] non-fouling biosurfaces,[162-164] conductive electronic layers,[165-167] and anti-corrosive coatings.[168-171] Consequently, much research focuses on optimizing performance and understanding film structure to reduce costs and enhance economic viability. At the core of this is the need to understand how films form and the factors that alter their morphology. Thus, this section focuses on the primary film-formation method employed in this dissertation: the layer-by-layer (LBL) method for deposition of ultra-thin multilayer polymer films.

1.4 Layer-by-layer deposition of multilayer films

Among many methods for thin-film deposition including spin coating,[172,173] dip coating,[174] physical and chemical vapor deposition,[175,176] and surface-initiated polymerization,[177,178] the layer-by-layer (LBL) method is attractive for its precise

control over film formation and surface morphology. As Figure 1.10 shows, LBL deposition typically utilizes alternating layers of polycations and polyanions. Initially, immersion of a positively-charged substrate in a polyanion solution yields a negatively-charged polymer film attached to the surface through electrostatic interactions. Rinsing and immersion in water helps remove weakly adhered polyelectrolyte. Subsequent immersion of the negatively-charged film in a polycation solution produces a positively-charged film. Additional sequential immersion steps lead to the formation of multilayer films.[179-181]

An increase in entropy drives this process because adhesion of a single polyelectrolyte macromolecule releases numerous counter ions into solution.[182] Excess polyelectrolyte adsorption leads to charge overcompensation and reversal of the surface charge. Repeated immersions in oppositely charged polyelectrolytes form electrostatic interactions that again reverse the surface charge.[183] Thus, polyelectrolytes readily adsorb to charged interfaces. Additionally, some multilayer films incorporate hydrogen bonding[184,185] or covalent linkages between layers.[186]

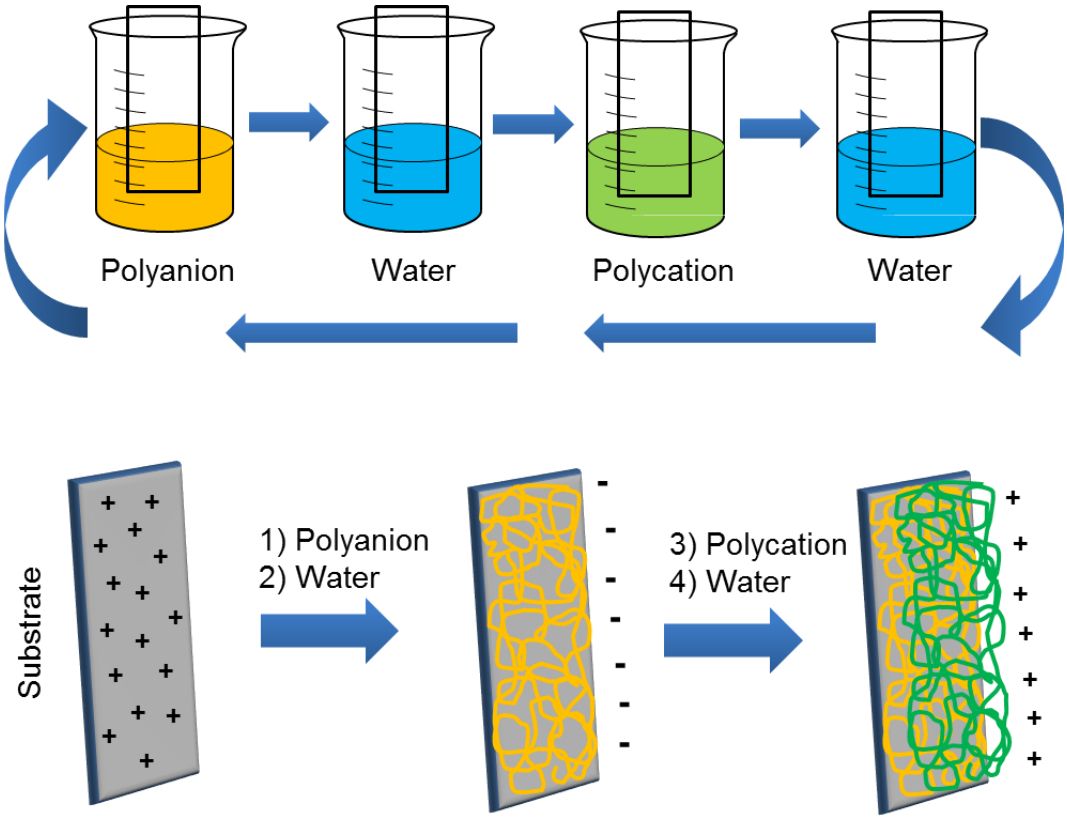

Figure 1.10. Schematic illustration of the layer-by-layer method for forming films on a positively-charge substrate. Sequential immersions in polycation and polyanion solutions with intermediate water rinses produce a single bilayer film.[183]

Polyelectrolytes suitable for LBL film formation include DNA,[187,188] proteins,[189] simple polymers[190] and other multiply-charged species such as nanoparticles[191] or viruses.[192] This dissertation focuses on LBL films prepared from synthetic, charged polymers, and some of the most common polyelectrolytes used in LBL adsorption include PSS,[193,194] PAH,[189] PDADMAC,[195] poly(acrylic

acid) (PAA),[196] and various branched and unbranched polyethyleneimines (PEI).[197] Figure 1.11 shows the structures of these polymers.

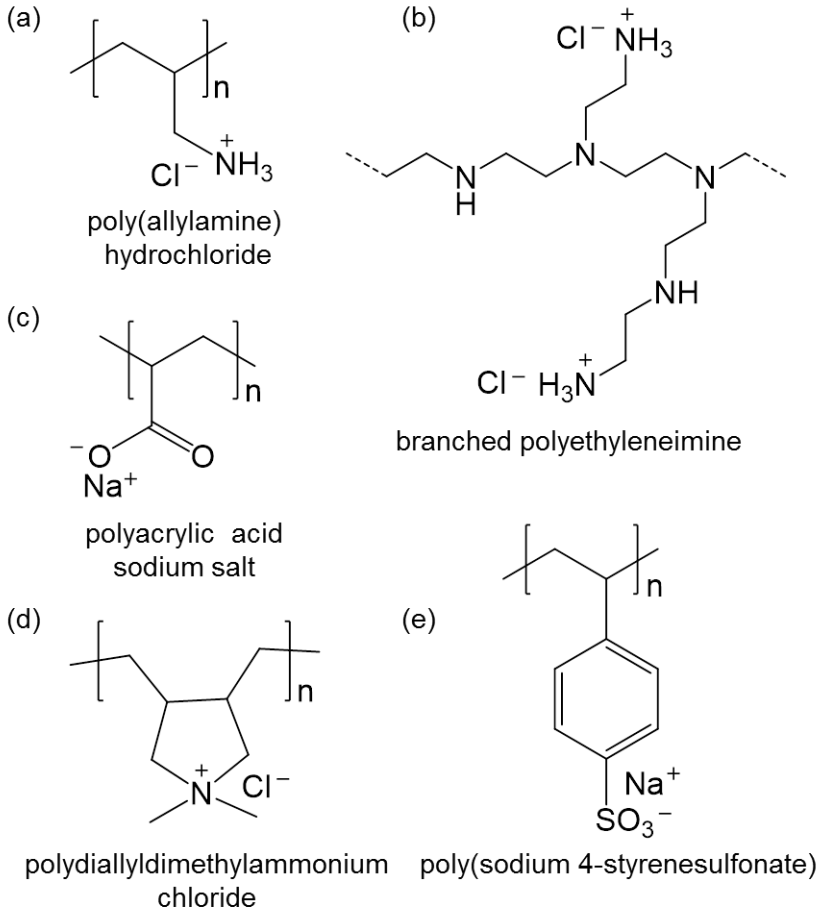

Figure 1.11. Structures of common polyelectrolytes used for LBL film formation.

1.4.1 Factors affecting PEM formation

PEM formation depends on the polyelectrolyte chemistry and morphology, the deposition temperature and pH, the supporting electrolyte composition and

concentration, adsorption time, and polyelectrolyte concentration. Choi *et al*. reported that PEMs prepared from star-shaped PAA and poly[2-(dimethylamino) ethyl methacrylate] (PDMAEMA) are two or three times thicker than comparable PEMs fabricated from linear PAA and PDMAEMA.[198] Subsequent studies with PAH and comb-like poly(2-hydroxyethyl methacrylate)-graft-poly- (acrylic acid) (PHEMA-g-PAA) generated films ~2 times thicker than those prepared from PAH and linear PAA. The comb-like structure produces thick films because of intra-molecular electrostatic repulsion and the large size of the copolymer.[199]

Several studies investigated the effect of temperature and pH on LBL adsorption. Tan *et al.* reported that the thicknesses of PSS/PDADMAC films adsorbed from solutions containing 1.0 M NaCl increase from 80 nm at a deposition temperature of 10°C to nearly 250 nm at a deposition temperature of 70°C. The heat provides the energy needed to overcome barriers to conformational changes in the polyelectrolytes, and the polymer sends loops and tails into solution above the surface to give a thicker film at higher temperature.[200] Later work by Salomaki determined that PAH/PSS film thicknesses increase linearly with increasing layer number at 55°C but exponentially with layer numbers at an adsorption temperature of 80°C. Higher diffusion rates within the polymer structure at high temperatures allow expanded geometries.[201] In addition, since the polyelectrolyte charge state depends on pH, film growth also varies with the pH of the deposition solutions. Schoeler, Poptoshev, and Caruso reported that LBL adsorption of PAA and [3-(2-methylpropionamido) propyl] trimethyl

ammonium chloride (AM-MAPTAC) gives films whose thickness increases exponentially with the number of layers when adsorption occurs at low pH. However, increasing the deposition pH to >6 leads to highly-charged PAA that causes a large charge mismatch between the polyanion and polycation and desorption of AM-MAPTAC 10.[202]

Supporting electrolytes play a significant role in PEM deposition. Dubas and Schlenoff reported that 10-bilayer PSS/PDADMAC films adsorbed in the absence of supporting electrolyte were only ~ 200 Å thick, but the thickness increased more than 10-fold when depositing polyelectrolytes from solutions containing 2 M NaCl. With no salt, polyelectrolytes extend to maximize the distance between like charges, and this extension leads to very thin films. In contrast, in the presence of supporting electrolyte additional ions screen charges on the polymer chains and allow formation of coils and, consequently, thicker layers.[203] Guzman *et al* noted similar results and that PEM growth switches from a linear to an exponential pattern at high supporting electrolyte concentrations, likely due to increased charge screening.[204]

Additionally, the identity of the supporting electrolyte affects deposition. Dubas *et al.* reported that less-hydrated cations lead to thicker films presumably because strongly bound ions (less hydrated) effectively increase the ion concentration.[203] Similarly, the supporting electrolyte anion affects growth of PSS/PAH films. In studies with sodium salts of the Hofmeister series from cosmotropic to chaotropic anions (F^-, $HCOO^-$, BrO_3^-, Cl^-, ClO^{3-}, Br^-, NO_3^-, ClO_4^-)

and 10-bilayer films, Salomaki and coworkers found chaotropic anions produce the thickest films. Such anions strongly screen the polyelectrolyte charges, leading to a loopy secondary structure that increases film thickness. Cosmotropic anions bind much less strongly to polycations, allowing polyelectrolytes to deposit in a more planar form.[205] Furthermore, multivalent anions can increase PEM thickness by formation of anionic bridges that produce voids in the film.[206]

The time employed to adsorb PEMs varies widely and is likely limited by mass transport of the polymer to the charged surface. Studies of film thickness and adsorption times are complicated by a large range of reported pH conditions, polyelectrolyte structures, and polymer molecular weights. However, Garg *et al*. found that in absorption of PAH/poly(1-[p-(3′-carboxy-4′-hydroxyphenylazo)benzenesulfonamido]-1,2-ethandiyl) (PCBS) films, 95% of polyelectrolyte absorption occurs in the first 66 seconds or less of exposure to the solution.[207] Similarly, Guzman showed that 75-80% of the mass of PSS/PDADMAC films deposits during a fast kinetic period after the initial substrate immersion in the polyelectrolyte solution where reorganization of the polymer chain occurs, mainly within the first 10 s.[208]

Studies focused on optimizing deposition show that the amount of adsorbed polyelectrolyte in PEM films increases with increasing polyelectrolyte concentration.[209,210] Thicknesses of 5-bilayer PSS/PDADMAC films increased ~25% when the concentration of the deposition solution rose from 2 mM to 50 mM in 1.0 M NaCl, but this increase is less dramatic than increases due to higher

supporting electrolyte concentrations.[203] Khopade and Caruso showed that the amount of adsorbed poly(amidoamine) dendrimer (PAMAM) or PSS increased by as much as 100% when the concentration of one polyelectrolyte was increased to 5 mM while the other remained at 1 mM during adsorption of PAMAM/PSS films.[211] Dendrimer concentration predominantly controls film deposition, presumably because its structure allows greater conformational flexibility and is less restricted to planar deposition.

LBL techniques allow sequential adsorption and specific tailoring of film thickness. Figure 1.12 shows the linear growth of PSS/PAH films as a function of the number of adsorbed bilayers, and the regular growth results from the thin and uniform deposition for this polyelectrolyte system.[212] In chapters 3 and 4, I discuss ion transport through such films.

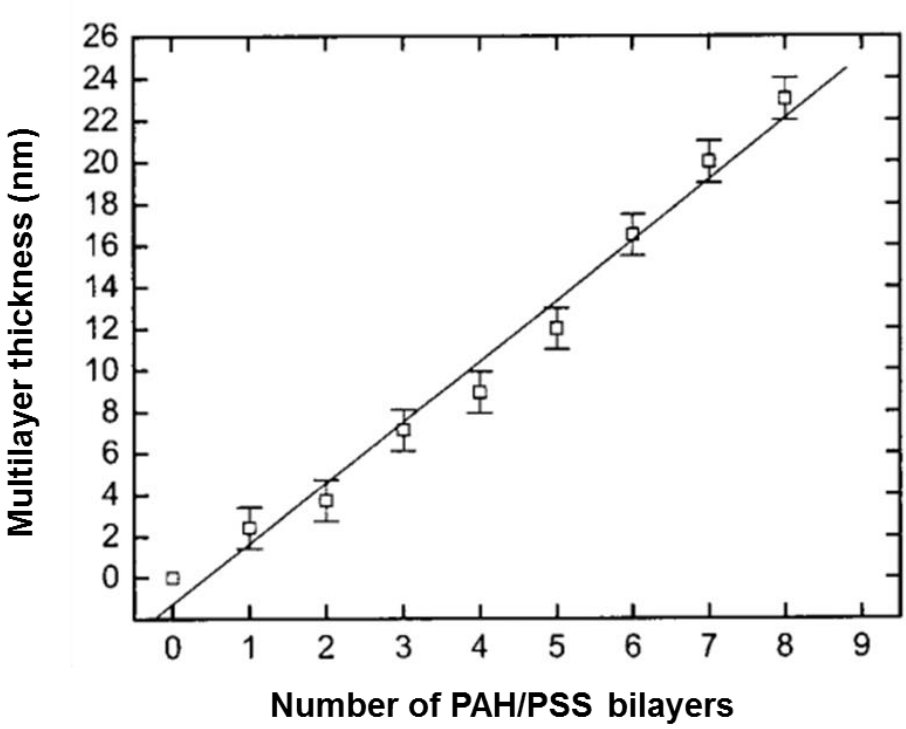

Figure 1.12. Total thickness of PAH/PSS multilayer films adsorbed on latex particles from solutions containing 0.25 M NaCl determined by single-particle light scattering. (reprinted with permission from *Langmuir* 2002, *18*, 2964-2966)[212]

1.5 Dissertation outline

This dissertation examines ion separations that use ion-exchange polymers and polyelectrolyte-modified membranes in NF and ED. Chapter 2 explores the current efficiency and selectivity in ED through PAH/PSS films deposited on commercial cation-exchange membranes. Nafion membranes are attractive for ED because of their durability and high cation over anion selectivity, but these membranes exhibit very low selectivity among cations. Membranes modified with

$(PAH/PSS)_5PAH$ films show K^+/Mg^{2+} selectivities >1000 in ED, and, remarkably, these selectivities reach 20,000 when the K^+ and Mg^{2+} concentration is 0.1 M. However, transmembrane potential measurements indicate that PEMs give rise to a diffusion-limited current, above which water splitting likely occurs.

Chapter 3 further investigates the selectivity and transport properties of PAH/PSS films in ED for recovery and purification of more-valuable cations. Li^+/Co^{2+} and K^+/La^{3+} selectivities remain >1000 in ED, and PEMs prove selective with as a few as 1.5 bilayers. Despite unprecedented selectivities, low limiting currents and poor film stability in strong electric fields remain a challenge. Nevertheless, this work demonstrates that ED is a potentially useful tool for separations, particularly in applications where low concentrations of monovalent ions are undesirable.

Chapter 4 investigates NF membranes modified with PEMs for dye removal from commercial wastewater from clothing manufacturing. In addition, I briefly explore electrically driven ion transport near and through ion-exchange polymers in a microfluidic cross-channel device as a method to de-salt water.

The final chapter summarizes this work and explores future directions such as the to better understand limiting currents in PEMs and the performance of these films in conditions more typical of commercial ED.

REFERENCES

REFERENCES

(1) White, N.; Misovich, M.; Yaroshchuk, A.; Bruening, M. L. *ACS Appl. Mater. Interfaces* **2015**, *7*, 6620-6628.

(2) Zabochnicka-Swiatek, M.; *Best Practice Guide on Metals Removal from Drinking Water by Treatment*; IWA Publishing: London, **2012**.

(3) Tiger, H. L.; Sussman, S. *Ind. Eng. Chem.* **1943**, *35*, 186-192.

(4) Kammerer, J.; Carle, R.; Kammerer, D. R. *J. Agric. Food Chem.* **2011**, *59*, 22-42.

(5) Omana, D. A.; Wang, J. P.; Wu, J. P. *J Chromatogr B* **2010**, *878*, 1771-1776.

(6) Klein, G.; Cherney, S.; Ruddick, E. L.; Vermeule.T. *Desalination* **1968**, *4*, 158-&.

(7) Greenleaf, J. E.; Lin, J. C.; Sengupta, A. K. *Environ. Prog.* **2006**, *25*, 300-311.

(8) Tiravanti, G.; Petruzzelli, D.; Passino, R. *Water Sci. Technol.* **1997**, *36*, 197-207.

(9) Clifford, D.; Liu, X. S. *J Am Water Works Ass* **1993**, *85*, 135-143.

(10) Radchenko, V.; Engle, J. W.; Wilson, J. J.; Maassen, J. R.; Nortier, F. M.; Taylor, W. A.; Birnbaum, E. R.; Hudston, L. A.; John, K. D.; Fassbender, M. E. *J Chromatogr A* **2015**, *1380*, 55-63.

(11) Samuelson, O. *Pharmazie* **1967**, *22*, 279-&.

(12) Jungbauer, A.; Hahn, R. *Method Enzymol* **2009**, *463*, 349-371.

(13) Skoog, D. A.; Holler, F. J.; Crouch, S. R.; *Principles of Instrumental Analysis*, 6th ed.; Thomson Brooks/Cole: Belmont, CA, **2007**.

(14) Fritz, J. S. *Anal. Chem.* **1987**, *59*, 335A-344A.

(15) Walton, H. F. *Anal. Chem.* **1968**, *40*, R51-&.

(16) Haddad, P. R. *Anal. Chem.* **2001**, *73*, 266a-273a.

(17) Cassidy, R. M.; Elchuk, S. *Anal. Chem.* **1982**, *54*, 1558-1563.

(18) Elchuk, S.; Cassidy, R. M. *Anal. Chem.* **1979**, *51*, 1434-1438.

(19) *Rare Earth Elements: A Review of Production, Processing, Recycling, and Associated Environmental Issues*, United States Environmental Protection Agency, **2012**.

(20) Baker, R. W.; *Membrane Technology and Applications*, 2nd ed.; J. Wiley: Chichester ; New York, **2004**.

(21) Schaep, J.; Van der Bruggen, B.; Uytterhoeven, S.; Croux, R.; Vandecasteele, C.; Wilms, D.; Van Houtte, E.; Vanlergberghe, F. *Desalination* **1998**, *119*, 295-301.

(22) Mika, A. M.; Childs, R. F.; Dickson, J. M. *Desalination* **1999**, *121*, 149-158.

(23) Jin, W. Q.; Toutianoush, A.; Tieke, B. *Langmuir* **2003**, *19*, 2550-2553.

(24) Van der Bruggen, B.; Schaep, J.; Maes, W.; Wilms, D.; Vandecasteele, C. *Desalination* **1998**, *117*, 139-147.

(25) Budd, P. M.; Msayib, K. J.; Tattershall, C. E.; Ghanem, B. S.; Reynolds, K. J.; McKeown, N. B.; Fritsch, D. *J. Membr. Sci.* **2005**, *251*, 263-269.

(26) Baker, R. W. *Ind. Eng. Chem. Res.* **2002**, *41*, 1393-1411.

(27) Koros, W. J.; Mahajan, R. *J. Membr. Sci.* **2001**, *181*, 141-141.

(28) Ning, W. J.; Wijeratne, S.; Dong, J. L.; Bruening, M. L. *ACS Appl. Mater. Interfaces* **2015**, *7*, 2575-2584.

(29) Tan, Y. J.; Wang, W. H.; Zheng, Y.; Dong, J. L.; Stefano, G.; Brandizzi, F.; Garavito, R. M.; Reid, G. E.; Bruening, M. L. *Anal. Chem.* **2012**, *84*, 8357-8363.

(30) Greenlee, L. F.; Lawler, D. F.; Freeman, B. D.; Marrot, B.; Moulin, P. *Water Res.* **2009**, *43*, 2317-2348.

(31) Li, D.; Wang, H. T. *J. Mater. Chem.* **2010**, *20*, 4551-4566.

(32) Li, L. X.; Dong, J. H.; Nenoff, T. M.; Lee, R. *J. Membr. Sci.* **2004**, *243*, 401-404.

(33) Sata, T.; Yang, W. K. *J. Membr. Sci.* **2002**, *206*, 31-60.

(34) Vallejo, E.; Pourcelly, G.; Gavach, C.; Mercier, R.; Pineri, M. *J. Membr. Sci.* **1999**, *160*, 127-137.

(35) Cheng, C.; White, N.; Shi, H.; Robson, M.; Bruening, M. L. *Polymer* **2014**, *55*, 1397-1403.

(36) Yip, N. Y.; Tiraferri, A.; Phillip, W. A.; Schiffman, J. D.; Elimelech, M. *Environ. Sci. Technol.* **2010**, *44*, 3812-3818.

(37) Cath, T. Y.; Childress, A. E.; Elimelech, M. *J. Membr. Sci.* **2006**, *281*, 70-87.

(38) Sheng, C. J.; Wijeratne, S.; Cheng, C.; Baker, G. L.; Bruening, M. L. *J. Membr. Sci.* **2014**, *459*, 169-176.

(39) Noble, R. D. *J. Membr. Sci.* **1991**, *60*, 297-306.

(40) Cussler, E. L.; Aris, R.; Bhown, A. *J. Membr. Sci.* **1989**, *43*, 149-164.

(41) Lawson, K. W.; Lloyd, D. R. *J. Membr. Sci.* **1997**, *124*, 1-25.

(42) Alklaibi, A. M.; Lior, N. *Desalination* **2005**, *171*, 111-131.

(43) Loeb, S. *Science* **1975**, *189*, 654-655.

(44) Hartanto, Y.; Yun, S.; Jin, B.; Dai, S. *Water Res.* **2015**, *70*, 385-393.

(45) Coday, B. D.; Xu, P.; Beaudry, E. G.; Herron, J.; Lampi, K.; Hancock, N. T.; Cath, T. Y. *Desalination* **2014**, *333*, 23-35.

(46) Purwasasmita, M.; Kurnia, D.; Mandias, F. C.; Khoiruddin; Wenten, I. G. *Food Bioprod. Process.* **2015**, *94*, 180-186.

(47) Fallanza, M.; Ortiz, A.; Gorri, D.; Ortiz, I. *J. Membr. Sci.* **2013**, *444*, 164-172.

(48) Perry, R. H.; Green, D. W.; *Perry's Chemical Engineers' Handbook*; McGraw Hill: New York, **1997**.

(49) Wijmans, J. G.; Baker, R. W. *J. Membr. Sci.* **1995**, *107*, 1-21.

(50) Benito, Y.; Ruiz, M. L. *Desalination* **2002**, *142*, 229-234.

(51) Lee, K. P.; Arnot, T. C.; Mattia, D. *J. Membr. Sci.* **2011**, *370*, 1-22.

(52) Schaep, J.; Van der Bruggen, B.; Vandecasteele, C.; Wilms, D. *Sep. Purif. Technol.* **1998**, *14*, 155-162.

(53) Bowen, W. R.; Welfoot, J. S. *Chem. Eng. Sci.* **2002**, *57*, 1121-1137.

(54) Yaroshchuk, A.; Martinez-Llado, X.; Llenas, L.; Rovira, M.; de Pablo, J. *J. Membr. Sci.* **2011**, *368*, 192-201.

(55) Csefalvay, E.; Pauer, V.; Mizsey, P. *Desalination* **2009**, *240*, 132-142.

(56) Bowen, W. R.; Mukhtar, H. *J. Membr. Sci.* **1996**, *112*, 263-274.

(57) Schaep, J.; Vandecasteele, C.; Mohammad, A. W.; Bowen, W. R. *Sep. Purif. Technol.* **2001**, *22-3*, 169-179.

(58) Childress, A. E.; Elimelech, M. *Environ. Sci. Technol.* **2000**, *34*, 3710-3716.

(59) Ouyang, L.; Malaisamy, R.; Bruening, M. L. *J. Membr. Sci.* **2008**, *310*, 76-84.

(60) Stanton, B. W.; Harris, J. J.; Miller, M. D.; Bruening, M. L. *Langmuir* **2003**, *19*, 7038-7042.

(61) Malaisamy, R.; Bruening, M. L. *Langmuir* **2005**, *21*, 10587-10592.

(62) Rahimpour, A.; Jahanshahi, M.; Mortazavian, N.; Madaeni, S. S.; Mansourpanah, Y. *Appl. Surf. Sci.* **2010**, *256*, 1657-1663.

(63) Fang, W. X.; Shi, L.; Wang, R. *J. Membr. Sci.* **2013**, *430*, 129-139.

(64) Gonzalez-Munoz, M. J.; Rodriguez, M. A.; Luque, S.; Alvarez, J. R. *Desalination* **2006**, *200*, 742-744.

(65) Murthy, Z. V. R.; Chaudhari, L. B. *Chem. Eng. J. (Lausanne)* **2009**, *150*, 181-187.

(66) Berg, P.; Hagmeyer, G.; Gimbel, R. *Desalination* **1997**, *113*, 205-208.

(67) Koyuncu, I. *Desalination* **2002**, *143*, 243-253.

(68) Wen, X.; Ma, P.; Chaoliang, Z.; He, Q.; Deng, X. *Sep. Purif. Technol.* **2006**, *49*, 230-236.

(69) Gopalakrishnan, A.; Mathew, M. L.; Chandran, J.; Winglee, J.; Badireddy, A. R.; Wiesner, M.; Aravindakumar, C. T.; Aravind, U. K. *ACS Appl. Mater. Interfaces* **2015**, *7*, 3699-3707.

(70) Manegold, E.; Kalauch, K. *Kolloid Z* **1939**, *86*, 93-101.

(71) Meyer, K. H.; Straus, W. *Helv. Chim. Acta* **1940**, *23*, 795-800.

(72) Kressman, T. R. E. *Nature* **1950**, *165*, 568-568.

(73) Juda, W.; Mcrae, W. A. *J. Am. Chem. Soc.* **1950**, *72*, 1043-1044.

(74) Flett, D. S.; *Ion Exchange Membranes*; Ellis Horwood Ltd: Chichester, **1983**.

(75) Katz, W. E. *Desalination* **1979**, *28*, 31-40.

(76) Allison, R. P. *Desalination* **1995**, *103*, 11-18.

(77) Banasiak, L. J.; Kruttschnitt, T. W.; Schafer, A. I. *Desalination* **2007**, *205*, 38-46.

(78) Choi, P.; Jalani, N. H.; Datta, R. *J. Electrochem. Soc.* **2005**, *152*, E84-E89.

(79) Nandan, D.; Mohan, H.; Iyer, R. M. *J. Membr. Sci.* **1992**, *71*, 69-80.

(80) Kreuer, K. D. *J. Membr. Sci.* **2001**, *185*, 29-39.

(81) Molau, G. E. *J. Membr. Sci.* **1981**, *8*, 309-330.

(82) Nagarale, R. K.; Gohil, G. S.; Shahi, V. K. *Adv. Colloid Interface Sci.* **2006**, *119*, 97-130.

(83) Choi, J. H.; Kim, S. H.; Moon, S. H. *J. Colloid Interface Sci.* **2001**, *241*, 120-126.

(84) Vyas, P. V.; Shah, B. G.; Trivedi, G. S.; Ray, P.; Adhikary, S. K.; Rangarajan, R. *J. Membr. Sci.* **2001**, *187*, 39-46.

(85) Volodina, E.; Pismenskaya, N.; Nikonenko, V.; Larchet, C.; Pourcelly, G. *J. Colloid Interface Sci.* **2005**, *285*, 247-258.

(86) Fang, J.; Shen, P. K. *J. Membr. Sci.* **2006**, *285*, 317-322.

(87) Yee, R. S. L.; Rozendal, R. A.; Zhang, K.; Ladewig, B. P. *Chem. Eng. Res. Des.* **2012**, *90*, 950-959.

(88) Mikhailenko, S. U. D.; Wang, K. P.; Kaliaguine, S.; Xing, P. X.; Robertson, G. P.; Guiver, M. D. *J. Membr. Sci.* **2004**, *233*, 93-99.

(89) Merle, G.; Wessling, M.; Nijmeijer, K. *J. Membr. Sci.* **2011**, *377*, 1-35.

(90) Gu, S.; Cai, R.; Luo, T.; Chen, Z. W.; Sun, M. W.; Liu, Y.; He, G. H.; Yan, Y. S. *Angew. Chem., Int. Ed. Engl.* **2009**, *48*, 6499-6502.

(91) Bauer, B.; Strathmann, H.; Effenberger, F. *Desalination* **1990**, *79*, 125-144.

(92) Hsu, W. Y.; Gierke, T. D. *J. Membr. Sci.* **1983**, *13*, 307-326.

(93) Mauritz, K. A.; Moore, R. B. *Chem. Rev. (Washington, DC, U. S.)* **2004**, *104*, 4535-4585.

(94) Park, C. H.; Lee, C. H.; Guiver, M. D.; Lee, Y. M. *Prog. Polym. Sci.* **2011**, *36*, 1443-1498.

(95) Rikukawa, M.; Sanui, K. *Prog. Polym. Sci.* **2000**, *25*, 1463-1502.

(96) Peighambardoust, S. J.; Rowshanzamir, S.; Amjadi, M. *Int. J. Hydrogen Energy* **2010**, *35*, 9349-9384.

(97) Cooke, B. A. *Electrochim. Acta* **1961**, *3*, 307-317.

(98) Forgacs, C.; Spiegler, K. S.; Sinkovic, J.; Ishibash.N; Leibovit.J. *Desalination* **1972**, *10*, 181-&.

(99) Tanaka, Y. *J. Membr. Sci.* **2003**, *216*, 149-164.

(100) Tanaka, Y. *J. Membr. Sci.* **1991**, *57*, 217-235.

(101) Dlugolecki, P.; Anet, B.; Metz, S. J.; Nijmeijer, K.; Wessling, M. *J. Membr. Sci.* **2010**, *346*, 163-171.

(102) Tanaka, Y. *J. Membr. Sci.* **2003**, *215*, 265-279.

(103) Verbrugge, M. W.; Hill, R. F. *J. Electrochem. Soc.* **1990**, *137*, 886-893.

(104) Guzmangarcia, A. G.; Pintauro, P. N.; Verbrugge, M. W.; Hill, R. F. *AIChE J.* **1990**, *36*, 1061-1074.

(105) Kim, Y.; Walker, W. S.; Lawler, D. F. *Desalination* **2011**, *274*, 54-63.

(106) Koter, S.; Piotrowski, P.; Kerres, J. *J. Membr. Sci.* **1999**, *153*, 83-90.

(107) Krol, J. J.; Wessling, M.; Strathmann, H. *J. Membr. Sci.* **1999**, *162*, 145-154.

(108) Rubinstein, I.; Zaltzman, B. *Phys. Rev. E* **2000**, *62*, 2238-2251.

(109) Shaffer, L. H.; Mintz, M. S. In *Principles of Desalination*; Spiegler, K. S., Ed.; Academic Press: New York, 1966, p 200-289.

(110) Strathmann, H. In *Membrane Separation Systems*; Baker, R. W., Cussler, E. L., Eykamp, W. J., Koros, W. J., Riley, R. L., Strathmann, H., Eds.; Noyes Data Corp.: Park Ridge, NJ, 1991, p 396-448.

(111) Seto, T.; Ehara, L.; Komori, R.; Yamaguchi, A.; Miwa, T. *Desalination* **1978**, *25*, 1-7.

(112) Strathmann, H. *Desalination* **2010**, *264*, 268-288.

(113) Amor, Z.; Malki, S.; Taky, M.; Bariou, B.; Mameri, N.; Elmidaoui, A. *Desalination* **1998**, *120*, 263-271.

(114) Amor, Z.; Bariou, B.; Mameri, N.; Taky, M.; Nicolas, S.; Elmidaoui, A. *Desalination* **2001**, *133*, 215-223.

(115) Sata, T.; Mizutani, Y. *J. Polym. Sci., Part A: Polym. Chem.* **1979**, *17*, 1199-1213.

(116) Sata, T.; Yamaguchi, T.; Matsusaki, K. *J. Membr. Sci.* **1995**, *100*, 229-238.

(117) Simons, R. *J. Membr. Sci.* **1993**, *78*, 13-23.

(118) Xu, T. W. *Resour. Conserv. Recy.* **2002**, *37*, 1-22.

(119) Mazrou, S.; Kerdjoudj, H.; Cherif, A. T.; Molenat, J. *J. Appl. Electrochem.* **1997**, *27*, 558-567.

(120) Mazrou, S.; Kerdjoudj, H.; Cherif, A. T.; Elmidaoui, A.; Molenat, J. *New J. Chem.* **1998**, *22*, 355-359.

(121) Gineste, J. L.; Pourcelly, G.; Lorrain, Y.; Persin, F.; Gavach, C. *J. Membr. Sci.* **1996**, *112*, 199-208.

(122) Xu, T. W.; Yang, W. H. *Chem. Eng. Process.* **2002**, *41*, 519-524.

(123) Ferrer, J. S. J.; Laborie, S.; Durand, G.; Rakib, M. *J. Membr. Sci.* **2006**, *280*, 509-516.

(124) Trivedi, G. S.; Shah, B. G.; Adhikary, S. K.; Indusekhar, V. K.; Rangarajan, R. *React. Funct. Polym.* **1997**, *32*, 209-215.

(125) Koter, S.; Warszawski, A. *Pol. J. Environ. Stud.* **2000**, *9*, 45-56.

(126) Li, H.; Mustacchi, R.; Knowles, C. J.; Skibar, W.; Sunderland, G.; Dalrymple, I.; Jackman, S. A. *Tetrahedron* **2004**, *60*, 655-661.

(127) Kim, Y. H.; Moon, S. H. *J. Chem. Technol. Biotechnol.* **2001**, *76*, 169-178.

(128) Lee, E. G.; Moon, S. H.; Chang, Y. K.; Yoo, I. K.; Chang, H. N. *J. Membr. Sci.* **1998**, *145*, 53-66.

(129) Madzingaidzo, L.; Danner, H.; Braun, R. *J. Biotechnol.* **2002**, *96*, 223-239.

(130) Akerberg, C.; Zacchi, G. *Bioresour. Technol.* **2000**, *75*, 119-126.

(131) Habova, V.; Melzoch, K.; Rychtera, M.; Sekavova, B. *Desalination* **2004**, *162*, 361-372.

(132) Alvarez, F.; Alvarez, R.; Coca, J.; Sandeaux, J.; Sandeaux, R.; Gavach, C. *J. Membr. Sci.* **1997**, *123*, 61-69.

(133) Novalic, S.; Kongbangkerd, T.; Kulbe, K. D. *J. Membr. Sci.* **2000**, *166*, 99-104.

(134) Yu, L. X.; Lin, A. G.; Zhang, L. P.; Chen, C. X.; Jiang, W. J. *Chem. Eng. J. (Lausanne)* **2000**, *78*, 153-157.

(135) Cauwenberg, V.; Peels, J.; Resbeut, S.; Pourcelly, G. *Sep. Purif. Technol.* **2001**, *22-3*, 115-121.

(136) Eliseeva, T. V.; Krisilova, E. V.; Shaposhnik, V. A.; Bukhovets, A. E. *Desalin. Water Treat.* **2010**, *14*, 196-200.

(137) Macheix, J. J.; Fleuriet, A.; Billot, J.; *Fruit Phenolics*; CRC Press: Boca Raton, FL, **1990**.

(138) Zemel, G. P.; Sims, C. A.; Marshall, M. R.; Balaban, M. *J. Food Sci.* **1990**, *55*, 562-563.

(139) Tronc, J. S.; Lamarche, F.; Makhlouf, J. *J. Agric. Food Chem.* **1998**, *46*, 829-833.

(140) Tronc, J. S.; Lamarche, F.; Makhlouf, J. *J. Food Sci.* **1997**, *62*, 75-&.

(141) Quoc, A. L.; Lamarche, F.; Makhlouf, J. *J. Agric. Food Chem.* **2000**, *48*, 2160-2166.

(142) Quoc, A. L.; Mondor, M.; Lamarche, F.; Ippersiel, D.; Bazinet, L.; Makhlouf, J. *Food Res. Int.* **2006**, *39*, 755-760.

(143) Calle, E. V.; Ruales, J.; Dornier, M.; Sandeaux, J.; Sandeaux, R.; Pourcelly, G. *Desalination* **2002**, *149*, 357-361.

(144) Vera, E.; Sandeaux, J.; Persin, F.; Pourcelly, G.; Dornier, M.; Ruales, J. *J. Food Eng.* **2007**, *78*, 1427-1438.

(145) Vera, E.; Sandeaux, J.; Persin, F.; Pourcelly, G.; Dornier, M.; Piombo, G.; Ruales, J. *J. Food Eng.* **2007**, *78*, 1439-1445.

(146) Rozoy, E.; Boudesocque, L.; Bazinet, L. *J. Agric. Food Chem.* **2015**, *63*, 642-651.

(147) Bazinet, L.; Brianceau, S.; Dube, P.; Desjardins, Y. *Sep. Purif. Technol.* **2012**, *87*, 31-39.

(148) Greiter, M.; Novalin, S.; Wendland, M.; Kulbe, K. D.; Fischer, J. *J. Membr. Sci.* **2002**, *210*, 91-102.

(149) *Electromat Electrodialysis*; GE Water & Process Technologies; 2010

(150) Bazinet, L.; Lamarche, F.; Ippersiel, D. *Trends Food Sci. Technol.* **1998**, *9*, 107-113.

(151) Kilara, A.; Sharkasi, T. Y. *Crit. Rev. Food Sci.* **1986**, *23*, 323-395.

(152) Nash, A. M.; Wolf, W. J. *Cereal Chem.* **1967**, *44*, 183-&.

(153) Bazinet, L.; Lamarche, F.; Labrecque, R.; Ippersiel, D. *J. Agric. Food Chem.* **1997**, *45*, 2419-2425.

(154) Bazinet, L.; Lamarche, F.; Labrecque, R.; Toupin, R.; Boulet, M.; Ippersiel, D. *Food Technol-Chicago* **1997**, *51*, 52-&.

(155) Krogman, K. C.; Druffel, T.; Sunkara, M. K. *Nanotechnology* **2005**, *16*, S338-S343.

(156) Nielsen, K. H.; Orzol, D. K.; Koynov, S.; Carney, S.; Hultstein, E.; Wondraczek, L. *Sol. Energy Mater. Sol. Cells* **2014**, *128*, 283-288.

(157) Kubota, S.; Kanomata, K.; Suzuki, T.; Ahmmad, B.; Hirose, F. *J. Coat. Technol. Res.* **2015**, *12*, 37-47.

(158) Amiri, M.; Amali, E.; Nematollahzadeh, A. *Sensor Actuat. B-Chem.* **2015**, *216*, 551-557.

(159) Ravalli, A.; Marrazza, G.; Ciui, B.; Cristea, C.; Sandulescu, R.; Di Camillo, D.; Lozzi, L. *Lect. Notes Electr. En.* **2015**, *319*, 123-127.

(160) Huynh, T. P.; Sharma, P. S.; Sosnowska, M.; D'Souza, F.; Kutner, W. *Prog. Polym. Sci.* **2015**, *47*, 1-25.

(161) Rahman, M. M.; Li, X. B.; Kim, J.; Lim, B. O.; Ahammad, A. J. S.; Lee, J. J. *Sensor Actuat. B-Chem.* **2014**, *202*, 536-542.

(162) Yang, W. J.; Neoh, K. G.; Kang, E. T.; Teo, S. L. M.; Rittschof, D. *Prog. Polym. Sci.* **2014**, *39*, 1017-1042.

(163) Zhao, C.; Li, L. Y.; Guo, M. M.; Zheng, J. *Chem. Pap.* **2012**, *66*, 323-339.

(164) Mizrahi, B.; Khoo, X.; Chiang, H. H.; Sher, K. J.; Feldman, R. G.; Lee, J. J.; Irusta, S.; Kohane, D. S. *Langmuir* **2013**, *29*, 10087-10094.

(165) Forrest, S. R. *Nature* **2004**, *428*, 911-918.

(166) Katz, H. E.; Huang, J. *Annu. Rev. Mater. Res.* **2009**, *39*, 71-92.

(167) Garnier, F.; Hajlaoui, R.; Yassar, A.; Srivastava, P. *Science* **1994**, *265*, 1684-1686.

(168) Racicot, R.; Clark, R. L.; Liu, H. B.; Yang, S. C.; Alias, M. N.; Brown, R. *P. Soc. Photo-Opt. Ins.* **1995**, *2528*, 251-258.

(169) Chauveau, E.; Marestin, C.; Mercier, R.; Brunaux, A.; Martin, V.; Nogueira, R. P.; Percheron, A.; Roche, V.; Waton, H. *J. Appl. Polym. Sci.* **2015**, *132*.

(170) Balgude, D.; Sabnis, A. *J. Sol-Gel Sci. Technol.* **2012**, *64*, 124-134.

(171) Zhang, F.; Chen, S. G.; Dong, L. H.; Lei, Y. H.; Liu, T.; Yin, Y. S. *Appl. Surf. Sci.* **2011**, *257*, 2587-2591.

(172) Hall, D. B.; Underhill, P.; Torkelson, J. M. *Polym. Eng. Sci.* **1998**, *38*, 2039-2045.

(173) Lawrence, C. J. *Phys. Fluids* **1988**, *31*, 2786-2795.

(174) Grosso, D. *J. Mater. Chem.* **2011**, *21*, 17033-17038.

(175) Helmersson, U.; Lattemann, M.; Bohlmark, J.; Ehiasarian, A. P.; Gudmundsson, J. T. *Thin Solid Films* **2006**, *513*, 1-24.

(176) Limb, S. J.; Labelle, C. B.; Gleason, K. K.; Edell, D. J.; Gleason, E. F. *Appl. Phys. Lett.* **1996**, *68*, 2810-2812.

(177) Jeon, N. L.; Choi, I. S.; Whitesides, G. M.; Kim, N. Y.; Laibinis, P. E.; Harada, Y.; Finnie, K. R.; Girolami, G. S.; Nuzzo, R. G. *Appl. Phys. Lett.* **1999**, *75*, 4201-4203.

(178) Edmondson, S.; Osborne, V. L.; Huck, W. T. S. *Chem. Soc. Rev.* **2004**, *33*, 14-22.

(179) Decher, G.; Hong, J. D.; Schmitt, J. *Thin Solid Films* **1992**, *210*, 831-835.

(180) Decher, G.; Hong, J. D. *Ber Bunsen Phys. Chem.* **1991**, *95*, 1430-1434.

(181) Decher, G.; Hong, J. D. *Makromol. Chem-M Symp.* **1991**, *46*, 321-327.

(182) Bucur, C. B.; Sui, Z.; Schlenoff, J. B. *J. Am. Chem. Soc.* **2006**, *128*, 13690-13691.

(183) Decher, G. *Science* **1997**, *277*, 1232-1237.

(184) Fu, Y.; Bai, S. L.; Cui, S. X.; Qiu, D. L.; Wang, Z. Q.; Zhang, X. *Macromolecules* **2002**, *35*, 9451-9458.

(185) Sukhishvili, S. A.; Granick, S. *Macromolecules* **2002**, *35*, 301-310.

(186) Richert, L.; Boulmedais, F.; Lavalle, P.; Mutterer, J.; Ferreux, E.; Decher, G.; Schaaf, P.; Voegel, J. C.; Picart, C. *Biomacromolecules* **2004**, *5*, 284-294.

(187) Sukhorukov, G. B.; Mohwald, H.; Decher, G.; Lvov, Y. M. *Thin Solid Films* **1996**, *284*, 220-223.

(188) Lvov, Y.; Decher, G.; Sukhorukov, G. *Macromolecules* **1993**, *26*, 5396-5399.

(189) Caruso, F.; Niikura, K.; Furlong, D. N.; Okahata, Y. *Langmuir* **1997**, *13*, 3427-3433.

(190) Cho, J.; Quinn, J. F.; Caruso, F. *J. Am. Chem. Soc.* **2004**, *126*, 2270-2271.

(191) Caruso, F.; Lichtenfeld, H.; Giersig, M.; Mohwald, H. *J. Am. Chem. Soc.* **1998**, *120*, 8523-8524.

(192) Lvov, Y.; Haas, H.; Decher, G.; Mohwald, H.; Mikhailov, A.; Mtchedlishvily, B.; Morgunova, E.; Vainshtein, B. *Langmuir* **1994**, *10*, 4232-4236.

(193) Chen, W.; McCarthy, T. J. *Macromolecules* **1997**, *30*, 78-86.

(194) Cheng, C.; Yaroshchuk, A.; Bruening, M. L. *Langmuir* **2013**, *29*, 1885-1892.

(195) Tedeschi, C.; Mohwald, H.; Kirstein, S. *J. Am. Chem. Soc.* **2001**, *123*, 954-960.

(196) Dotzauer, D. M.; Dai, J. H.; Sun, L.; Bruening, M. L. *Nano Lett.* **2006**, *6*, 2268-2272.

(197) Ai, H.; Jones, S. A.; Lvov, Y. M. *Cell Biochem. Biophys.* **2003**, *39*, 23-43.

(198) Choi, I.; Suntivich, R.; Plamper, F. A.; Synatschke, C. V.; Muller, A. H. E.; Tsukruk, V. V. *J. Am. Chem. Soc.* **2011**, *133*, 9592-9606.

(199) Ma, Y. D.; Dong, J. L.; Bhattacharjee, S.; Wijeratne, S.; Bruening, M. L.; Baker, G. L. *Langmuir* **2013**, *29*, 2946-2954.

(200) Tan, H. L.; McMurdo, M. J.; Pan, G. Q.; Van Patten, P. G. *Langmuir* **2003**, *19*, 9311-9314.

(201) Salomaki, M.; Vinokurov, I. A.; Kankare, J. *Langmuir* **2005**, *21*, 11232-11240.

(202) Schoeler, B.; Poptoschev, E.; Caruso, F. *Macromolecules* **2003**, *36*, 5258-5264.

(203) Dubas, S. T.; Schlenoff, J. B. *Macromolecules* **1999**, *32*, 8153-8160.

(204) Guzman, E.; Ritacco, H.; Rubio, J. E. F.; Rubio, R. G.; Ortega, F. *Soft Matter* **2009**, *5*, 2130-2142.

(205) Salomaki, M.; Tervasmaki, P.; Areva, S.; Kankare, J. *Langmuir* **2004**, *20*, 3679-3683.

(206) Dressick, W. J.; Wahl, K. J.; Bassim, N. D.; Stroud, R. M.; Petrovykh, D. Y. *Langmuir* **2012**, *28*, 15831-15843.

(207) Garg, A.; Heflin, J. R.; Gibson, H. W.; Davis, R. M. *Langmuir* **2008**, *24*, 10887-10894.

(208) Guzman, E.; Ritacco, H.; Ortega, F.; Svitova, T.; Radke, C. J.; Rubio, R. G. *J. Phys. Chem. B* **2009**, *113*, 7128-7137.

(209) Wang, L. Y.; Fu, Y.; Wang, Z. Q.; Fan, Y. G.; Zhang, X. *Langmuir* **1999**, *15*, 1360-1363.

(210) Voigt, U.; Jaeger, W.; Findenegg, G. H.; Klitzing, R. V. *J. Phys. Chem. B* **2003**, *107*, 5273-5280.

(211) Khopade, A. J.; Caruso, F. *Langmuir* **2002**, *18*, 7669-7676.

(212) Schwarz, B.; Schonhoff, M. *Langmuir* **2002**, *18*, 2964-2966.

CHAPTER 2

Coating of Nafion Membranes with Polyelectrolyte Multilayers to Achieve High Monovalent/Divalent Cation Electrodialysis Selectivities

Portions of this chapter reprinted from N White, M Misovich, A Yaroshchuk, and ML Bruening. *ACS Appl. Mater. Interfaces* **2015**, *7*, 6620-6628.

2.1 Introduction

Electrodialysis (ED) is a membrane-based separation technique for applications such as preconcentrating brines,[1] recovering organic acids from waste-salt solutions,[2] organic acid production,[3] treating wastewater effluent,[4] demineralizing milk by-products[5] and desalting brackish water.[6,7] In commercially viable configurations, alternating anion- and cation-exchange membranes in flow-cells create parallel diluate and concentrate streams to enable high throughput.[8] Under an applied current or potential, cations leave the diluate compartment through the cation-exchange membrane, whereas anions leave in the opposite direction through the anion-exchange membrane. Thus, ED effectively removes ions from feed streams, but typical ion-exchange membranes exhibit low selectivities among ions. Such selectivities are important when employing ion-exchange membranes in some ED applications, e.g. removal of SO_4^{2-} from sea salt, or other functions such as prevention of vanadium crossover in redox flow batteries.[9-12]

Although variation of current density and concentration polarization may provide some control over ion-transport selectivity,[13] the development of ED for

separating ions requires ion-exchange membranes with high selectivities. Sata and coworkers showed that polycation or polyanion coatings on ion-exchange membranes enhance selectivity among cations or anions, respectively.[14-16] Deposition of protonated polyethylenimine (PEI) on cation-exchange membranes increases monovalent/divalent cation selectivity, and control over the hydrophobicity and cross-linking at the membrane surface leads to Na^+/Ca^{2+} selectivities up to 7.[14] Additionally, increasing the hydrophilicity of anion-exchange membranes with adsorbed ethylene glycols increases SO_4^{2-}/Cl^- selectivities from <0.1 to 0.8.[17,18] Rakib and co-workers observed a Na^+/Cr^{3+} selectivity of 10-20 using an electrodeposited PEI film on a Nafion cation-exchange membrane.[19] Nevertheless, these selectivities are relatively modest. In this study, we examine whether adsorption of polyelectrolyte multilayers on ion-exchange membranes can yield even higher selectivities.

With the development of alternating adsorption of polycations and polyanions to form ultrathin coatings,[20] several research groups began investigating whether polyelectrolyte multilayers (PEMs) can serve as ultrathin membrane skins that show high selectivity among cations or anions.[21-23] In many cases, monovalent ions move through these membranes more readily than multivalent ones, presumably because of enhanced electrostatic and size-based exclusion of highly hydrated, multiply charged ions. Although Michaels and coworkers formed membranes from polyelectrolyte complexes nearly 50 years ago,[24] layer-by-layer adsorption of polyelectrolytes offers much more control over

the film structure to increase selectivity. For example, in diffusion dialysis Krassemann and Tieke showed Na^+/Mg^{2+} selectivities as high as 110 with 60-bilayer poly(styrene sulfonate) (PSS)/protonated poly(allylamine) (PAH) films on poly(acrylonitrile)/poly(ethylene terephthalate) supports.[25] Other work showed K^+/Mg^{2+} diffusion dialysis selectivities >300 with 4-bilayer films on porous alumina substrates.[26] ED through such membranes recently gave similarly high selectivities,[27] but the substrates were not ion-exchange membranes, which will limit their utility in ED applications that require transport of only cations or only anions through a membrane.

A few recent studies employed layer-by-layer polyelectrolyte deposition to enhance the selectivity of ion-exchange membranes. Abdu and co-workers formed polyethyleneimine/PSS films on a Neosepta CMX ion-exchange membrane to generate a permselective layer while minimizing membrane resistance.[28] The Na^+/Ca^{2+} selectivity varied with the charge and number of polyelectrolyte multilayers but was at most 1.4.[28] Mulyati *et al.* found that anion-exchange membranes modified with PSS and poly(allylamine hydrochloride) (PAH) exhibit Cl^-/SO_4^{2-} selectivities of ~2.5. These membranes also showed enhanced fouling resistance but required at least 15 bilayers for these effects.[29]

This research utilizes $(PAH/PSS)_5PAH$ films as selective barriers on commercial cation-exchange membranes (Nafion 115) to separate monovalent and multivalent cations in ED. Adsorption of these films yields K^+/Mg^{2+} ED selectivities that exceed 1000. Furthermore, we investigate the effect of source-

phase electrolyte concentration and current density on selectivity and current efficiency because concentration polarization strongly affects ED.[30] Current-potential curves and pH measurements provide additional insight into limiting currents and water splitting in this system. Membranes coated with $(PAH/PSS)_5PAH$ films may prove useful for purifying salts containing divalent ions because these membranes remain selective when the divalent or monovalent ion is in excess.

2.2 Experimental section

2.2.1 Materials

Poly(sodium 4-styrenesulfonate) (M_w = 70,000 Da) and poly(allylamine hydrochloride) (M_w = 15,000 Da) were purchased from Sigma-Aldrich. Inorganic salts were obtained from Columbus Chemical and used as received. Nafion N115 membranes were acquired from Ion Power (New Castle, DE, thickness 127 μm), and AMI-7001 anion-exchange membranes were a gift from Membranes International (Ringwood, NJ). Deionized water (Milli-Q Reference Ultrapure Water Purification System, 18 MΩ·cm) was used to prepare aqueous solutions. For membrane oxidation, 30% H_2O_2 (Fisher) and 98% H_2SO_4 (EMD Chemical) were separately diluted to 3% H_2O_2 and 1.0 M H_2SO_4, respectively. The pH of polyelectrolyte solutions was adjusted with 0.1 M HCl or NaOH.

2.2.2 Film Formation and Characterization

Nafion membrane discs (25 mm diameter) were punched from a membrane sheet using a mechanical die. Following a literature procedure for Nafion oxidation, membranes were rinsed in deionized water prior to 30-min sequential immersions in the following solutions which were heated to 100°C: 3% H_2O_2, deionized water, 1.0 M H_2SO_4, and deionized water.[12,31] Rinsing with room-temperature deionized water from a wash bottle also occurred for 20 sec after the immersions in H_2O_2 and H_2SO_4. This oxidation process likely exposes sulfonate groups at the Nafion surface to enhance negative surface charge. All ED experiments and I-V curves with bare Nafion employed oxidized membranes.

Layer-by-layer polyelectrolyte adsorption was performed by immersing oxidized membranes in alternating polycation (PAH in 1.0 M NaCl) and polyanion (PSS in 0.5 M NaCl) solutions for 5 min each. Polyelectrolyte solutions (pH = ~2.3) contained 0.02 M of the polymer repeating unit. Adsorption began with the polycation, which should adhere to the Nafion via electrostatic interactions. Membranes were rinsed with deionized water from a wash bottle for ~30 sec after each deposition step to remove weakly adsorbed polyelectrolytes, and films contained a total of 5.5 bilayers ($(PAH/PSS)_5PAH$). In a few cases noted in the text, adsorption occurred using a holder to limit film formation to only one side of the membrane. X-ray photoelectron spectroscopy (XPS) using a Perkin Elmer Phi 5600 ESCA instrument with a magnesium Kα X-ray source at a 45° take off angle was employed for film characterization.

2.2.3 Electrodialysis

Initially, coated Nafion membranes were inserted between two homemade 100-mL glass cells clamped together with an o-ring (3.1 cm^2 of exposed membrane area), and platinum wire electrodes were inserted into each compartment.[27] The anode and cathode were in the source and receiving phases, respectively, so that cations migrated to the receiving phase and anions toward the source phase. Using a CH Instruments model 604 potentiostat, a potential was applied across a resistor (499 Ω) to generate a constant 4.0 mA current (1.27 mA cm^{-2}). In some experiments, the voltage was increased or decreased using the same resistor to produce higher or lower current densities. (The resistor was connected between the potentiostat terminals for the working and the reference electrodes, and the reference electrode terminal was also connected to the Pt anode of the electrodialysis cell. The cathode was connected to the counter electrode terminal of the potentiostat).[27] Both source and receiving phases were stirred vigorously to limit concentration polarization. Sample aliquots were withdrawn periodically over 90 min from both source and receiving cells, but generally only the receiving phase was analyzed, although the source phase was occasionally analyzed to verify concentration. Cation analysis was performed with an axial Varian 710-ES Inductively Coupled Plasma Optical Emission Spectrophotometer (ICP-OES) equipped with a Varian SPS 3 autosampler. Individual cation standards were prepared from nitrate (K^+ and Mg^{2+}) or carbonate (Ca^{2+}) salts, and serial dilutions were performed to generate a calibration curve.

Concentrations in the standard solutions were verified using Specpure® ICP-OES standards obtained from Alfa Aesar. For each condition, ED was performed with three membranes, and uncertainties in fluxes, selectivities, and transference numbers represent standard deviations of values for the different membranes. Diffusion dialysis was performed with the same cell without an applied current.

ED data were plotted as total moles of cation passed through the membrane as a function of time, and fluxes were calculated by dividing the slope in these plots by the membrane area. To allow for ion exchange between the membrane and the solution, we determined the slopes only from data acquired after 30 min of dialysis. The reported K^+/Mg^{2+} selectivities in these experiments are simply the ratio of K^+ and Mg^{2+} fluxes when the source phase contains equal concentrations of the two ions. Finally transference numbers, t_i, were calculated using equation 2.1, where J_i is the flux of ion i in moles cm^{-2} s^{-1}, z_i is the ion charge, F is Faraday's constant, and I is the current density in A cm^{-2}.

$$t_i = \frac{J_i z_i F}{I} \tag{2.1}$$

In a few cases, current-voltage curves were obtained using the four-point method in a homemade two-compartment cell similar to the electrodialysis cell described above (Figure 2.1). Reference electrodes (Ag/AgCl, 3 M KCl, CH Instruments model 111) were brought to within ~4 mm of the membrane surface using homemade Haber-Luggin capillaries incorporating borosilicate glass frits (Ace glass, size E) to minimize solution leakage. The capillaries were affixed to ground-glass joints to ensure reproducible placement of the reference electrodes

near the center of the membrane, and platinum wire electrodes were used for the anode and cathode. Current-voltage curves were obtained with solutions containing 0.01 M KNO_3 and 0.1 M $Mg(NO_3)_2$ on both sides of the membrane, and the current was increased stepwise at >30-second intervals to achieve steady state. The excess $Mg(NO_3)_2$ reduces solution resistance without greatly altering K^+ transport through the PEM. Over the course of these measurements, the source-phase pH decreases from 5.5 to 2.3, and the receiving-phase pH increases from 5.5 to 5.8.

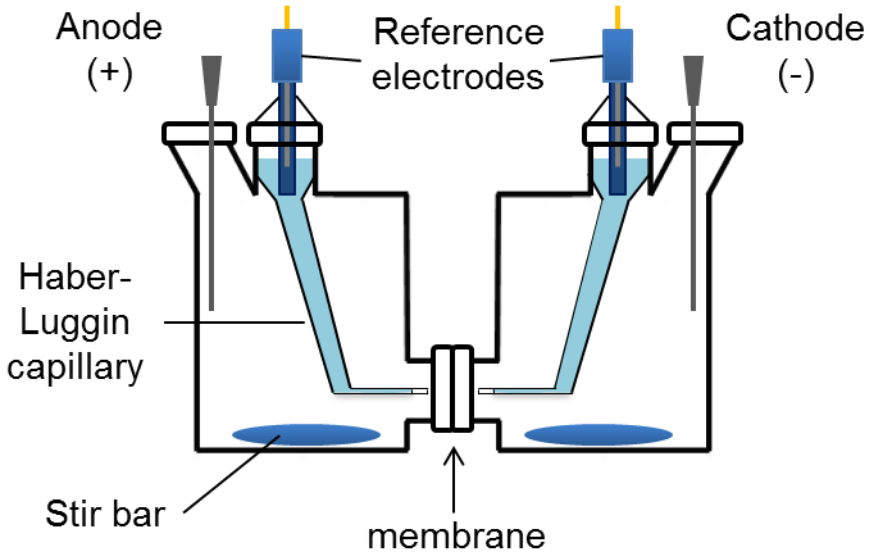

Figure 2.1. Home-built cell for measuring transmembrane potentials in ED. The Haber-Luggin capillaries reduce the impact of bulk-solution resistance and facilitate measurement of electrochemical behavior near the membrane surface.

Some experiments aimed to decrease proton transport employed the homemade 3-compartment ED cell illustrated in Figure 2.2. Following the manufacturer's protocol, an anion exchange membrane (AEM) was preconditioned in a 5% NaCl solution for 24 hours at 40 °C. The AEM was rinsed with deionized water to remove excess salt and clamped between the left and center cells with an o-ring (3.1 cm^2 of exposed area). The modified cation-exchange membrane (CEM) was inserted between the center and right cells with an identical o-ring. Platinum wire electrodes were inserted in the left and right compartments, and all three compartments were stirred vigorously to minimize concentration polarization. A potential was applied between the electrodes using a DC power supply (Protek, 3006B). Voltage was adjusted periodically throughout the experiment to maintain ~4 mA of current (1.27 mA cm^{-2}), as measured in series using a multimeter (TEK DMM249). The resistance between the electrodes typically increased throughout the ED as expected. Additional studies on the extent of water splitting used a similar 4-compartment electrodialysis cell to isolate the anode and cathode from the source and receiving phases, respectively. This setup is similar to that in Figure 2.2 but contains an addition cell for the cathode and a bare Nafion membrane that isolates the cathode compartment. Electrodialysis was performed with 0.01 M KNO_3 in the anode and source cells and 0.01 M $NaNO_3$ in the receiving and cathode cells. The current density was first maintained at under-limiting (0.32 mA cm^{-2}) levels for 160 minutes before immediately switching to overlimiting (2.54 mA cm^{-2}) levels for 20 minutes to ensure equal charge passage

at each current level. The pH in the source and receiving phases was monitored periodically.

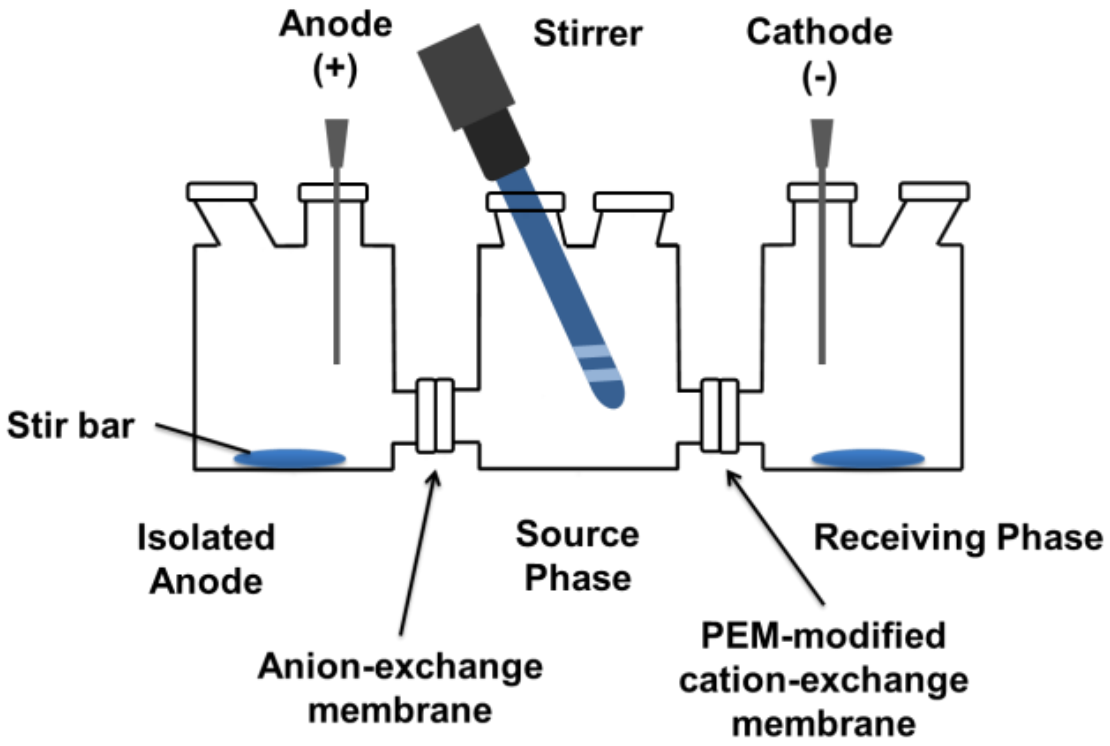

Figure 2.2. Home-built ED apparatus comprised of three 100-mL glass cells filled with salt or acid solutions and connected by 2.5-cm #15 flat joints with embedded tracks for o-rings to eliminate leaking. A multimeter was used to measure current that depended on the potential applied between the electrodes.

2.3 Results and Discussion

Our previous work showed monovalent/divalent-ion selectivities >300 in ED through porous alumina membranes coated with $(PSS/PAH)_5$ films.[27] However, such membranes allow passage of both anions and cations, which is undesirable in some ED applications. Thus, this section initially examines layer-by-layer methods to coat ion-exchange membranes with polyelectrolyte films. Later subsections investigate whether the high selectivities of PSS/PAH multilayer films deposited on alumina membranes translate to films on commercial cation-exchange membranes. Studies of ED as a function of current density and source-phase concentration show remarkably high selectivities, but both selectivity and current efficiency depend on the feed concentrations and current density.

2.3.1 Modification of Nafion Membranes

Nafion membranes are attractive for PEM adsorption because they have smooth, essentially defect-free surfaces. In contrast, other cation-exchange membranes that we obtained have large μm-sized surface voids that the thin multilayer film likely cannot bridge (see Figure 2A.1 in the appendix). Elemental analysis with XPS confirms the adsorption of $(PAH/PSS)_n$ films on oxidized Nafion (Table 2.1), as the elemental composition of the surface changes with successive depositions steps. The pretreated bare membrane contains a large fraction of fluorine because Nafion is a perfluorinated copolymer, but the fluorine fraction decreases after adsorption of polyelectrolytes and is essentially zero after

formation of a $(PAH/PSS)_3PAH$ film. Because of the limited escape depth for photoelectrons, XPS probes primarily the top ~5 nm of a surface and is most sensitive near the surface. Thus, the near-complete disappearance of fluorine signals after adsorption of 3.5 PAH/PSS bilayers suggests that the PEM is at least 5 nm thick.[32] The small amount of fluorine reported after adsorption of a $(PAH/PSS)_5PAH$ film stems from noise in the area of the fluorine signal. Sulfur and nitrogen signals increase as the fluorine signal decreases, confirming the adsorption of PSS (sulfur atoms) and PAH (nitrogen atoms).

Table 2.1. XPS elemental compositions for Nafion 115 membranes before and after coating with $(PAH/PSS)_xPAH$ films.

Number of (PAH/PSS) bilayers	**Fluorine (%)**	**Sulfur (%)**	**Nitrogen (%)**	**Carbon (%)**	**Oxygen (%)**
0	57.1	1.3	1.2	32.4	8.0
1.5, $(PAH/PSS)_1PAH$	11.5	4.7	5.1	58.0	19.7
3.5, $(PAH/PSS)_3PAH$	0.0	6.7	6.7	59.5	26.7
5.5 $(PAH/PSS)_5PAH$	0.4	7.4	6.8	55.7	28.4

2.3.2 Electrodialysis with bare and modified cation-exchange membranes

Initial ED experiments employed a 2-compartment cell with 0.01 M KNO_3 and 0.01 M $Mg(NO_3)_2$ in the source phase (anode chamber) and 0.01 M HNO_3 in the receiving phase (cathode chamber). The 0.01 M HNO_3 maintains electrical conductivity and neutralizes hydroxide formed at the cathode to prevent precipitation of $Mg(OH)_2$ in the receiving phase. We use nitrate rather than chloride salts to avoid generation of Cl_2, which may damage the PEM.[27,33] Figure 2.3 shows the amounts of K^+ and Mg^{2+} in the receiving phase as a function of time during constant-current (1.27 mA cm^{-2}) ED. The amount of K^+ in the receiving phase increases nearly linearly with ED time, and the slight decrease in flux at long times for bare Nafion membranes likely stems from an increase in the proton concentration in the source phase and a corresponding increase in the fraction of current carried by H^+. The pH of the source phase decreased from 4.6 to ~2.3 over the course of the ED for both modified and bare membranes. (Note that pH values <4 are below the calibration range of the meter and not very accurate.)

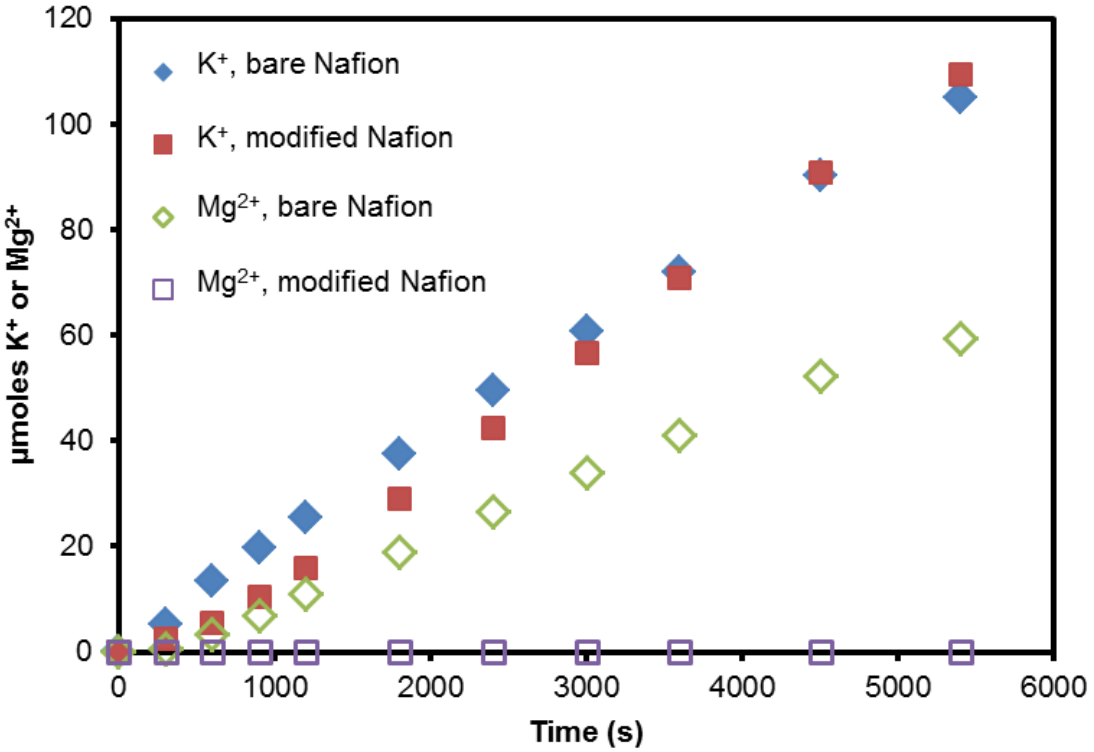

Figure 2.3. Moles of K^+ and Mg^{2+} in the receiving phase as a function of time during ED with initial solutions containing 0.01 M KNO_3 and 0.01 M $Mg(NO_3)_2$ in the source phase and 0.01 M HNO_3 in the receiving phase. Electrodialysis occurred in a 2-compartment experiment using bare (diamonds) and $(PAH/PSS)_5PAH$-modified (squares) Nafion 115 membranes and a 1.27 mA cm^{-2} current density.

Unmodified Nafion membranes show high passage of both K^+ and Mg^{2+}. In experiments with 3 replicate membranes, the average fluxes of K^+ (6.4 ± 0.3 nmol cm^{-2} s^{-1}) and Mg^{2+} (3.6 ± 0.1 nmol cm^{-2} s^{-1}) reflect an average selectivity of only

1.8 ± 0.1 at a current density of 1.27 mA cm^{-2}. The K^+ flux through membranes coated with $(PAH/PSS)_5PAH$ films is 6.9 ± 0.2 nmol cm^{-2} s^{-1}, or approximately the same as that through the bare Nafion. In contrast, Mg^{2+} flux was < 5 pmol cm^{-2} s^{-1} for all three replicate membranes, which gives rise to a K^+/Mg^{2+} selectivity >1000 for the $(PAH/PSS)_5PAH$-coated membrane. This selectivity is similar to the value of >300 for $(PSS/PAH)_5$ films on porous alumina and is much higher than the typical selectivities of <10 for ion-exchange membranes.[14,17-19,28,34]

In addition to selectivity, high current efficiencies are important to minimize the energy required for ED. The current efficiency (or the fraction of current carried through the membrane by a given ion, also known as the transference number, t_i) for K^+ is 0.53 for $(PAH/PSS)_5PAH$-modified Nafion membranes at a current density of 1.27 mA cm^{-2}. In contrast, Mg^{2+} carries <<1% of the total current. Thus, other unwanted ions carry ~50% of the current through the membrane. Presuming that the Nafion is essentially 100% cation selective, protons must carry ~ 50% of the current through $(PAH/PSS)_5PAH$-modified Nafion. In aqueous solutions, the proton electrophoretic mobility is approximately 5 times the mobility of K^+, so proton transference numbers >0.5 are feasible at the end of the experiments when the source-phase pH is ~2.3.[33] However, at the initial source-phase pH of 4.6, protons should not carry significant current. Some protons may diffuse from the acidic receiving phase to the source phase and migrate across the membrane. However, due to the cation-selectivity of Nafion, this would likely require coupled diffusion of protons to the source phase and

cations to the receiving phase. Such a process would not decrease the *calculated* K^+ and Mg^{2+} transference numbers, as these calculations assume all cation transport occurs through electromigration and yet measure cation transport to the receiving phase by any process (see equation 2.1). Diffusion dialysis experiments (no applied potential) show a K^+ flux that is only 7% of the flux in ED through $(PAH/PSS)_5PAH$-modified Nafion. Thus, most of the K^+ transport occurs due to electromigration. In contrast, diffusive fluxes are >50% of ED fluxes through bare Nafion, and in some cases this leads to a sum of calculated transference numbers >1.

Some of the non-K^+ current through modified membranes may stem from water splitting that occurs in an ion-depleted region near the polyelectrolyte/Nafion interface. At overlimiting currents high local potential gradients in this region may separate H^+ and OH^- ions that form due to dissociation of water (see below). Our previous measurements of transmembrane diffusion potentials suggest that PEMs are anion selective,[26] whereas Nafion is nearly ideally cation selective. Because cations likely carry <50% of the current in the PEM and nearly all the current in Nafion, positive currents give rise to significant cation depletion near the source-phase PEM/Nafion interface (i.e. cation electromigration through the PEM to the Nafion interface is less than that away from this interface toward the receiving phase, see Figure 2.4). Concurrent anion depletion occurs because few anions come to the interface through the Nafion, but anions likely carry more than 50% of the current in the PEM and thus migrate away from the PEM/Nafion interface

toward the source phase. At steady state, diffusion toward the PEM/Nafion interface leads to constant ion fluxes throughout the modified membrane. The electric field in the depleted, low-conductivity region must be high to maintain a constant current, and at sufficiently high fields water will split into OH^- and H^+ to provide current-carrying species. This should primarily occur near the PEM/Nafion interface where depletion is greatest. In this non-electrode process, water dissociates into H^+ and OH^-, and the electric field separates these ions. Moreover, Wessling's group recently showed that some PEMs act as water-splitting catalysts.[28,35]

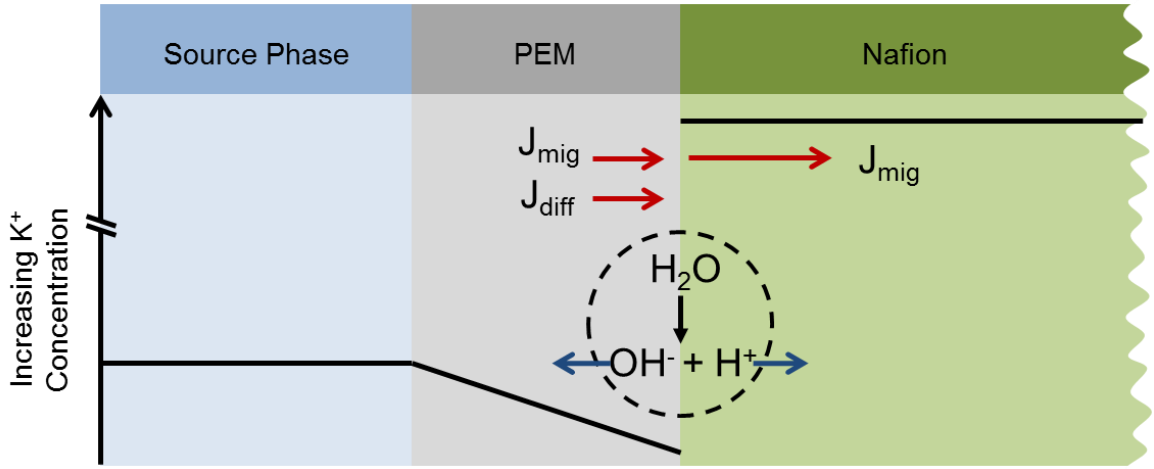

Figure 2.4. Schematic, qualitative diagram of the K^+ concentration profile (black lines) during ED through a PEM-coated Nafion membrane. The red arrows qualitatively represent the magnitudes of the fluxes due to electromigration, J_{mig}, and diffusion, J_{diff}, of cations in the PEM and/or Nafion. The sum of electromigration and diffusion in the PEM should equal the flux due to electromigration in Nafion, where diffusion is negligible compared to electromigration. Due to possible proton gradients, the concentration of K^+ may not be constant in the Nafion. The PEM/Nafion interface near the receiving phase (not shown) should show ion accumulation rather than depletion.

Water splitting should only occur at the high potentials required to drive the current density beyond the diffusion-limited value, I_{lim}. Equation 2.2 gives an approximate expression for the K^+ limiting current density based on the assumptions that the dominant concentration polarization occurs at the PEM/Nafion interface, that diffusive transport in Nafion is negligible, and that

convection is negligible throughout the membrane. (See the appendix for a derivation of this equation).[36] In this equation,

$$I_{lim} \approx \frac{P_s \cdot c \cdot F}{\Delta t_+} \quad (2.2)$$

P_s is the diffusion permeance of the PEM, *c* is the KNO_3 concentration in the source phase, *F* is the Faraday constant and Δt_+ is the difference in the K^+ transference numbers in Nafion and the PEM. Previous diffusion dialysis experiments with bare porous alumina and porous alumina coated with $(PSS/PAH)_4$ films give a PEM permeance of 3.8 μm/s for KCl.[26] Moreover, transmembrane potential measurements suggest that the PEM K^+ transference number is ~0.3 in 0.01 M KCl.[26] Assuming that the $(PAH/PSS)_5PAH$ coating on Nafion has approximately the same properties as the porous alumina-supported film, that KCl and KNO_3 transport properties are similar, and that Nafion is ideally selective (i.e., in KNO_3 the K^+ transference number is 1), the limiting current density for a 0.01 M KNO_3 solution should be ~0.5 mA cm^{-2}. This value is a factor of 2 lower than the ~1.27 mA cm^{-2} employed to obtain the data in Figure 2, which is consistent with possible water splitting at this current density. However, as mentioned above, transport of protons from the increasingly acidic anodic source phase will also decrease K^+ transference numbers, particularly at the end of the ED.

2.3.3 Current−Voltage Curves and Evidence for Water Splitting.

Current-voltage curves often provide insight into limiting currents and, hence, the processes occurring at membranes in ED. Typically, the I-V curve for an ion-exchange membrane exhibits three regions. At low current densities, the potential drop across the membrane is directly proportional to the current. As the current density approaches its diffusion-limited value (I_{lim}), the ion concentration near the interface decreases rapidly causing an increase in resistance and consequently a large potential drop that gives rise to a smaller slope or a plateau. Further increases in current density result in less-dramatic changes in the membrane voltage drop, presumably because electroconvection and/or water splitting bring additional ions to the interface.[28,37,38] The intersection of the plateau region and the linear region serves as an estimate of I_{lim}.

As Figure 2.5 shows, the current density-voltage curve for a $[PAH/PSS]_5PAH$-modified membrane shows linear, plateau and overlimiting regions, with a limiting current density around 0.6 mA cm^{-2}, which is comparable to the value calculated using equation 2.2. Bare, oxidized Nafion exhibits only an ohmic profile under the same conditions because its limiting current is much higher due to the absence of the restrictive film and more importantly passage of both Mg^{2+} and K^{+}. These experiments employ a 10-fold excess of Mg^{2+} to minimize solution resistance. The Mg^{2+} does not pass significantly through the PEM and thus has a negligible effect on I_{lim} for the modified membrane, but it will greatly increase I_{lim} for the bare Nafion. When we performed the same experiment

without a membrane in the cell, the solution resistance was only slightly smaller than the total resistance with the bare Nafion membrane (see Figure 2A.2). Subtracting the solution resistance from the total resistance leads to values of 6 and 120 Ωcm^2 for the area resistances of Nafion and the $[PAH/PSS]_5PAH$-modified Nafion, respectively. Given that the Nafion conduction results from both 0.1 M Mg^{2+} and 0.01 M K^+ and the modified membrane utilizes only the 0.01 M K^+, the resistance of the modified membrane to K^+ electromigration is likely about twice the resistance of the bare Nafion to this ion.

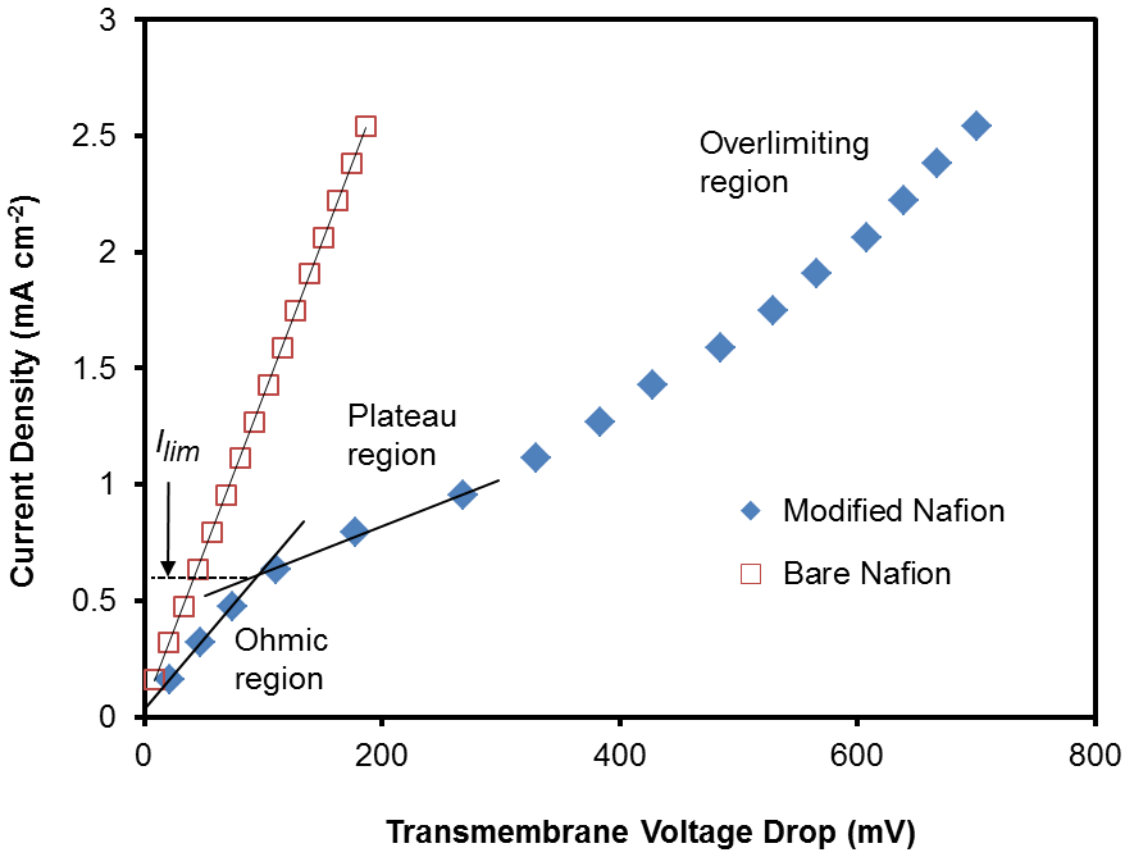

Figure 2.5. Current-voltage curves for bare (open squares) and $[PAH/PSS]_5PAH$-modified (filled diamonds) Nafion membranes. The experiments employed a two-compartment cell with solutions containing 0.01 M KNO_3 and 0.1 M $Mg(NO_3)_2$ on both sides of the membrane. The limiting current was determined from the intersection of the lines from the ohmic and plateau regions.

Water splitting should occur at high membrane potential drops and lead to changes in the pH of the source and receiving phases. However, protons and hydroxide ions generated electrolytically at the anode and cathode, respectively, also affect pH, so monitoring pH changes due to water splitting requires isolation

of the anode and cathode with cation- and anion-exchange membranes, respectively. In such experiments we employ a 4-compartment cell with 0.01 M KNO_3 solutions in the anode and source phases and 0.01 M $NaNO_3$ solutions in the receiving and cathode phases to allow monitoring of K^+ flux and also avoid any pH changes due to formation of $Mg(OH)_2$. After passing 9.6 C of charge through the membrane using an underlimiting current density of 0.32 mA cm^{-2} (160 min of current) the pH of the source and receiving phases remained around 5.5. In contrast, during subsequent passage of 9.6 C at an overlimiting current density of 2.54 mA cm^{-2} (20 min of current), the pH of the source phase gradually increased to 7.0 and the receiving-phase pH dropped to around 4.0. Assuming that 50% of the current results in water splitting at this overlimiting current density, the pH in the receiving phase should drop to around 3.3. However, some of the protons will pass from the receiving phase into the cathode compartment, which is highly basic (pH 11 at the end of the experiment). Moreover, the anion-exchange membrane may not provide a perfect barrier to proton transport from the anode compartment to the source phase. Despite the qualitative nature of this experiment, it provides strong evidence that water splitting accounts for a substantial change in the pH of each compartment at high current densities and leads to some of the decrease in current efficiency at overlimiting current densities. As expected extensive water splitting only occurs at relatively high transmembrane potentials.[39]

2.3.4 Effect of current density on K^+/Mg^{2+} separations

We further examined selectivity and current efficiency in ED at current densities ranging from 0.32 to 2.54 mA cm^{-2} for source-phase solutions containing 0.01 M KNO_3 and 0.01 M $Mg(NO_3)_2$. Figure 2.6 shows the K^+ and Mg^{2+} fluxes from these experiments with coated Nafion membranes. For current densities at and below 2.22 mA cm^{-2}, the K^+ flux increases with current density (see the supporting information, Table 2A.1, for flux values). However, on going from 2.22 to 2.54 mA cm^{-2}, the K^+ flux declines 30% and the Mg^{2+} flux increases 5-fold. Table 2.2 further shows that the K^+ transference number declines at the highest current density, where the most water splitting should occur.[28,40] The initially continuous increase in K^+ flux and subsequent drop with increasing overlimiting current densities are difficult to explain and suggest complicated mass transport through the membrane. Wessling and coworkers recently found that PEMS can cause hydrodynamic instabilities at the surface of ion-exchange membranes, which should affect transport and overlimiting currents.[41]

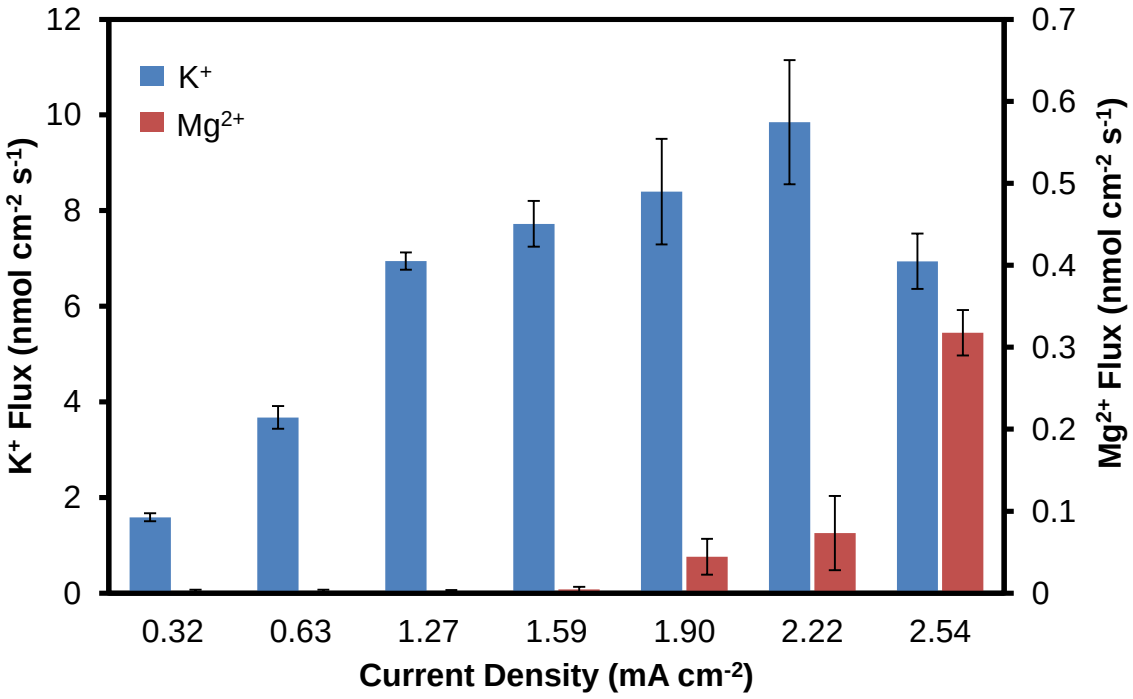

Figure 2.6. K^+ and Mg^{2+} fluxes as a function of applied current density in 2-cell ED experiments with 0.01 M HNO_3 in the receiving phase. The source phase initially contained 0.01 M KNO_3 and 0.01 M $Mg(NO_3)_2$. Note the different scales for K^+ and Mg^{2+} flux.

Table 2.2. K^+/Mg^{2+} selectivities and cation transference numbers in ED through $(PAH/PSS)_5PAH$-modified Nafion membranes as a function of current density. The source phase contained 0.01 M KNO_3 and 0.01 M $Mg(NO_3)_2$.

Current Density (mA cm^{-2})	K^+/Mg^{2+} Selectivity	K^+ Transference	Mg^{2+} Transference
2.54	22.1 ± 3.5	0.26 ± 0.02	0.024 ± 0.002
2.22	176 ± 104	0.43 ± 0.06	0.006 ± 0.004
1.90	245 ± 171	0.43 ± 0.02	0.004 ± 0.002
1.59	>1000	0.47 ± 0.03	<0.0007
1.27	>1000	0.53 ± 0.01	<0.0007
0.63	>1000	0.56 ± 0.04	<0.0007
0.32	>480	0.48 ± 0.02	<0.002

Interestingly, coating both sides of the Nafion membranes with $(PAH/PSS)_5PAH$ films yields greater selectivities than coating either side alone. Specifically, for a current density of 2.54 mA cm^{-2}, K^+/Mg^{2+} selectivities are 7.8 ± 1.6 with a $(PAH/PSS)_5PAH$ film only on the side of the membrane facing the source phase and 10.0 ± 3.8 when the films is on the side facing the receiving phase. With a $(PAH/PSS)_5PAH$ coating on both sides of the membrane, the K^+/Mg^{2+} selectivity is 22.1 ± 3.5 (Table 2.2). Thus, selectivity approximately doubles when coating both sides of the membrane.

The increased Mg^{2+} transport at high current densities may result from water splitting, which produces not only protons but also stoichiometric amounts of OH^- ions that migrate towards the anode in the source phase. This should result in a locally high pH near the source phase/membrane interface where hydroxyl ions may form $Mg(OH)_x$ complexes with the incoming Mg^{2+} ions. The PEM permeability to the low concentration of neutral, soluble $Mg(OH)_2$ may be much higher than to Mg^{2+} ions, and we speculate that diffusion of this neutral species across the PEM might be the principal mechanism that enhances magnesium transfer at the higher overlimiting currents (Figure 2.6 and Table 2.2). Notably, to form a significant fraction of $Mg(OH)_x$ species, the pH value at the source-phase membrane surface must reach a threshold value of 9-11 (assuming that the Mg^{2+} concentration does not considerably increase in this region). This threshold value, which may only appear at the higher current densities, occurs locally near the PEM and is much different from the bulk solution pH. Additionally, a high local pH may alter film permeability to increase Mg^{2+} flux.

2.3.5 ED with different source-phase concentrations

To further investigate the effect of current density on separations, we performed ED with different concentrations of salt in the source phase. The KNO_3 and $Mg(NO_3)_2$ source-phase concentrations were ≥0.01 M to avoid excessive solution resistance, and the receiving phase always contained 0.01 M HNO_3. This series of experiments used a current density of 2.54 mA cm^{-2}, which gives a

detectable Mg^{2+} flux at low salt concentrations. As Figure 2.7 shows, although the applied current is constant, K^+ flux nearly doubles from 6.94 ± 0.58 nmol cm^{-2} s^{-1} to 13.5 ± 0.6 nmol cm^{-2} s^{-1} when the source phase concentration increases from 0.01 M to 0.02 M in both KNO_3 and $Mg(NO_3)_2$. This provides further evidence that in a 0.01 M KNO_3 solutions this applied current density is overlimiting for K^+. Simultaneously, Mg^{2+} flux *drops* from 318 ± 28 pmol cm^{-2} s^{-1} to 149 ± 47 pmol cm^{-2} s^{-1}, perhaps because of less water splitting. Further increasing the source-phase KNO_3 and $Mg(NO_3)_2$ concentrations to 0.1 M increases the K^+ flux to 25.2 ± 1.6 nmol cm^{-2} s^{-1}, and Mg^{2+} flux falls below its detection limit (<1 pmol cm^{-2} s^{-1})).

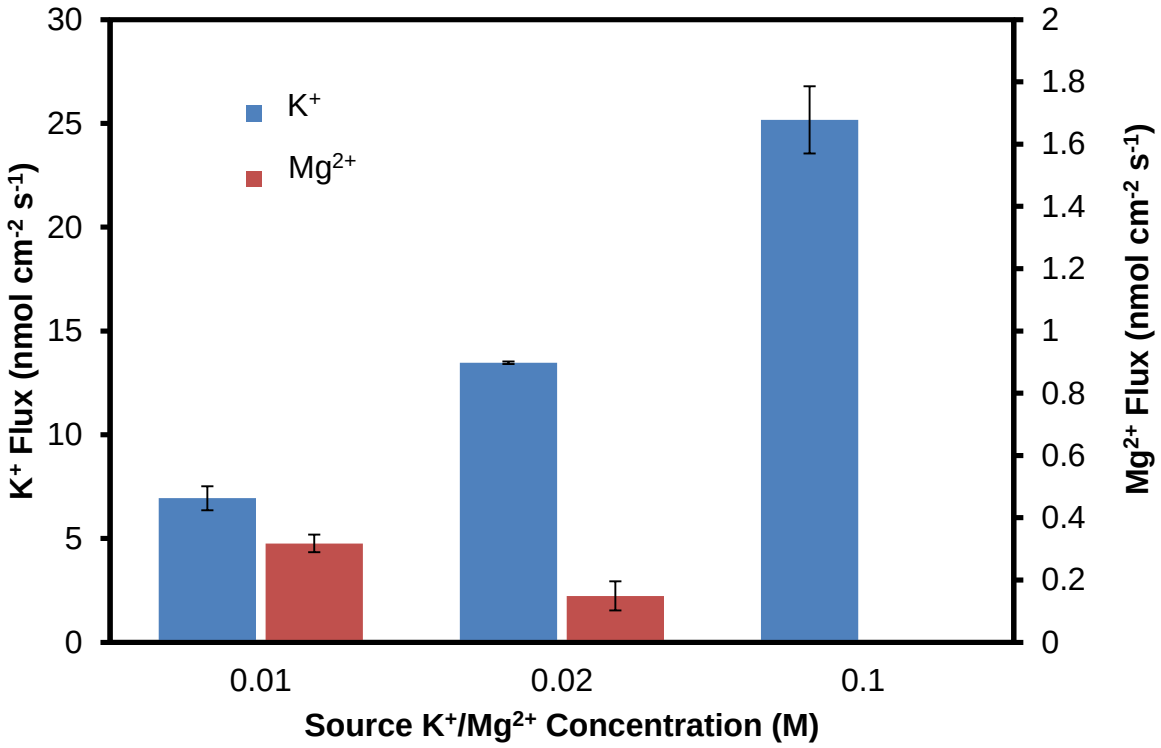

Figure 2.7. K^+ and Mg^{2+} fluxes as a function of the KNO_3 and $Mg(NO_3)_2$ source-phase concentrations in 2-compartment ED with 0.01 M HNO_3 in the receiving phase and a 2.54 mA cm^{-2} current density. Note the different scales for K^+ and Mg^{2+}; the Mg^{2+} flux was undetectable (<1 pmol cm^{-2} s^{-1}) with KNO_3 and $Mg(NO_3)_2$ source-phase concentrations of 0.1 M.

The increase in K^+ flux and simultaneous decrease in Mg^{2+} flux on raising the source-phase concentrations from 0.01 to 0.1 M lead to a remarkable increase in selectivity from 22 to >20,000 (see Table 2.3). Furthermore, the transference number for K^+ approaches unity with 0.1 M KNO_3 and 0.1 M $Mg(NO_3)_2$ in the source phase. The current density is constant in this series of

experiments and should fall below the limiting value at high source-phase concentrations. Based on equation 2.2 and the permeance value mentioned previously, the limiting current density for 0.1 M KNO_3 is ~5 mA cm^{-2}, which is twice the applied current density. Below the limiting current, local electric fields are small and little water splitting occurs, so Mg(OH)x species should not form and decrease K^+/Mg^{2+} selectivity. Moreover, proton transport from the source to the receiving phase is negligible in the presence of 0.1 M K^+, so the K^+ transference number is high.

Table 2.3. K^+/Mg^{2+} selectivities and cation transference numbers in ED through $(PAH/PSS)_5PAH$-modified Nafion membranes. For the feed solution with 0.1 M salts, selectivity and Mg^{2+} transference number are estimated from the minimum detectable Mg^{2+} flux. The current density was 2.54 mA cm^{-2}.

Source-Phase Concentration (M)	**K^+/Mg^{2+} Selectivity**	**K^+ Transference**	**Mg^{2+} Transference**
0.01	22.1 ± 3.5	0.26 ± 0.02	0.024 ± 0.002
0.02	96 ± 26	0.51 ± 0.01	0.011 ± 0.004
0.1	>20000	0.96 ± 0.06	<0.0001

We also investigated the utility of these membranes in separating K^+ and Mg^{2+} from source-phase solutions where the KNO_3 and $Mg(NO_3)_2$ concentrations

are not the same. In all experiments, the receiving phase was 0.01 M HNO_3 and the current density was 2.54 mA cm^{-2}. When the source-phase contained 0.1 M KNO_3 and 0.01 M $Mg(NO_3)_2$, the K^+ flux was 24.7 ± 0.3 nmol cm^{-2} s^{-1} and the Mg^{2+} flux was not detectable. The high KNO_3 concentration in these experiments again ensures that K^+ is the dominant current carrier, and the K^+ transference number is 0.938 ± 0.010.

In the reciprocal ED experiment, where the source phase contains 0.01 M KNO_3 and 0.1 M $Mg(NO_3)_2$, the K^+ flux is 9.9 ± 0.6 nmol cm^{-2} s^{-1} and the Mg^{2+} flux is 272 ± 98 pmol cm^{-2} s^{-1} giving rise to a K^+/Mg^{2+} flux ratio of 40 ± 14. However, this number does not account for the Mg^{2+} to K^+ concentration ratio of 10 in the source phase, and the true selectivity in this separation is 400 ± 140. Because of the low KNO_3 concentration, the K^+ transference number is 0.38 ± 0.02, and protons from water splitting probably carry much of the remainder of the current in Nafion. Interestingly, the Mg^{2+} flux remained virtually unchanged from 318 ± 28 pmol cm^{-2} s^{-1} at a 0.01 M source-phase concentration to 272 ± 98 pmol cm^{-2} s^{-1} at a 0.1 M concentration, even with a constant KNO_3 concentration of 0.01 M. Despite the low K^+ transference number at an overlimiting K^+ flux, these membranes remain highly selective when the divalent cation is in large excess. This should prove useful in applications that require the removal of small concentrations of contaminants and would most likely be implemented using low current densities applied over larger membrane areas in flow-through cells with low solution thicknesses. Prior studies suggest that Mg^{2+} adsorption in PEMs may

increase surface charge to maintain a low flux of Mg^{2+} ions, even as the Mg^{2+} concentration increases.[42] Additionally, at the high Mg^{2+} concentration, $Mg(OH)^+$ rather than $Mg(OH)_2$ species may result from OH^- formed in water splitting. The membrane may be much more permeable to low concentrations of neutral, soluble $Mg(OH)_2$ than to $Mg(OH)^+$.

2.3.6 Electrodialysis in a 3-compartment cell

With 0.01 M KNO_3 in the source phase, the low K^+ transference numbers even at underlimiting currents (Table 2) suggest electromigration of H^+ from the source phase, particularly as this phase becomes more acidic due to proton generation at the anode. To investigate the extent of unwanted ED proton current that is not associated with water splitting, we employed a 3-compartment cell that separates the proton-generating anode from the source phase using an anion-exchange membrane. This strategy is typical for ED applications that employ multiple compartments. Compared to the 2-compartment experiments described above, ED of 0.01 M KNO_3 and 0.01 M $Mg(NO_3)_2$ in a 3-compartment cell increases the K^+ flux from 6.9 ± 0.2 to 8.9 ± 0.1 nmol cm^{-2} s^{-1} upon application of the same 1.27 mA cm^{-2} current density. This increases the K^+ current efficiency from 0.53 to 0.67. (Figure 2.8 shows data from a representative experiment.) Additionally, Mg^{2+} flux is still very low (<23 pmol cm^{-2} s^{-1})) with the 3-compartment cell, and the minimum K^+/Mg^{2+} selectivity with 3 different membranes was above 350.

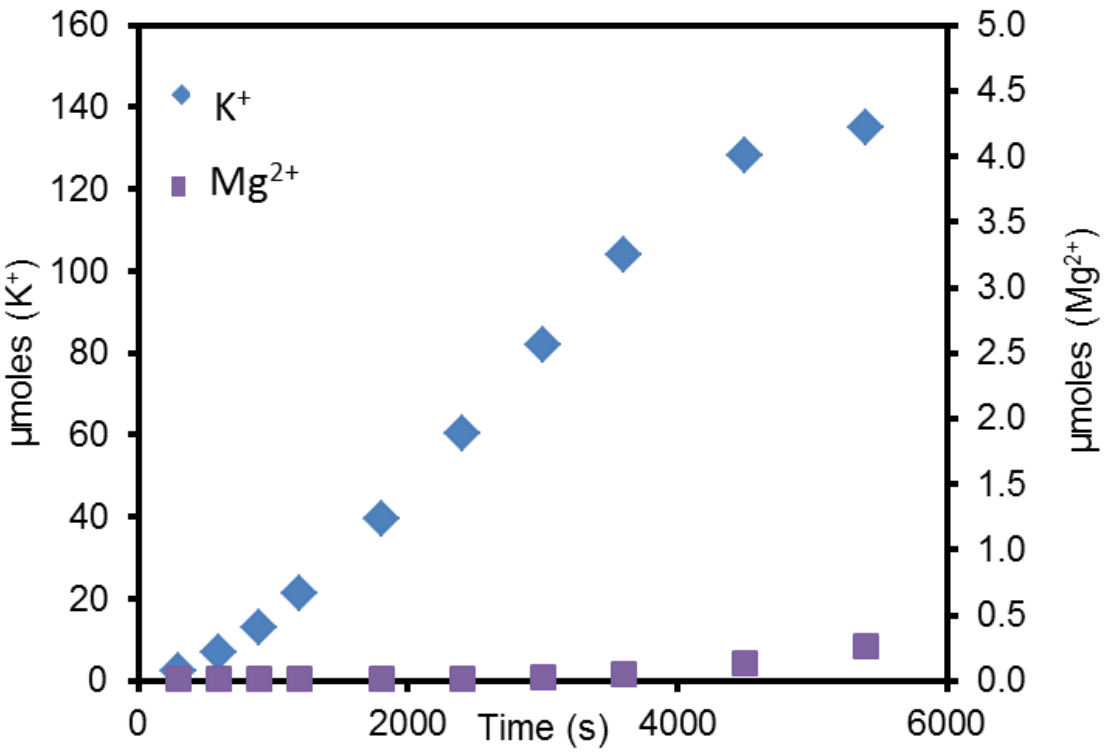

Figure 2.8. Moles of K^+ and Mg^{2+} in the receiving phase as a function of time in a 3-compartment ED experiment with 0.01 M KNO_3 and 0.01 M $MgNO_3$ in the source phase and 0.01 M HNO_3 in the receiving phase. 0.01 M HNO_3 was also used in the isolated anode cell.

Overall, the fraction of the current carried by K^+ increases ~25% on going from the 2-compartment to the 3-compartment cell (see Table 2 for the 2-compartment data). Nevertheless, other ions still carry ~30% of the current in this system. Similar to the 2-compartment experiments, the pH of the source phase is around 4.5 at the start of the experiment, so initially the mobility of protons in the membrane would have to be 2orders of magnitude higher than the mobility of K^+ to

account for such large H^+ currents. By the end of the experiment the source-phase pH decreases to 3.5 (compared to ~2.3 in the 2-compartment experiment, the anion-exchange membrane likely does not completely block proton transport), so a proton transference of 0.3 would still require a high proton mobility in the membrane if no water splitting occurs. Thus, these experiments suggest some water splitting under these conditions.

2.3.7 Selectivities among other cations

Experiments with other cations also show remarkable selectivity. At a current density of 1.27 mA cm^{-2} with a source phase containing 0.01 M KNO_3 and 0.01 M $Ca(NO_3)_2$, and a receiving phase of 0.01M HNO_3, K^+/Ca^{2+} selectivities and K^+ transference numbers are similar to those in corresponding ED with 0.01 M KNO_3 and 0.01 M $Mg(NO_3)_2$ in the source phase. Specifically, K^+ flux is 5.94 ± 0.27 nmol cm^{-2} s^{-1} and Ca^{2+} flux is 18 ± 12 pmol cm^{-2} s^{-1}, representing an average K^+/Ca^{2+} selectivity of 430 ± 220. Uncertainty in the very low Ca^{2+} flux causes the large uncertainty in selectivity. Compared to K^+/Mg^{2+}, slightly lower values for K^+/Ca^{2+} selectivities are consistent with the larger diffusion coefficient and lower hydration energy for Ca^{2+} compared to Mg^{2+}.[33]

Transference numbers in these experiments are 0.451 ± 0.021 for K^+ and 0.003 ± 0.002 for Ca^{2+}. In the corresponding control experiment, flux through unmodified Nafion membranes is 6.24 ± 0.25 nmol cm^{-2} s^{-1} for K^+ and 3.86 ± 0.05 nmol cm^{-2} s^{-1} for Ca^{2+}, representing an average K^+/Ca^{2+} selectivity of only 1.62 ±

0.05. Again, the multilayer film provides a relatively small resistance to K^+ transport while essentially preventing transport of the multivalent cation. These selectivities are 1-2 orders of magnitude higher than those previously reported for commercial membranes in Na^+/Ca^{2+} separations with below-limiting currents.[14] Such high selectivities may lead to new ED applications.

2.4 Conclusions

Alternating adsorption of polycations and polyanions on Nafion cation-exchange membranes leads to remarkable monovalent/divalent cation selectivities in ED. Either at high source-phase concentrations or low current densities, the K^+/Mg^{2+} selectivity of Nafion membranes coated with $(PAH/PSS)_5PAH$ is >1000. Selectivities are still >350 when the concentration of one cation exceeds the other by a factor of 10. However, with low source-phase K^+ and Mg^{2+} concentrations, selectivities decline when the current greatly exceeds the K^+ diffusion-limited value, perhaps because water splitting in the membrane increases permeability to Mg^{2+} or leads to a small amount of neutral, soluble $Mg(OH)_2$ that can diffuse through the membrane. Current-voltage curves and pH monitoring confirm both the K^+ limiting current and water splitting at overlimiting currents. At 0.1 M KNO_3 source-phase concentrations, the K^+ transference number approaches 1, presumably because the current is well below the K^+ diffusion-limited value and H^+ transport is insignificant. Future work should investigate the long-term stability of these membranes and their use for recovery of more valuable cations.

Additionally, modelling of the system will enhance understanding of boundary conditions and the concentration-dependence of ion transport.

APPENDIX

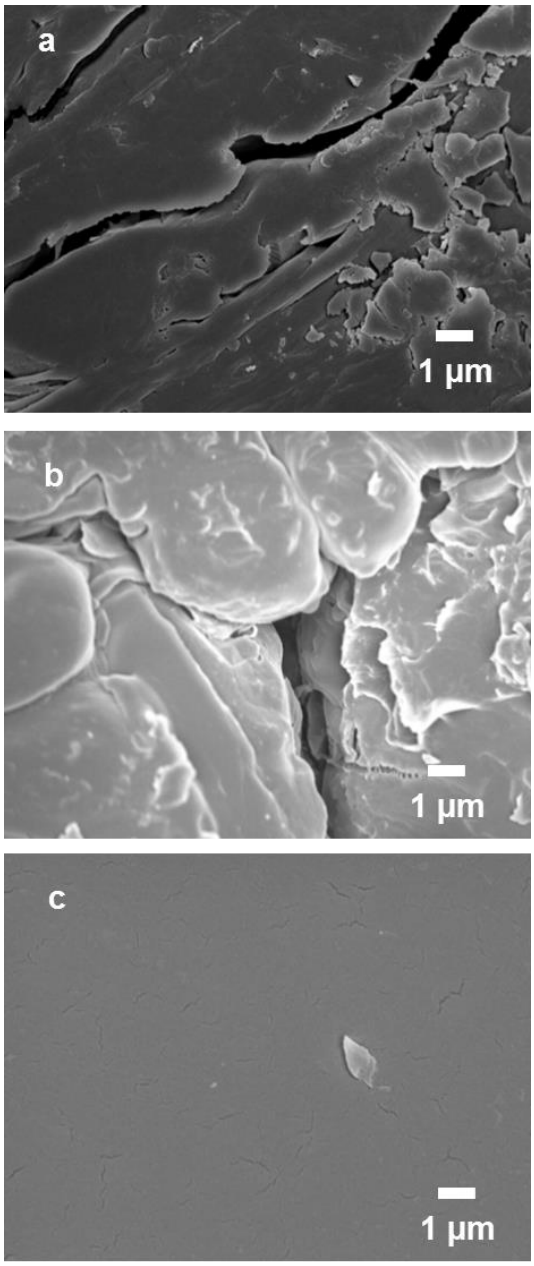

Figure 2A.1. SEM images of several commercial cation-exchange membranes: (a) CMI-7000, (b) Excellion, and (c) Nafion. Note the large (>1 µm) defects in (a) and (b), whereas Nafion has a smooth, essentially defect-free surface suitable for polyelectrolyte deposition. Preliminary attemps to coat CMI-7000 and Excellion with polyelectrolyte multilayers did not give highly selective membranes.

Limiting Current. The dominant concentration polarization in ED through PEM-coated Nafion membranes should occur in the PEM because of its low permeance. Equation 2A.1 defines the PEM permeance, P_i^{PEM}, which reflects both partitioning and diffusivity for species *i* in the film as well as the film thickness. In this equation, J_i is the diffusive flux through the film and ΔC is the concentration difference between the two solution phases immediately adjacent to the film. We previously

$$P_i^{PEM} = \frac{J_i}{\Delta C} \tag{2A.1}$$

determined the permeance of PEMs on porous alumina. A series resistance model gave P_{KCl}^{PEM} =3.8 μm/s for a $(PSS/PAH)_4$ film.[26] We assume $P_{KNO_3}^{PEM}$ will be similar for a $(PAH/PSS)_5PAH$ film on Nafion, but the value may be lower due to the extra polyelectrolyte layers. Nitrate and chloride salts should behave similarly. In ED, we estimate the limiting current from the permeance of the PEM by assuming: (a) the concentrations of K^+ and NO_3^- at the PEM/Nafion interface are essentially zero, (b) no convection, i.e., electroosmotic and osmotic flow are negligible, and (c) the concentration gradient for K^+ in Nafion is small enough that diffusion is negligible compared to electromigration.[36] The last assumption is reasonable given the high thickness of the Nafion support compared to the PEM. With these assumptions, at steady state the sum of diffusive, J_{diff}^{PEM}, and electromigration, J_{mig}^{PEM}, fluxes in the PEM must equal the migration flux, J_{mig}^{Nafion}, in the Nafion membrane according to equation 2A.2.

$$J_{diff}^{PEM} + J_{mig}^{PEM} = J_{mig}^{Nafion} \tag{2A.2}$$

Rearranging equation 2A.1 with the assumption that the concentration at the PEM/Nafion interface is close to zero gives equation 2A.3 where c_{source} is the source-phase KNO_3 concentration. (This equation

$$J_{KNO_3,diff}^{PEM} = P_{KNO_3}^{PEM} c_{source} \tag{2A.3}$$

assumes minimal concentration polarization in the source phase. Note that the diffusive fluxes for K^+ and NO_3^- are equal, so we use a salt permeability.) The migratory K^+ flux is simply the current density, *I*, multiplied by the transference number, t_{K^+} and divided by the Faraday constant, *F*. Thus substituting for diffusion and electromigration fluxes in equation 2A.2 and noting that equation 2A.3 is valid only for the limiting current, I_{lim} , gives equation 2A.4.

$$P_{KNO_3}^{PEM} c_{source} + \frac{I_{lim}\, t_{K^+,PEM}}{F} = \frac{I_{lim}\, t_{K^+,Nafion}}{F} \tag{2A.4}$$

Solving for I_{lim} yields equation 2A.5.

$$I_{lim} = \frac{P_{KNO_3}^{PEM} c_{source} F}{\Delta t_{K^+}};\ \Delta t_{K^+} = t_{K^+,Nafion} - t_{K^+,PEM} \tag{2A.5}$$

For a source-phase concentration of 0.01 M KNO_3, $P_{KNO_3}^{PEM} = 3.8 \frac{\mu m}{sec}$, and $\Delta t_{K^+} = 0.7$, equation 2A.4 gives $I_{lim} = 0.52\ \frac{mA}{cm^2}$.

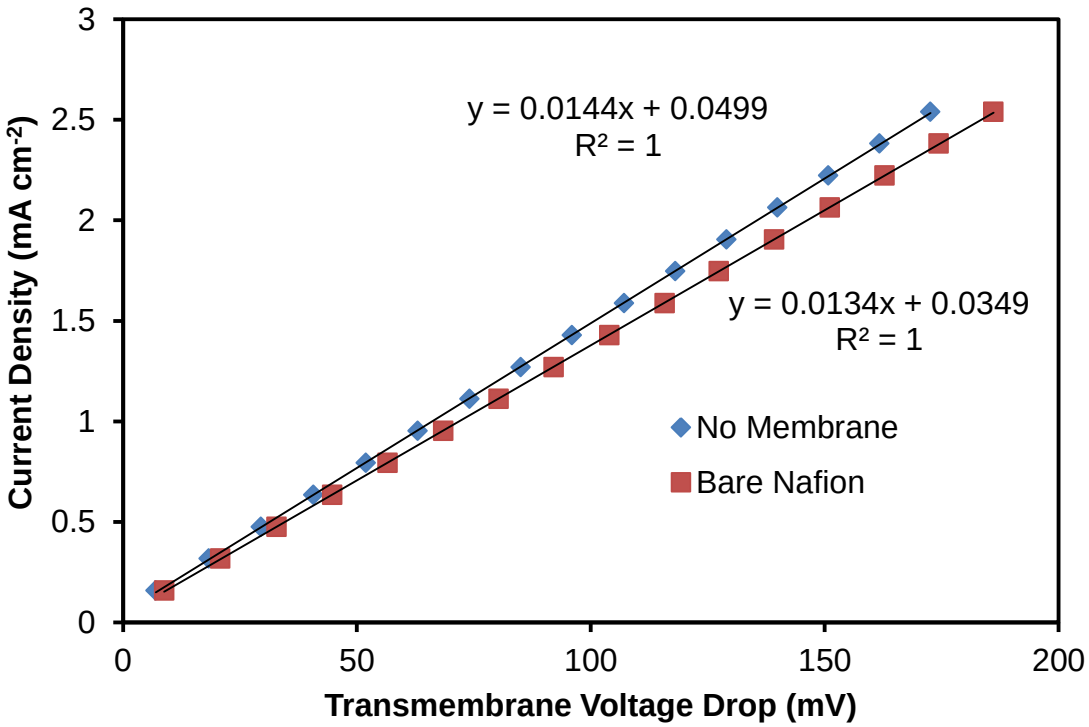

Figure 2A.2. Current-voltage curves obtained in a two-compartment cell separated by bare oxidized Nafion (squares) or no membrane (diamonds). Both compartments contained 0.01 M KNO_3 and 0.1 M $Mg(NO_3)_2$. The small difference in slopes indicates that the bare Nafion membrane adds minimal resistance (~5 Ω cm^2) to the system.

Table 2A.1. Average fluxes for K^+ and Mg^{2+} ions as a function of applied current during ED using $(PAH/PSS)_5PAH$-coated Nafion membranes and a source phase containing 0.01 M KNO_3 and 0.01 M $Mg(NO_3)_2$. The receiving phase contained 0.01 M HNO_3. Large standard deviations in Mg^{2+} flux are due in part to the low concentrations of this ion in the receiving phase.

Current (mA)	Current Density ($mA\ cm^{-2}$)	K^+ Flux ($nmol\ cm^{-1}\ s^{-1}$)	Mg^{2+} Flux ($pmol\ cm^{-1}\ s^{-1}$)
8	2.54	6.28 ± 0.58	318 ± 28
7	2.22	9.85 ± 1.30	73 ± 45
6	1.90	8.40 ± 1.10	44 ± 22
5	1.59	7.72 ± 0.48	5 ± 3
4	1.27	6.94 ± 0.18	2 ± 2
2	0.63	3.67 ± 0.24	2 ± 2
1	0.32	1.59 ± 0.08	3 ± 1

REFERENCES

REFERENCES

(1) Tanaka, Y.; Ehara, R.; Itoi, S.; Goto, T. *J. Membr. Sci.* **2003**, *222*, 71-86.

(2) Wang, Z. X.; Luo, Y. B.; Yu, P. *J. Membr. Sci.* **2006**, *280*, 134-137.

(3) Huang, C. H.; Xu, T. W.; Zhang, Y. P.; Xue, Y. H.; Chen, G. W. *J. Membr. Sci.* **2007**, *288*, 1-12.

(4) Smagghe, F.; Mourgues, J.; Escudier, J. L.; Conte, T.; Molinier, J.; Malmary, C. *Bioresour. Technol.* **1992**, *39*, 185-189.

(5) Bazinet, L. *Critical Reviews in Food Science and Nutrition* **2005**, *45*, 307-326.

(6) Seto, T.; Ehara, L.; Komori, R.; Yamaguchi, A.; Miwa, T. *Desalination* **1978**, *25*, 1-7.

(7) Kim, D. H. *Desalination* **2011**, *270*, 1-8.

(8) Silva, V.; Poiesz, E.; van der Heijden, P. *J. Appl. Electrochem.* **2013**, *43*, 1057-1067.

(9) Luo, Q. T.; Zhang, H. M.; Chen, J.; Qian, P.; Zhai, Y. F. *J. Membr. Sci.* **2008**, *311*, 98-103.

(10) Suuar, T.; Skyllas-Kazacos, M. *J. Membr. Sci.* **2003**, *222*, 249-264.

(11) Weber, A. Z.; Mench, M. M.; Meyers, J. P.; Ross, P. N.; Gostick, J. T.; Liu, Q. H. *J. Appl. Electrochem.* **2011**, *41*, 1137-1164.

(12) Xi, J. Y.; Wu, Z. H.; Teng, X. G.; Zhao, Y. T.; Chen, L. Q.; Qiu, X. P. *J. Mater. Chem.* **2008**, *18*, 1232-1238.

(13) Galama, A. H.; Daubaras, G.; Burheim, O. S.; Rijnaarts, H. H. M.; Post, J. W. *J. Membr. Sci.* **2014**, *452*, 219-228.

(14) Sata, T.; Yang, W. K. *J. Membr. Sci.* **2002**, *206*, 31-60.

(15) Sata, T.; Mizutani, Y. *J. Polym. Sci., Part A: Polym. Chem.* **1979**, *17*, 1199-1213.

(16) Sata, T.; Yamane, R.; Mizutani, Y. *J. Polym. Sci., Part A: Polym. Chem.* **1979**, *17*, 2071-2085.

(17) Sata, T.; Yamaguchi, T.; Matsusaki, K. *J. Phys. Chem.* **1995**, *99*, 12875-12882.

(18) Sata, T.; Mine, K.; Higa, M. *J. Membr. Sci.* **1998**, *141*, 137-144.

(19) Lambert, J.; Avila-Rodriguez, M.; Durand, G.; Rakib, M. *J. Membr. Sci.* **2006**, *280*, 219-225.

(20) Decher, G. *Science* **1997**, *277*, 1232-1237.

(21) Hollman, A. M.; Bhattacharyya, D. *Langmuir* **2004**, *20*, 5418-5424.

(22) Li, X. F.; De Feyter, S.; Chen, D. J.; Aldea, S.; Vandezande, P.; Du Prez, F.; Vankelecom, I. F. J. *Chem. Mater.* **2008**, *20*, 3876-3883.

(23) Farhat, T. R.; Schlenoff, J. B. *J. Am. Chem. Soc.* **2003**, *125*, 4627-4636.

(24) Michaels, A. S. *Ind Eng Chem* **1965**, *57*, 32-&.

(25) Krasemann, L.; Tieke, B. *Langmuir* **2000**, *16*, 287-290.

(26) Cheng, C.; Yaroshchuk, A.; Bruening, M. L. *Langmuir* **2013**, *29*, 1885-1892.

(27) Cheng, C.; White, N.; Shi, H.; Robson, M.; Bruening, M. L. *Polymer* **2014**, *55*, 1397-1403.

(28) Abdu, S.; Marti-Caatayud, M. C.; Wong, J. E.; Garcia-Gabaldon, M.; Wessling, M. *ACS Appl. Mater. Interfaces* **2014**, *6*, 1843-1854.

(29) Mulyati, S.; Takagi, R.; Fujii, A.; Ohmukai, Y.; Matsuyama, H. *J. Membr. Sci.* **2013**, *431*, 113-120.

(30) Tanaka, Y. *J. Membr. Sci.* **2004**, *244*, 1-16.

(31) Jiang, S. P.; Tang, H. L. *Colloids Surf., A* **2012**, *407*, 49-57.

(32) Skoog, D. A.; Holler, F. J.; Crouch, S. R.; *Principles of Instrumental Analysis*, 6th ed.; Thomson Brooks/Cole: Belmont, CA, **2007**.

(33) Vanýsek, P. In *CRC Handbook of Chemistry and Physics*; 94 ed.; CRC Press: 2014, p 77.

(34) Van der Bruggen, B.; Koninckx, A.; Vandecasteele, C. *Water Res.* **2004**, *38*, 1347-1353.

(35) Abdu, S.; Sricharoen, K.; Wong, J. E.; Muljadi, E. S.; Melin, T.; Wessling, M. *ACS Appl. Mater. Interfaces* **2013**, *5*, 10445-10455.

(36) Yaroshchuk, A. *J. Membr. Sci.* **2012**, *396*, 43-49.

(37) Krol, J. J.; Wessling, M.; Strathmann, H. *J. Membr. Sci.* **1999**, *162*, 145-154.

(38) Rubinstein, I.; Zaltzman, B. *Phys Rev E* **2000**, *62*, 2238-2251.

(39) Strathmann, H.; Rapp, H. J.; Bauer, B.; Bell, C. M. *Desalination* **1993**, *90*, 303-323.

(40) Kang, M. S.; Choi, Y. J.; Moon, S. H. *Korean J. Chem. Eng.* **2004**, *21*, 221-229.

(41) Wessling, M.; Morcillo, L. G.; Abdu, S. *Scientific Reports* **2014**, *4*, 4294.

(42) Lu, O. Y.; Malaisamy, R.; Bruening, M. L. *J. Membr. Sci.* **2008**, *310*, 76-84.

CHAPTER 3

Highly Selective Separations of Multivalent and Monovalent Cations in Electrodialysis Through Nafion Membranes Coated with Polyelectrolyte Multilayers

Portions of this chapter reprinted from N White, M Misovich, E Alemayehu, A Yaroshchuk, and ML Bruening. *Polymer*, **2016**.
DOI: 0.1016/j.polymer.2015.12.019

3.1 Introduction

Electrodialysis (ED) is a membrane-based separation technique for applications such as brackish-water desalination,[1-3] wastewater treatment,[4] dairy-byproduct demineralization,[5] and production of organic acids[6] and concentrated brines.[7,8] Typical commercial ED systems employ feed solutions flanked by cation and anion-exchange membranes, and an applied current leads to migration of both cations and anions out of the feed solution.[9] Although ED effectively removes charged species from feed streams, commercial ED membranes exhibit low selectivities among different cations or anions. Such selectivities are important in applications such as preventing vanadium crossover in redox flow batteries or purifying salts or drinking water.[10-13]

Several groups employed polyelectrolyte adsorption to enhance the selectivity of ion-exchange membranes. Sata and coworkers showed that polyanion coatings on cation-exchange membranes enhance the selectivity for cations over anions, and polycation coatings have the opposite effect.[14-16] Polyethyleneimine (PEI) deposition on AMX anion-exchange membranes

increased monovalent anion selectivity, and modification under basic conditions led to NO_3^-/SO_4^{2-} selectivities up to 20.[17] Other studies using PEI coatings on cation-exchange membranes showed that cross-linking of the film and control over hydrophobicity give Na^+/Ca^{2+} selectivities as high as 7.[16] Additionally, electrochemical deposition of PEI films on Nafion cation-exchange membranes produced Na^+/Cr^{3+} selectivities >10.[18] However, these selectivities are relatively modest, so in this study we explore adsorption of multilayer polyelectrolyte films on cation-exchange membranes to increase selectivity.

The discovery of simple layer-by-layer polyelectrolyte adsorption[19] spurred exploration into whether polyelectrolyte multilayers (PEMs) can act as selective barriers for ion transport,[20-25] and a few groups deposited PEMs on ion-exchange membranes to impart selectivity. Mulyati *et al.* reported that modification of an anion-exchange membrane with $(PSS/PAH)_7PSS$ films reverses the Cl^-/SO_4^{2-} selectivity from 0.8 to 2.5.[10] Other work with 60-bilayer poly(styrenesulfonate) (PSS)/protonated poly(allylamine) (PAH) films on poly(acrylonitrile)/poly(ethylene terephthalate) produced Na^+/Mg^{2+} selectivities exceeding 100 in diffusion dialysis.[26] Abdu and coworkers modified Neosepta CMX ion-exchange membranes with polyethylenimine/PSS films to alternate ion permselectivity based on the terminal layer, but Na^+/Ca^{2+} selectivities were less than 1.5.[27]

This research builds on our previous studies of PEM-coated membranes that show remarkable K^+/Mg^{2+} ED selectivities >1000.[28,29] In this paper, we first demonstrate that $(PAH/PSS)_5PAH$-modified Nafion also exhibits Li^+/Co^{2+} and

K^+/La^{3+} selectivities >1000. Using these pairs of ions, we investigate the effect of the source-phase salt concentrations on selectivity and transference numbers because concentration polarization greatly affects ED. Current-voltage curves and elemental characterization of fouled membranes give insight into limiting currents and water-splitting near the PEM-Nafion interface, a phenomenon that decreases the current carried by target ions.[27] Additionally, longer-term (48 h) ED reveals challenges to PEM stability, possibly because the electric field causes electromigration of the charged polyelectrolytes to degrade the film. We also study how varying the number of bilayers in the PEM affects the flux, transference number, and selectivity of coated membranes. The high selectivities of PEM-coated membranes make them very attractive for ED separations, and future work should aim at increasing limiting currents and membrane stability.

3.2 Experimental section

3.2.1 Materials

Poly(sodium 4-styrenesulfonate) (M_w = 70000 Da), poly (allylamine hydrochloride) (M_w = 15000 Da), sodium nitrate, lanthanum(III) acetate ($La(OAc)_3$) hydrate, and potassium acetate (K(OAc)) were purchased from Sigma-Aldrich. Magnesium nitrate was obtained from Mallinckrodt, and lithium nitrate was purchased from Spectrum. All salts were used as received without further purification. For the acidic receiving phase, 69% HNO_3 (Fisher) was diluted with

deionized water to give 0.01 M HNO_3. Nafion 115 membranes were acquired from Ion Power (New Castle, DE, thickness 127 μm), and deionized water (Milli-Q Reference Ultrapure Water Purification System, 18 MΩ·cm) was used to prepare aqueous solutions. For membrane oxidation, 30% H_2O_2 (Fisher) and 98% H_2SO_4 (Macron) were separately diluted to 3% H_2O_2 and 1.0 M H_2SO_4. The pH of polyelectrolyte solutions was adjusted with 0.1 M HCl or 0.1 M NaOH. Nafion 117 solution (5% w/w) was purchased from Sigma-Aldrich and diluted to 0.5% with isopropanol.

3.2.2 Film formation and characterization

As previously described,[29] Nafion membranes were cut into 25-mm disks with a mechanical die and pretreated according to literature methods to oxidize and clean the surface. Membranes were first rinsed with deionized water then sequentially immersed for 30 min in the following solutions heated to 100 °C: 3% H_2O_2, deionized water, 1.0 M H_2SO_4, and deionized water.[13,30] Rinsing with room-temperature deionized water also occurred after each immersion. All experiments with unmodified and modified Nafion employed oxidized membranes.

We performed layer-by-layer adsorption by sequentially immersing membranes in 0.02 M PAH in 1.0 M NaCl, rinsing with deionized water to remove weakly adhered polyelectrolyte, immersing in 0.02 M PSS in 0.5 M NaCl, and again rinsing with deionized water. This process was repeated to form multiple bilayers, and films were terminated with PAH adsorption to give them a positive

surface charge. In one case noted in the text, the final immersion in PAH was eliminated to yield a negatively-charged film.

Reflectance FTIR spectra were obtained using a Thermo Nicolet 6700 FTIR spectrometer with a Pike grazing angle (80°) apparatus. Bare Au-coated silicon wafers treated with UV/O_3 served as a background. To create substrates for polyelectrolyte adsorption, wafers were spin-coated with a 0.5% v/v Nafion solution for 30 s at 2000 rpm before pretreatment with H_2O_2/H_2SO_4 and polyelectrolyte adsorption using the procedure employed for modifying Nafion membranes.

3.2.3 Electrodialysis

Nafion membranes were sandwiched between two 100-mL homemade glass cells separated by an o-ring (3.1 cm^2 effective membrane area). Platinum wire electrodes were placed in each compartment such that upon application of an electric field cations could move across the membrane from the source phase to the receiving phase. Using a CH Instruments model 604 potentiostat, a specific potential between working and reference electrode terminals was applied across a 499 Ω resistor to generate a constant current during ED. The reference electrode terminal was also attached to the Pt electrode in the source phase, and the counter electrode terminal was attached to the Pt electrode in the receiving phase.[29] To produce current-voltage curves, the voltage across the resistor was

varied from 0.05 V to 4.0 V. Both source and receiving phases were stirred briskly to minimize concentration polarization. During ED, sample aliquots were removed periodically over 2 h from both the source and receiving phases, but generally only the receiving phase was analyzed. The source phase was periodically analyzed to verify the salt concentration. Metal-cation analysis was accomplished with an axial Varian 710-ES Inductively Coupled Plasma Optical Emission Spectrophotometer equipped with a Varian SPS 3 autosampler. Individual cation standards were prepared from nitrate (Li^+ and Co^{2+}) or acetate (La^{3+} and K^+) salts, and serial dilutions were performed to make a calibration curve. Each experiment was performed in triplicate using a different membrane each time, and uncertainties in the results represent standard deviations of values for the different membranes.

ED data are plotted as total moles of cation in the permeate phase as a function of time, and fluxes were calculated by dividing the slope of this line by the membrane area. To allow for ion exchange and equilibration between the membrane and solution, slopes were determined from only the final 90 min of 2 h of ED. The reported selectivities represent the ratios of monovalent to multivalent ion fluxes when the source phase contains equal concentrations of both cations. Selectivities are shown as > values to show the minimum selectivity observed with three different membranes because variations in the very low multivalent ion flux can lead to large deviations in calculated selectivities. Furthermore, transference numbers, t_i, were calculated using equation 3.1, where J_i is the flux of ion *i* in

moles cm^{-2} s^{-1}, z_i is the ion charge, F is the Faraday constant, and I is the current density in A cm^{-2}.

$$t_i = \frac{J_i z_i F}{I} \tag{3.1}$$

Parallel experiments with current-voltage curves were performed using the four-point method in a homemade two-compartment electrodialysis cell similar to the one described above. Haber-Luggin capillaries filled with 1 M KCl and fitted with borosilicate glass frits (Ace glass, size E) to minimize leakage were used to bring the capillary-filling solution/source phase interface to within ~4 mm of the membrane surface. The capillaries containing the references electrodes (Ag/AgCl, 3 M KCl, CH Instruments model 111) were attached to ground-glass joints to ensure their reproducible placement near the center of the membrane. Platinum wire electrodes were used for both the anode and cathode. Current-voltage curves were obtained with solutions containing 0.01 M $LiNO_3$ or K(OAc) and 0.1 M $Co(NO_3)_2$ or $La(OAc)_3$ on both sides of the membranes. The current was increased stepwise and held at a constant value for at least 30 s to reach a constant voltage. Between steps to new current values, the applied current was turned off until the transmembrane potential was <10 mV. The excess multivalent cation in these experiments decreases solution resistance, but due to its low permeability it should not greatly affect K^+ or Li^+ transport through the PEM.

In a few ED experiments, membranes modified with $(PAH/PSS)_5PAH$ films were deliberately fouled using a high current density (2.54 mA cm^{-2}) with 0.01 M $LiNO_3$ and 0.01 M $Co(NO_3)_2$ in the source phase and 0.01 M HNO_3 in the receiving

phase. A blue precipitate formed on the membrane within 30 minutes, but the current was maintained for 1 h to ensure a thicker coating. Subsequently, the membrane was air-dried before coating with 8 nm of gold using a Pelco SC-7 Auto Sputter Coater coupled to a Pelco FTM-2 Film Thickness Monitor. The fouled membrane was characterized with a JEOL 7500F scanning electron microscope (SEM) equipped with a cold field-emission emitter (2 kV accelerating voltage, 4.5 mm working distance), and elemental analysis of the precipitate was performed with energy dispersive spectroscopy (EDS) and INCA software.

3.2.4 Membrane durability

Experiments aimed to evaluate the stability of PEMs in electric fields employed the two-compartment electrodialysis cell described previously. ED was performed for a total of 48 h with the same $(PAH/PSS)_5PAH$ membrane at a current density of 0.63 mA cm^{-2}. These experiments used 0.02 M $LiNO_3$ and 0.02 M $Co(NO_3)_2$ in the source phase and 0.01 M HNO_3 in the receiving phase. At 2-h ED intervals the cell was rinsed with deionized water, and ED solutions were replaced. Sample aliquots were taken at the end of each 2-h period and analyzed for cation content. After 12, 22, and 30 h of ED, the membrane was stored overnight in deionized water while still mounted in the cell. Ions probably diffuse out of the membrane during storage, causing a ‘lag effect’ after which the membranes must re-equilibrate with the source and receiving solutions. In Figure

3.6, small dips in ion passage at 22 and 30 h likely occur due to this overnight storage.

3.3 Results and Discussion

Our previous work showed monovalent/divalent-ion selectivities >300 in ED through porous alumina membranes coated with $(PSS/PAH)_5$ films,[28] and selectivities as high as 20,000 with Nafion membranes coated with $(PAH/PSS)_5PAH$ films.[29] High selectivities originate from both the large hydration sphere of the divalent ion and electrostatic exclusion of multiply-charged ions. However, those studies only investigated K^+ and Mg^{2+} transport. This section first examines whether the high selectivities previously observed with K^+ and Mg^{2+} also occur with Li^+ and Co^{2+} as well as K^+ and La^{3+}. We also investigate limiting currents and water splitting, which creates metal-hydroxide precipitates on membrane surfaces. Finally, we explore membrane durability and how ED varies with the number of adsorbed PAH/PSS bilayers on Nafion membranes.

3.3.1 Electrodialysis with bare and modified cation-exchange membranes

Initial ED experiments with bare and modified membranes employed a 2-compartment cell with 0.01 M $LiNO_3$ and 0.01 M $Co(NO_3)_2$ in the source phase (anode compartment) and 0.01 M HNO_3 in the receiving phase (cathode compartment). The acidic receiving phase maintains electrical conductivity while

neutralizing hydroxide produced at the cathode to prevent $Co(OH)_2$ precipitation. We used nitrate salts because ED with chloride sometimes generates Cl_2 which may damage the PEM.[28] Figure 3.1 shows the amounts of Li^+ or Co^{2+} in the receiving phase as a function of ED time. Unmodified Nafion membranes show high passage of both Li^+ and Co^{2+}. In experiments with three replicate membranes, the average fluxes of Li^+ (1.9 ± 0.4 nmol cm^{-2} s^{-1}) and Co^{2+} (3.0 ± 0.7 nmol cm^{-2} s^{-1}) indicate an average Li^+/Co^{2+} selectivity of only 0.66 ± 0.08 at the applied current density of 0.63 mA cm^{-2}. Interestingly, the K^+/Mg^{2+} selectivity of bare Nafion membranes is >1.[29] The Li^+/Co^{2+} selectivity of 0.66 likely reflects a low Li^+ electrical mobility. In aqueous solutions, K^+ is about twice as mobile as Li^+.[31]

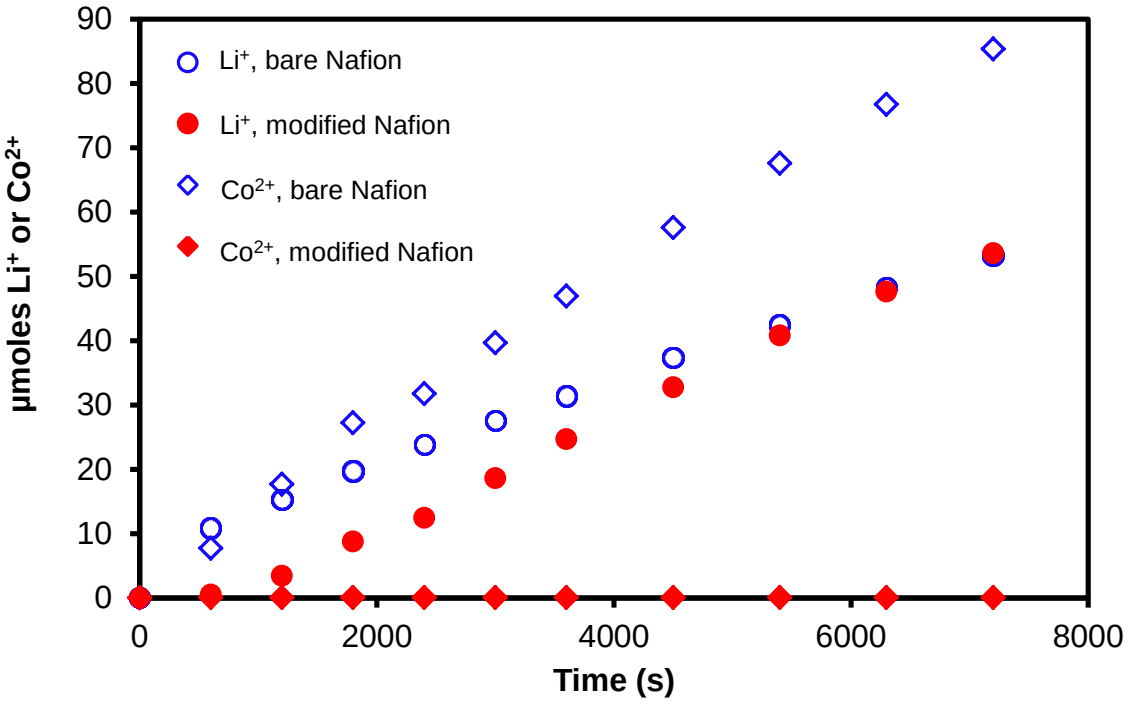

Figure 3.1. Moles of Li^+ and Co^{2+} in the receiving phase as a function of time during ED (current density of 0.63 mA cm^{-2}) through bare Nafion membranes (open symbols) or Nafion coated with a $(PAH/PSS)_5PAH$ film (filled symbols). The source phase initially contained 0.01 M $LiNO_3$ and 0.01 M $Co(NO_3)_2$, and the receiving phase was initially 0.01 M HNO_3. The membrane area was 3.14 cm^2.

With $(PAH/PSS)_5PAH$-coated Nafion, the Li^+ concentration increases approximately linearly after a brief induction period. In one experiment, we immersed the membrane overnight in the source phase prior to ED, and the induction period disappeared. In all experiments, plots of Li^+ receiving-phase concentration versus time were linear ($R^2 > 0.995$) over the final 90 min of ED.

Nevertheless, at the end of the ED, the Li^+ flux may decline slightly because the source-phase pH decreases from 4.7 to 2 over the course of the experiment, presumably due to protons generated at the anode. As the pH decreases, protons should carry a larger fraction of the current.

Based on the last 90 min of ED in Figure 3.1 and in other replicate experiments, the Li^+ flux through $(PAH/PSS)_5$PAH-coated Nafion is 3.0 ± 0.2 nmol cm^{-2} s^{-1} (current density of 0.63 mA cm^{-2}) . The Li^+ flux through the PEM-coated Nafion is higher than through the native membrane because Co^{2+} carries >50% of the current through the bare Nafion. In contrast, the Co^{2+} flux was <2 pmol cm^{-2} s^{-1} through three replicate $(PAH/PSS)_5$PAH-coated Nafion membranes, so the Li^+/Co^{2+} selectivity of these membranes is >1500. This value is similar to the K^+/Mg^{2+} selectivities of >1000 reported[29] for the same membranes and is much higher than the typical monovalent/divalent-ion selectivities of <10 for monovalent-ion selective ion-exchange membranes.[16,18,32-35] Interestingly, in ED with PSS-terminated coatings ($(PAH/PSS)_5$ films), the Co^{2+} flux rises to 116 ± 34 pmol cm^{-2} s^{-1} whereas the Li^+ flux is again ~3.0 nmol cm^{-2} s^{-1}, so the Li^+/Co^{2+} selectivity is only 23.5 ± 6.8. Thus, positively-charged terminal layers are essential for achieving very high selectivities among cations, presumably because of electrostatic exclusion of the more highly charged ion. Additionally, swelling of (PAH/PSS) multilayers is likely lower for films terminated with a polycation,[36,37] and low swelling will increase size exclusion of highly hydrated divalent ions.

High current efficiencies are important for minimizing power consumption in ED separations. The current efficiency, quantified through the transference number, t_i, is the fraction of current carried by a particular ion. For $(PAH/PSS)_5$PAH-modified Nafion membranes at a current density of 0.63 mA cm^{-2}, $t_{Li^+}$is 0.45 whereas $t_{Co^{2+}}$ is essentially zero. Thus, other ions carry about 50% of the current in ED through $(PAH/PSS)_5$PAH-coated membranes. Assuming that anions do not pass through Nafion, protons (the only cations present besides Li^+ and Co^{2+}) must carry about 55% of the current in this cation-exchange membrane. Large proton transference numbers are reasonable at highly acidic pH, but this condition appears only toward the end of the ED experiments after electrolysis at the anode has generated sufficient protons for the source-phase pH to approach 2. At the initial source-phase pH of 4.7, protons generated at the anode should not carry a significant fraction of the current.

In the beginning of the ED, protons and hydroxide ions generated from water splitting near the PEM-Nafion interface probably carry much of the current. Inside the Nafion, only cations will carry current if this cation-exchange substrate is ideally selective, but the PEM allows transport of both anions and monovalent cations.[29] In fact, Cheng et al. showed that PEMs are somewhat anion-selective in the case of 1:1 salts.[28] Even assuming that Li^+ and NO_3^- have the same electrophoretic mobilities in the PEM, Li^+ should carry only half the current in this region (Figure 3.2). The disparity between the Li^+ transference number in Nafion (where it approaches unity) and in the PEM leads to an ion-depleted region near

the PEM-Nafion interface (i.e. cation and anion electromigration away from this interface is greater than toward it). To maintain a constant current throughout the membrane, the electric field in the ion-depleted region must be high and may reach the levels needed to cause water splitting, a non-electrode process characterized by water dissociation and separation to H^+ and OH^-. Furthermore, Wessling and coworkers showed that some PEMs can act as water-splitting catalysts.[27,34]

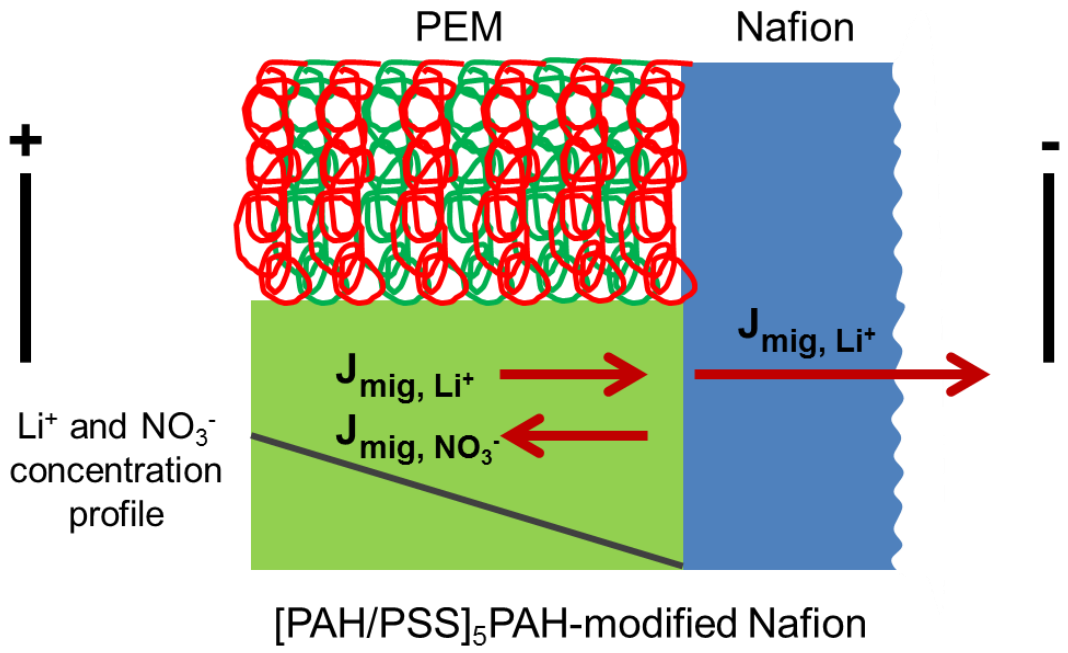

Figure 3.2. Ion transport through $(PAH/PSS)_5PAH$-modified cation-exchange membranes. Imbalanced Li^+ and NO_3^- electromigration at the PEM-Nafion interface generates an ion-depletion zone in the PEM. J_{mig} arrows represent the local flux of the ions due to electrical migration.

3.3.2 ED with different source-phase concentrations

We further examined selectivity and current efficiency in ED through $(PAH/PSS)_5PAH$-modified Nafion membranes with source phases containing 0.01 M, 0.02 M, or 0.1 M salts. We maintained at least 0.01 M salt concentrations to prevent excessive solution resistance, and the current density was 0.63 mA cm^{-2} in all of these experiments. Salts were either $LiNO_3$ and $Co(NO_3)_2$ or K(OAc) and $La(OAc)_3$ in the source phase, and the receiving phase remained 0.01 M HNO_3 for all experiments. Table 3.1 presents the Li^+ and Co^{2+} fluxes and the corresponding transference numbers and Li^+/Co^{2+} selectivities from these experiments. Interestingly, Li^+ flux is almost constant when the source-phase $LiNO_3$ and $Co(NO_3)_2$ concentrations increase from 0.01 to 0.02 M, but it nearly doubles when the source concentrations increase from 0.02 to 0.1 M. The Li^+ transference number approaches 1.0 at 0.1 M salt concentrations but is only ~0.45 at the lower source-phase salt concentrations. These data suggest that the current density is overlimiting for both 0.01 M and 0.02 M source-phase concentrations, giving rise to water splitting at the PEM-Nafion interface. However, we would expect the limiting current and the transference number to approximately double on doubling the source-phase salt concentrations from 0.01 to 0.02 M. Perhaps precipitation of $Co(OH)_2$ increases upon doubling the source-phase concentration and thus limits membrane permeability to Li^+ more with 0.02 M $Co(NO_3)_2$ rather than 0.01 M $Co(NO_3)_2$ in the source phase. We could not see any precipitate on membranes during ED under these conditions, but even a thin layer of precipitate might reduce

ion flux. The increase in Co^{2+} flux on going from 0.01 M to 0.02 M salts might stem from formation of $Co(OH)^{+}$ or some soluble $Co(OH)_2$ that can pass through the membrane more readily than Co^{2+}. At 0.1 M source-phase salt concentrations, the current density should be underlimiting, so water splitting will not occur to generate OH^- that precipitates Co^{2+}. Most remarkably, the Li^+/Co^{2+} selectivity is >600 for all conditions (Table 3.1).

Table 3.1. Li^+ and Co^{2+} fluxes, Li^+ transference numbers,[a] and Li^+/Co^{2+} selectivities as a function of source-phase cation concentrations during ED[b] through Nafion membranes coated with $(PAH/PSS)_5PAH$ films.

Li^+ or Co^{2+} Concentration (M)	**Li^+ Flux (nmol cm^{-2} s^{-1})**	**Co^{2+} Flux[c] (pmol cm^{-2} s^{-1})**	**Li^+ Transference**	**Selectivity[d]**
0.01	2.95 ± 0.21	1.29 ± 0.51	0.45 ± 0.03	>1600
0.02	3.18 ± 0.30	2.55 ± 1.71	0.48 ± 0.05	>630
0.1	6.79 ± 0.18	< 1	1.03 ± 0.02	>6500

[a]Co^{2+} transference numbers were <0.0013 for all replicates
[b]The source phase contained equal concentrations of $LiNO_3$ and $Co(NO_3)_2$, the receiving phase was 0.01 M HNO_3, and the current density was 0.63 mA cm^{-2}.
[c]Co^{2+} fluxes are close to the minimum detectable value, which leads to large uncertainties in selectivity.
[d]These values are the minimum selectivity observed in experiments with three replicate membranes.

Table 3.2 shows data for ED with K(OAc) and $La(OAc)_3$ in the source phase. Constant-current ED leads to greatly increasing K^+ flux when the source-phase K(OAc) and $La(OAc)_3$ concentrations change from 0.01 M to 0.02 M or 0.1 M. Remarkably, despite a constant current density, the K^+ flux increases nearly ten-fold from 0.46 ± 0.27 to 4.40 ± 0.02 nmol cm^{-2} s^{-1} when the salt concentration in the source phase doubles from 0.01 M to 0.02 M. Flux increases further when the source phase contains 0.1 M K(OAc) and $La(OAc)_3$, and t_{K^+} exceed unity. Transference numbers >1 suggest that diffusive transport of ions across the membrane is significant compared to electromigration. Our calculation of the transference number (see the experimental section) assumes that all of the K^+ in the receiving phase appears there due to electromigration. However, significant coupled diffusion of K^+ to the receiving phase and protons to the source phase could occur.

Table 3.2. K^+ and La^{3+} fluxes, K^+ transference numbers,[a] and K^+/La^{3+} selectivities as a function of source-phase cation concentrations during ED[b] through Nafion membranes coated with $(PAH/PSS)_5PAH$ films.

K^+ or La^{3+} Concentration (M)	**K^+ Flux (nmol cm^{-2} s^{-1})**	**La^{3+} Flux[c] (pmol cm^{-2} s^{-1})**	**K^+ Transference**	**Selectivity[d]**
0.01	0.46 ± 0.27	1.58 ± 1.00	0.07 ± 0.04	>93
0.02	4.40 ± 0.02	1.27 ± 0.46	0.69 ± 0.01	>2400
0.1	7.85 ± 0.69	<1	1.19 ± 0.10	>7000

[a]La^{3+} transference numbers were <0.0008 for all replicates
[b]The source phase contained equal concentrations of K(OAc) and $La(OAc)_3$, the receiving phase was 0.01 M HNO_3, and the current density was 0.63 mA cm^{-2}.
[c]La^{3+} fluxes are close to the minimum detectable value, which leads to large uncertainties in selectivity.
[d]These values are the minimum selectivity observed in experiments with three replicate membranes or the maximum detectable selectivity.

Compared to ED with Li^+ and Co^{2+}, the monovalent ion flux from a source phase of 0.01 M K(OAc) and $La(OAc)_3$ is very low, so t_{K^+} is below 10%. This low current efficiency presumably results from interfacial precipitation that decreases membrane permeability to both K^+ and La^{3+} much more than to hydroxide or protons. Hydroxide generated through water splitting near the PEM-Nafion interface likely forms $La(OH)_3$, which is highly insoluble in water.[38] In a separate set of experiments with 0.01 M KOAc and 0.01 M $La(OAc)_3$ in the source phase,

the K^+ flux increased from 0.46 ± 0.27 nmol cm^{-2} s^{-1} to 1.05 ± 0.47 nmol cm^{-2} s^{-1} upon *decreasing* current density from 0.63 mA cm^{-2} to 0.32 mA cm^{-2}. Additionally t_{K^+} increased from 0.07 ± 0.04 to 0.32 ± 0.14 leading to a K^+/La^{3+} selectivity >500 for three replicate membranes at the lower current density. These results provide strong evidence that overlimiting current densities cause formation of hydroxide compounds that adversely affect the permeability of PEM-coated membranes to monovalent cations. Decreasing the current density results in less precipitation to provide a more permeable film and, hence, higher K^+ flux despite the lower current.

In contrast to ED with nitrate salts where the source-phase acidity increases with time, in ED with acetate salts the source-phase pH remains around 5.5 throughout the experiment, so proton transport from this phase should not decrease K^+ transference numbers substantially. Thus, with 0.01 M and 0.02 M acetate salts in the source phase, transference numbers significantly <1 must stem predominantly from water splitting. Moreover, the formation of $La(OH)_x$ species due to water splitting might explain why La^{3+} flux increases at low source-phase concentrations where water splitting is most prevalent. As Table 3.2 shows, the selectivity of the films increases from ~100 with 0.01 M source-phase solutions to >2400 with 0.02 M solutions. Further increasing the source-phase concentration to 0.1 M increases selectivity to >7000. For comparison, the K^+/La^{3+} selectivity of unmodified Nafion membranes with 0.01 M K(OAc) and 0.01 M $La(OAc)_3$ in the source phase is only 1.61 ± 0.26.

We should note that K^+/La^{3+} selectivities stem in part from the formation of $La(OAc)_x$ complexes in the source phase. These large complexes likely have low electrophoretic mobilities in the PEM. Based on literature values for La^{3+}-OAc association constants,[39] we estimate that in a solution prepared with 0.01 M $La(OAc)_3$ and 0.01 M K(OAc) only ~15% of the La(III) exists as La^{3+} ions. $La(OAC)^{2+}$ and $La(OAc)_2^+$ complexes account for ~57% and ~28% of the La(III), respectively. In solutions made from 0.1 M $La(OAc)_3$ and 0.1 M K(OAc), the fractions of La^{3+}, $La(OAC)^{2+}$, $La(OAc)_2^+$, and $La(OAc)_3$ are around 3%, 25%, 42%, and 31%, respectively. The appendix provides the details of these estimations.

3.3.3 Effect of bilayer number on selectivity and current efficiency

Figure 3.3 shows reflectance-FTIR spectra of $(PAH/PSS)_xPAH$-modified Nafion films. Although subtraction of absorbances from the underlying Nafion leads to some uncertainty in the spectra (small negative peaks), the figure clearly shows that sulfonate absorbances of PSS (1200, 1130, 1033, and 1008 cm^{-1}) increase in intensity with the number of adsorbed PAH/PSS bilayers.[40] Previous X-ray photoelectron spectroscopy analysis showed the disappearance of fluorine signals after adsorption of $(PAH/PSS)_3PAH$ films, confirming that such films are at least 5 nm thick, or greater than the escape depth of Nafion fluorine photoelectrons.[29,41]

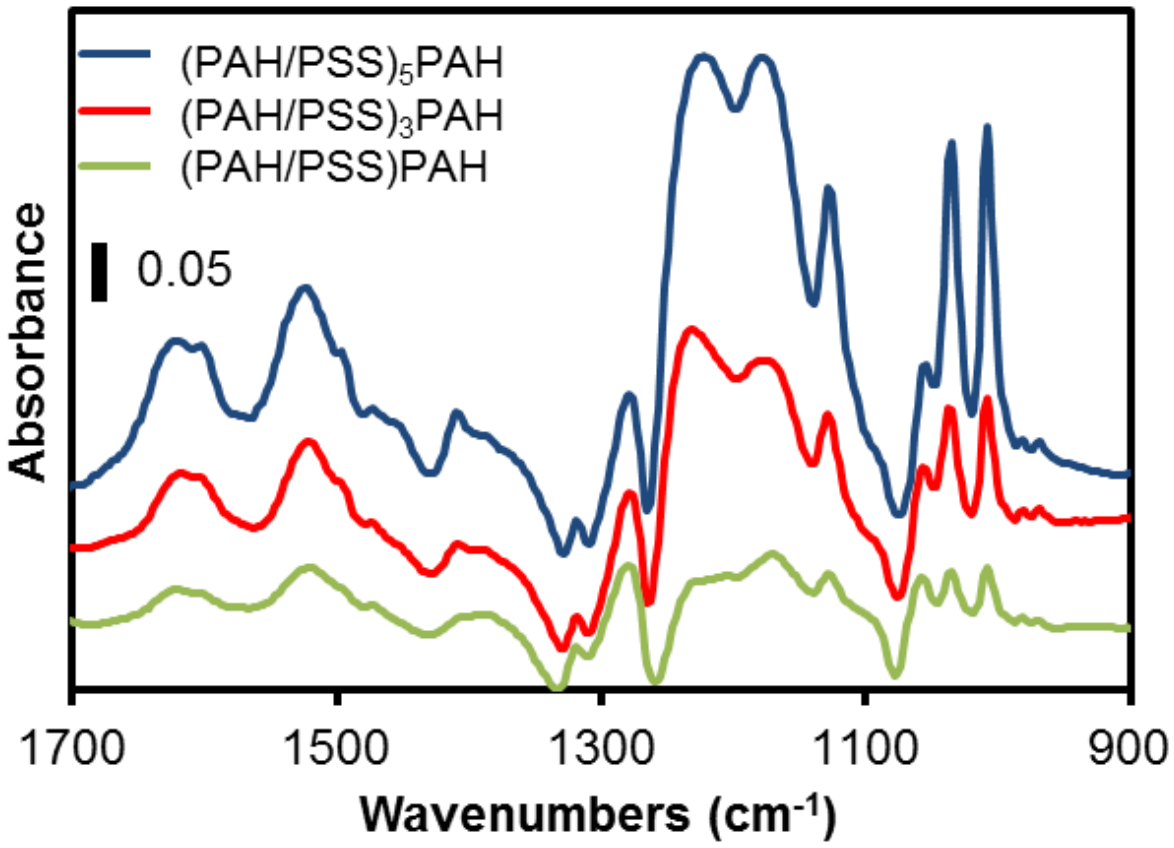

Figure 3.3. Reflectance-FTIR spectra (1700-900 cm^{-1}) of $(PAH/PSS)_5PAH$, $(PAH/PSS)_3PAH$, and (PAH/PSS)PAH-modified Nafion films on Au-coated Si wafers. The spectra were plotted after subtracting the spectrum of a Nafion film to minimize absorbances from Nafion. Wafers were spin-coated with a Nafion solution and oxidized prior to film deposition. The peaks at 1200, 1130, 1008 and 1033 cm^{-1} are due to the sulfonate groups in PSS, and additional peaks around 1500-1650 cm^{-1} stem from aromatic ring modes in PSS.

Because the amount of adsorbed polyelectrolyte increases with the number of deposited layers, we compared selectivity, flux, and current efficiency in ED through Nafion membranes coated with $(PAH/PSS)_5PAH$, $(PAH/PSS)_3PAH$, and PAH/PSS/PAH films. Surprisingly, at a constant applied current density, Li^+ flux through modified Nafion membranes decreases as the number of PAH/PSS bilayers in the film decreases (Table 3.3). As a result, Li^+ transference numbers decrease as well. Conversely, Table 3.3 shows that the Co^{2+} flux increases as the number of bilayers decreases, so the membrane Li^+/Co^{2+} selectivity declines from at least 1600 for all three replicate membranes with $(PAH/PSS)_5PAH$ films to only ~50 with PAH/PSS/PAH coatings. Nevertheless, the Co^{2+} transference number is <0.02 in all cases. Evidently, protons and hydroxide from water splitting carry an increased fraction of current as the number of bilayers declines.

Table 3.3. Li^+ and Co^{2+} fluxes, transference numbers, and Li^+/Co^{2+} selectivities during ED[a] through Nafion membranes coated with $(PAH/PSS)_5PAH$, $(PAH/PSS)_3PAH$, or (PAH/PSS)PAH films.

Film	Li^+ Flux (nmol cm^{-2} s^{-1})	Co^{2+} Flux (pmol cm^{-2} s^{-1})	Li^+ Transference	Co^{2+} Transference	Selectivity
$(PAH/PSS)_5$ PAH	2.95 ± 0.21	1.29 ± 0.51	0.45 ± 0.03	< 0.0006	>1600[b]
$(PAH/PSS)_3$ PAH	2.39 ± 0.10	3.85 ± 2.49	0.36 ± 0.02	< 0.002	>430[b]
(PAH/PSS) PAH	1.62 ± 0.10	37.3 ± 25.5	0.25 ± 0.01	< 0.018	23, 54, 108[c]

[a]The source phase contained 0.01 M $LiNO_3$ and 0.01 M $Co(NO_3)_2$, the receiving phase was 0.01 M HNO_3, and the current density was 0.63 mA cm^{-2}.
[b]These values are the minimum selectivity observed in experiments with three replicate membranes.
[c]These are the values from three replicate measurements. With adsorption of only a few polyelectrolyte layers, film coverage may differ significantly among replicate membranes and lead to large variations in selectivity.

Table 3.4 shows the trends in fluxes with the number of PAH/PSS bilayers during ED of K^+ and La^{3+} (acetate salts) through Nafion membranes. As noted above, flux and K^+ transference numbers are low with the $(PAH/PSS)_5PAH$ film on Nafion due to formation of a precipitate that decreases permeability. The K^+ Flux

increases nearly 10-fold upon going from $(PAH/PSS)_5PAH$ to $(PAH/PSS)_3PAH$ films on the membrane, perhaps because of less precipitation on the membrane surface due to a higher limiting current. However, PAH/PSS/PAH-coated membranes exhibit lower K^+ fluxes than $(PAH/PSS)_3PAH$-coated Nafion. La^{3+} flux increases slightly from <1 pmol cm^{-2} s^{-1} to 2.7 ± 1.9 pmol cm^{-2} s^{-1} upon changing from $(PAH/PSS)_3PAH$ to PAH/PSS/PAH films. Nevertheless, selectivity remains >500 even with only 1.5 bilayers on the Nafion (Table 3.4). K^+ transference numbers decline similarly to those of Li^+ upon moving from $(PAH/PSS)_3PAH$ to PAH/PSS/PAH films, but the transference numbers are higher for K^+ than for Li^+, probably because of the larger electrophoretic mobility of K^+.[31]

Table 3.4. K^+ and La^{3+} fluxes, transference numbers, and K^+/La^{3+} selectivities during ED[a] through Nafion membranes coated with $(PAH/PSS)_5PAH$, $(PAH/PSS)_3PAH$, or (PAH/PSS)PAH films.

Film	K^+ Flux (nmol cm^{-2} s^{-1})	La^{3+} Flux[b] (pmol cm^{-2} s^{-1})	K^+ Transference	La^{3+} Transference	Selectivity[c]
$(PAH/PSS)_5$ PAH	0.46 ± 0.27	1.58 ± 1.00	0.07 ± 0.04	< 0.0009	>90
$(PAH/PSS)_3$ PAH	4.32 ± 0.38	<1	0.66 ± 0.06	< 0.0003	>3500
(PAH/PSS) PAH	2.82 ± 0.14	2.70 ± 1.90	0.43 ± 0.02	< 0.0015	>500

[a]The source phase contained 0.01 M K(OAc) and 0.01 M $La(OAc)_3$, the receiving phase was 0.01 M HNO_3, and the current density was 0.63 mA cm^{-2}.
[b]La^{3+} fluxes are close to the minimum detectable value, which leads to large uncertainties in selectivity.
[c]These values are the minimum selectivity observed in experiments with three replicate membranes or the maximum detectable selectivity.

Although all of the membranes are essentially impermeable to multivalent ions, we expected the K^+ and Li^+ fluxes to increase with decreasing film thickness. A thinner film should lead to a stronger concentration gradient across the PEM to increase the supply of monovalent ions to the PEM-Nafion interface, thus

increasing the maximum current carried by that ion. This in turn should decrease the amount of water splitting at a specific current density. Experiments are not in accord with these expectations, and we are currently trying to understand why monovalent ion fluxes usually decrease with a decreasing number of bilayers in a PEM on Nafion. These unusual behaviors may stem from a low PEM thickness that is comparable to the thickness of an electrical double layer that forms inside this film.

3.3.4 Current density-voltage curves

Current density-voltage (*I-V)* curves often provide insight into limiting currents. *I-V* curves for ion-exchange membranes frequently exhibit three regions. At the lowest current densities, the potential drop across the membrane increases nearly linearly with increasing current density. As the applied current increases, cation electromigration inside Nafion increasingly exceeds the cation electromigration through the PEM, and a strong depletion zone forms near the interface (Figure 3.2). Equation 3.2 describes the theoretical limiting current density, I_{lim}, which occurs when the concentration of ions at the interface goes to

$$I_{lim} = \frac{P_s * c * F}{\Delta t_+} \qquad (3.2)$$

zero.[29] In this equation, P_s is the diffusion salt permeance of the PEM, c is the monovalent cation concentration in the source phase, F is the Faraday constant,

and Δt_+ is the difference in the monovalent cation transference numbers in the PEM and the Nafion.

Attainment of limiting conditions gives rise to a 'plateau' region in the *I-V* plot because further increases in current density require a large increase in potential. The intersection of the best-fit lines through the plateau and linear regions approximates the limiting current density (see the example in the inset of Figure 3.4). Further increases in current density lead to an overlimiting region where the potential drop across the film rises less dramatically with increases in current, presumably because water splitting or electroconvective forces supply additional ions at the interface.[34,42,43]

As Figure 3.4 shows, the *I-V* curves for membranes coated with $(PAH/PSS)_5PAH$, $(PAH/PSS)_3PAH$, and PAH/PSS/PAH films exhibit linear, ohmic regions only at very low current densities and transmembrane potentials <100 mV (inset). "Plateau" regions then appear where the transmembrane potential drop increases more rapidly with increasing current density. The limiting current in all three cases is <0.2 mA cm^{-2} and does not increase with a decreasing number of bilayers. As with measurements of ion flux (see Table 3.3), decreasing the film thickness unexpectedly does not increase permeability. Finally, Figure 3.4 shows that extensive water splitting at high current densities requires lower transmembrane potentials with thinner films. Wessling *et al.* recently reported a similar trend with poly(3,4- ethylenedioxythiophene):PSS/PEI multilayer films.[27]

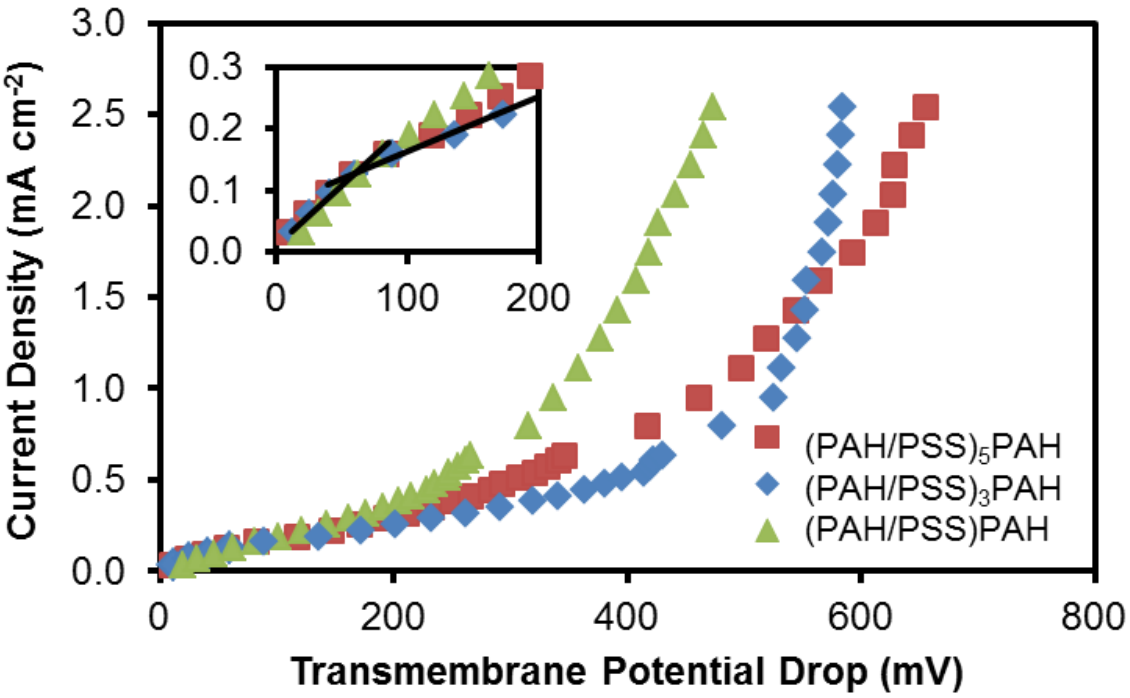

Figure 3.4. Current density as a function of transmembrane potential drop during electrodialysis through Nafion membranes coated with $(PAH/PSS)_5PAH$, $(PAH/PSS)_3PAH$, and PAH/PSS/PAH films. Electrodialysis employed solutions containing 0.01 M $LiNO_3$ and 0.1 M $Co(NO_3)_2$ in both the source and receiving phases. The inset shows an expanded view at low current densities along with best-fit lines from ohmic and "plateau" regions for the $(PAH/PSS)_3PAH$-coated membrane.

3.3.5 Characterization of membrane fouling

At overlimiting currents, water splitting near the PEM-Nafion interface gives protons that migrate toward the cathode and hydroxide ions that move toward the

anode. When the source phase contains transition-metal or lanthanide cations, insoluble hydroxide salts may form in the PEM or at its surface. Figure 3.5 shows SEM images of a fouled, $(PAH/PSS)_5PAH$-coated membrane after 1 h of ED at a highly overlimiting current. A thick cake-layer forms (images 3.5a and 3.5b), and EDS analysis of the precipitate confirms extensive amounts of cobalt (image 3.5c) and oxygen (image 3.5d) across the membrane. Table 3.5 shows the composition of the foulant in Figure 3.5b, and atomic percentages are reasonably consistent with $Co(OH)_2$, strongly suggesting that hydroxides from water splitting form insoluble cobalt hydroxides on the membrane surface at overlimiting current densities. The blue color of the foulant also suggests the presence of $Co(OH)_2$.

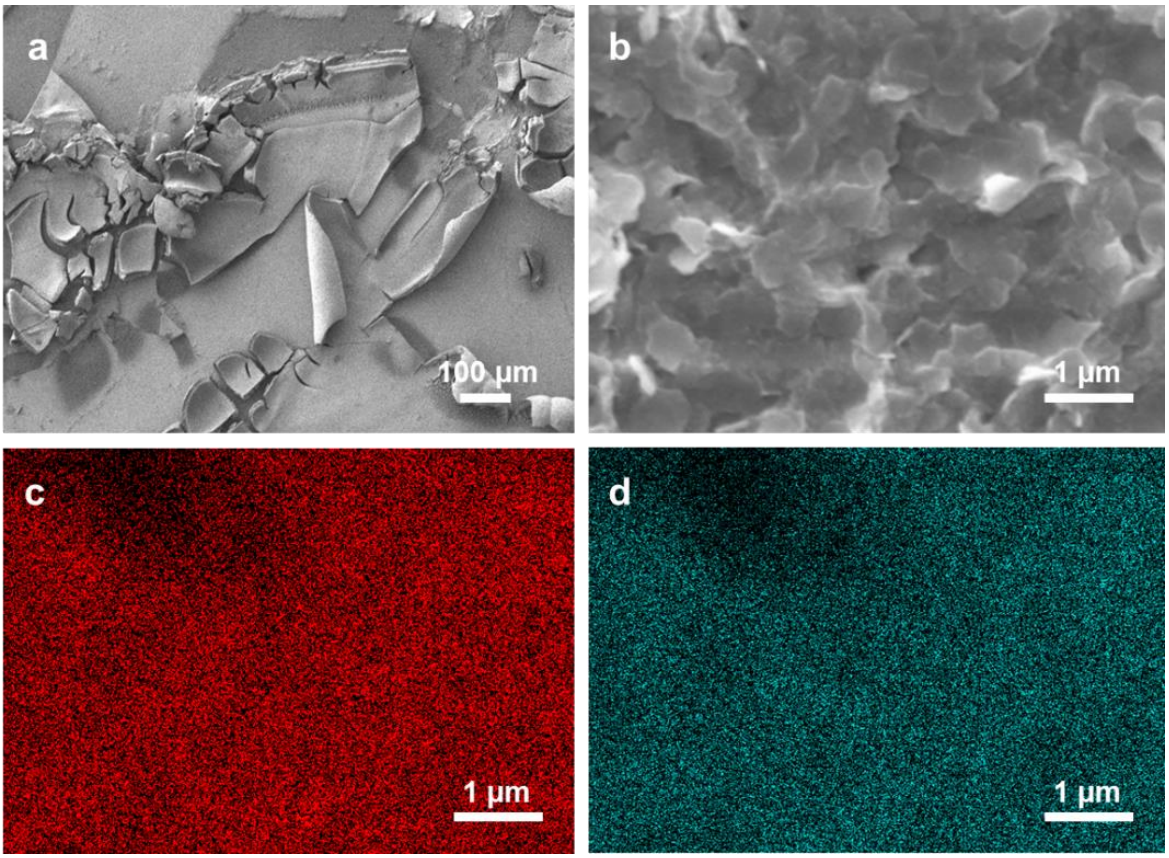

Figure 3.5. SEM images of fouled, $(PAH/PSS)_5PAH$-modified Nafion membranes at (a) low and (b) high magnifications. EDS imaging of the area in (b) shows extensive deposition of (c) cobalt (L_α line) and (d) oxygen (K_α line) in the fouled area. Fouling occurred during 1 h of ED at a current density of 2.54 mA cm^{-2} with 0.01 M $LiNO_3$ and 0.01 M $Co(NO_3)_2$ in the source phase and 0.01 M HNO_3 in the receiving phase.

Table 3.5. EDS elemental surface composition of a $(PAH/PSS)_5PAH$-modified Nafion membrane after fouling during 1 h of ED at 2.54 mA cm^{-2} with 0.01 M $LiNO_3$ and 0.01 M $Co(NO_3)_2$ in the source phase and 0.01 M HNO_3 in the receiving phase.

Element	C	O	F	Co
Weight %	4.67	30.06	1.94	63.33
Atomic %	11.29	54.5	2.96	31.20

3.3.6 Durability of membranes during ED

We evaluated the durability of membranes during 48 h of constant-current ED. Figure 3.6 shows the total quantity of Li^+ or Co^{2+} that passed into the receiving phase during 24 2-h periods (every 2 h, an aliquot of the receiving phase was collected for analysis prior to rinsing the cell with deionized water and adding fresh source- and receiving-phase solutions). During the first 6 h of ED, the total micromoles of Li^+ passing through the membrane during 2 h increased about 20%, perhaps due to conditioning of the membrane. The Co^{2+} flux was negligible initially but increased steadily after ~12 h of total ED, and the Li^+ flux decreased concurrently. Membrane selectivity during the first 12 h was >1000 but declined to ~25 after 48 h of ED. Electromigration of polyelectrolytes out of the PEM may lead to this selectivity decline. After 48 h, the selectivity is similar to that of a

membrane coated with either PAH/PSS/PAH or a PSS-terminated film ($(PSS/PAH)_5$). This lack of durability is a significant challenge, but either less hydrophobic base membranes or cross-linked PEMs may increase stability.

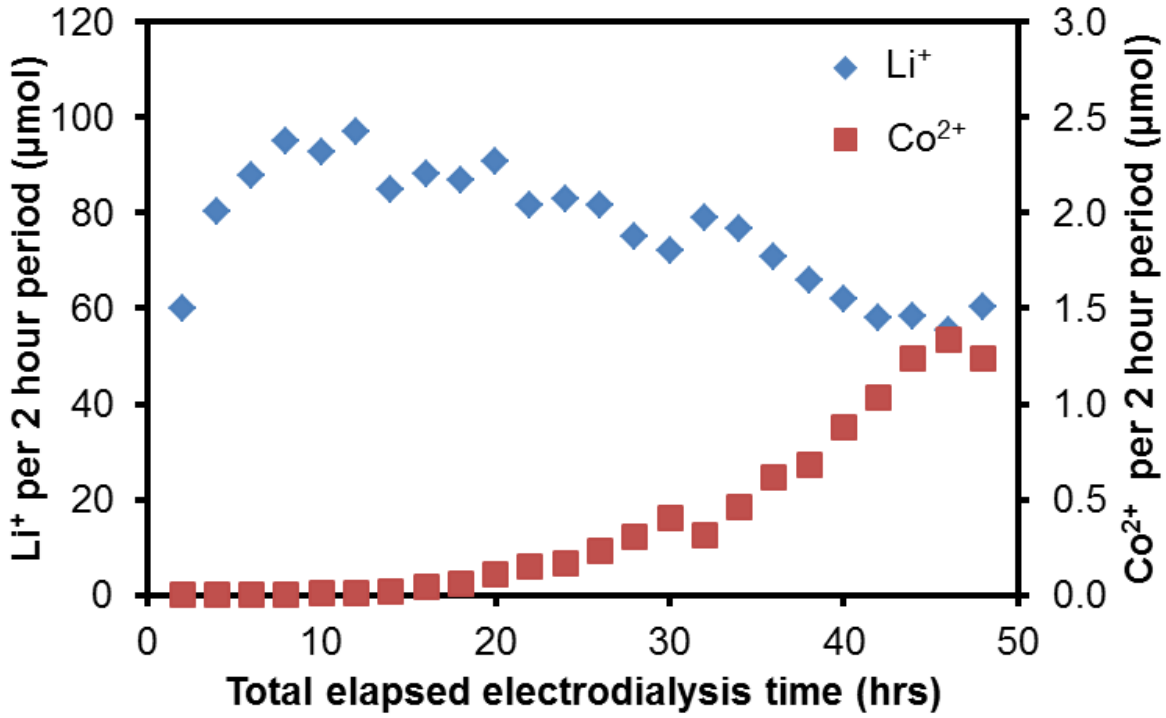

Figure 3.6. Total Li^+ and Co^{2+} passage (µmol) per 2-h sampling period during electrodialysis through a Nafion membrane modified with a $(PAH/PSS)_5PAH$ multilayer film. Electrodialysis used 0.02 M $LiNO_3$ and 0.02 M $Co(NO_3)_2$ in the source phase and 0.01 M HNO_3 in the receiving phase along with a current density of 0.63 mA cm^{-2}. Source- and receiving-phase solutions were changed after each 2-h interval prior to again performing electrodialysis with the same membrane.

3.4 Conclusions

Alternating adsorption of polycations and polyanions on Nafion yields membranes with high ED monovalent-ion selectivities for several pairs of monovalent/multivalent cations. Below overlimiting current densities, Li^+/Co^{2+} and K^+/La^{3+} selectivities are >1000 for ED through $(PAH/PSS)_5PAH$-coated Nafion membranes. Selectivities are >25 even for membranes modified with only 3 polyelectrolyte layers (PAH/PSS/PAH films). Transference numbers reach ~1 and selectivity is >5000 with high source-phase concentrations and underlimiting current densities. However, water splitting in the PEM reduces current efficiency at high current densities or low source-phase ion concentrations. Hydroxides formed from water splitting lead to precipitation of insoluble metal hydroxides on the membrane, which decreases current efficiency for monovalent ion transport. Current-voltage curves show that the limiting current does not increase with fewer bilayers in the $(PAH/PSS)_nPAH$ film, perhaps because the thickness of the electrical double layer inside the PEM is significant relative to the film thickness. Finally, ED for 48 h with the same membrane suggests that the films may be unstable in strong electric fields, as selectivity declines with extended ED time. To enhance the possible impact of these membranes, future work will explore methods to increase limiting current, stabilize PEMs, and form highly selective membranes on less-expensive cation-exchange substrates.

APPENDIX

Table 3A.1. Equilibrium constants, K, for formation of acetic acid and $La(OAc)_x$ complexes.[39]

Equilibrium	**Equilibrium Constant**	**Log K Employed for solutions Containing 0.1 M K(OAc) and 0.1 M $La(OAC)_3$[a]**	**Log K Employed for solutions Containing 0.01 M K(OAc) and 0.01 M $La(OAC)_3$[b]**
$H^+ + OAc \rightleftharpoons HOAc$	K_a	4.56	4.66
$La^{3+} + OAc \rightleftharpoons La(OAc)^{2+}$	K_1	1.70	2.18
$La^{3+} + 2OAc \rightleftharpoons La(OAc)_2^+$	K_2	2.68	3.47
$La^{3+} + 3OAc \rightleftharpoons La(OAc)_3$	K_3	3.29	3.53

[a]Values estimated based on literature data for solution with 0.1 M and 2.0 M ionic strength.
[b]Values estimated based on literature data for solutions with 0.0 M and 0.1 M ionic strength.

The equilibrium constants in Table 3A.1 suggest that $La(OAc)_x$ complexes will form at the salt concentrations we employed in electrodialysis (ED). Equations 3A.1-3A.3 give equilibrium expressions for $[La(OAC)]$, $[La(OAC)_2]$, and $[La(OAC)_3]$.

$$\frac{[La(OAC)]}{[La^{3+}][OAc]} = K_1 \text{ so } [La(OAC)] = K_1[La^{3+}][OAc] \quad \text{(3A.1)}$$

$$\frac{[La(OAC)_2]}{[La^{3+}][OAc]^2} = K_2 \text{ so } [La(OAC)_2] = K_2[La^{3+}][OAc]^2 \quad \text{(3A.2)}$$

$$\frac{[La(OAC)_3]}{[La^{3+}][OAc]^3} = K_3 \text{ so } [La(OAC)_3] = K_3[La^{3+}][OAc]^3 \quad \text{(3A.3)}$$

Equation 3A.4 gives the fraction of La(III) that does not bind OAc.

$$f_{La^{3+}} = \frac{[La^{3+}]}{[La^{3+}]+[La(OAC)]+[La(OAC)_2]+[La(OAC)_3]} \quad \text{(3A.4)}$$

Substituting equations 3A.1-3A.3 into 3A.4 we obtain equation 3A.5 for the fraction of free La^{3+}. Table 3A.1 lists estimates for the equilibrium constants.

$$f_{La^{3+}} = \frac{[La^{3+}]}{[La^{3+}]+K_1[La^{3+}][OAc]+K_2[La^{3+}][OAc]^2+K_3[La^{3+}][OAc]^3} =$$

$$\frac{1}{1+K_1[OAc]+K_2[OAc]^2+K_3[OAc]^3} \quad \text{(3A.5)}$$

Similarly, equations 3A.6-3A.8 give the fractions of the total La(III) contained in $La(OAc)$, $La(OAC)_2$, and $La(OAC)_3$ complexes.

$$f_{La(OAC)} = \frac{[La(OAC)]}{[La^{3+}]+[La(OAC)]+[La(OAC)_2]+[La(OAC)_3]} =$$

$$\frac{K_1[OAc]}{1+K_1[OAc]+K_2[OAc]^2+K_3[OAc]^3} \quad \text{(3A.6)}$$

$$f_{La(OAC)_2} = \frac{[La(OAC)_2]}{[La^{3+}]+[La(OAC)]+[La(OAC)_2]+[La(OAC)_3]} =$$

$$\frac{K_2[OAc]^2}{1+K_1[OAc]+K_2[OAc]^2+K_3[OAc]^3} \quad \text{(3A.7)}$$

$$f_{La(OAC)_3} = \frac{[La(OAC)_3]}{[La^{3+}]+[La(OAC)]+[La(OAC)_2]+[La(OAC)_3]} =$$

$$\frac{K_3[OAc]^3}{1+K_1[OAc]+K_2[OAc]^2+K_3[OAc]^3} \quad \text{(3A.8)}$$

To get concentrations, we simply multiply the fractions by the total concentration of La(III) species in the solution. However, we do not know the fraction of OAc that is free in solution. The fraction of free acetate depends on both protonation (equation 3A.9) and complexation of La(III).

$$\frac{[HOAc]}{[H^+][OAc]} = K_a \text{ so } [HOAc] = K_a[H^+][OAc] \quad \text{(3A.9)}$$

Thus, equations 3A.10-3A.12 describe the fraction of free OAc in solution.

$$f_{OAC} = \frac{[OAc]}{[OAc]+[HOAC]+[La(OAC)]+2[La(OAC)_2]+3[La(OAC)_3]} \quad \text{(3A.10)}$$

$$f_{OAC} = \frac{[OAc]}{[OAc]+K_a[H^+][OAc]+K_1[La^{3+}][OAc]+2K_2[La^{3+}][OAc]^2+3K_3[La^{3+}][OAc]^3} \quad \text{(3A.11)}$$

$$f_{OAC} = \frac{1}{1+K_a[H^+]+K_1[La^{3+}]+2K_2[La^{3+}][OAc]+3K_3[La^{3+}][OAc]^2} \quad \text{(3A.12)}$$

To solve for the concentrations of OAc and La(III) species, we first guessed a value of f_{OAC} and used it to calculate $[OAc]$ based on the total amount of OAc species in the solution. Subsequently, we substituted $[OAc]$ into equation 3A.5 to calculate $f_{La^{3+}}$ and, hence, $[La^{3+}]$. Substituting $[OAc]$ and $[La^{3+}]$ into equation 3A.12 gives a new estimate for f_{OAC}. We repeated the process until f_{OAC} converged to a constant value.

REFERENCES

REFERENCES

(1) Seto, T.; Ehara, L.; Komori, R.; Yamaguchi, A.; Miwa, T. *Desalination* **1978**, *25*, 1-7.

(2) Harkare, W. P.; Adhikary, S. K.; Narayanan, P. K.; Bhayani, V. B.; Dave, N. J.; Govindan, K. P. *Desalination* **1982**, *42*, 97-105.

(3) Kim, D. H. *Desalination* **2011**, *270*, 1-8.

(4) Jakobsen, M. R.; Fritt-Rasmussen, J.; Nielsen, S.; Ottosen, L. M. *J. Hazard. Mater.* **2004**, *106*, 127-132.

(5) Johnson, K. T.; Hill, C. G.; Amundson, C. H. *J. Food Sci.* **1976**, *41*, 770-777.

(6) Huang, C. H.; Xu, T. W.; Zhang, Y. P.; Xue, Y. H.; Chen, G. W. *J. Membr. Sci.* **2007**, *288*, 1-12.

(7) Tanaka, Y.; Ehara, R.; Itoi, S.; Goto, T. *J. Membr. Sci.* **2003**, *222*, 71-86.

(8) Reig, M.; Casas, S.; Aladjem, C.; Valderrama, C.; Gibert, O.; Valero, F.; Centeno, C. M.; Larrotcha, E.; Cortina, J. L. *Desalination* **2014**, *342*, 107-117.

(9) Grimm, J.; Bessarabov, D.; Sanderson, R. *Desalination* **1998**, *115*, 285-294.

(10) Mulyati, S.; Takagi, R.; Fujii, A.; Ohmukai, Y.; Matsuyama, H. *J. Membr. Sci.* **2013**, *431*, 113-120.

(11) Luo, Q. T.; Zhang, H. M.; Chen, J.; Qian, P.; Zhai, Y. F. *J. Membr. Sci.* **2008**, *311*, 98-103.

(12) Weber, A. Z.; Mench, M. M.; Meyers, J. P.; Ross, P. N.; Gostick, J. T.; Liu, Q. H. *J. Appl. Electrochem.* **2011**, *41*, 1137-1164.

(13) Xi, J. Y.; Wu, Z. H.; Teng, X. G.; Zhao, Y. T.; Chen, L. Q.; Qiu, X. P. *J. Mater. Chem.* **2008**, *18*, 1232-1238.

(14) Sata, T.; Mizutani, Y. *J. Polym. Sci., Part A: Polym. Chem.* **1979**, *17*, 1199-1213.

(15) Sata, T.; Yamane, R.; Mizutani, Y. *J. Polym. Sci., Part A: Polym. Chem.* **1979**, *17*, 2071-2085.

(16) Sata, T.; Yang, W. K. *J. Membr. Sci.* **2002**, *206*, 31-60.

(17) Guesmi, F.; Hannachi, C.; Hamrouni, B. *Ionics* **2012**, *18*, 711-717.

(18) Lambert, J.; Avila-Rodriguez, M.; Durand, G.; Rakib, M. *J. Membr. Sci.* **2006**, *280*, 219-225.

(19) Decher, G.; Hong, J. D. *Thin Solid Films* **1991**, *95*, 1430-1434.

(20) Li, X. F.; De Feyter, S.; Chen, D. J.; Aldea, S.; Vandezande, P.; Du Prez, F.; Vankelecom, I. F. J. *Chem. Mater.* **2008**, *20*, 3876-3883.

(21) Ahmadiannamini, P.; Li, X. F.; Goyens, W.; Meesschaert, B.; Vanderlinden, W.; De Feyter, S.; Vankelecom, I. F. J. *J. Membr. Sci.* **2012**, *403*, 216-226.

(22) Hoffmann, K.; Friedrich, T.; Tieke, B. *Polym. Eng. Sci.* **2011**, *51*, 1497-1506.

(23) Farhat, T. R.; Schlenoff, J. B. *J. Am. Chem. Soc.* **2003**, *125*, 4627-4636.

(24) Farhat, T. R.; Schlenoff, J. B. *Electrochem Solid St* **2002**, *5*, B13-B15.

(25) Rajesh, S.; Yan, Y.; Chang, H. C.; Gao, H. F.; Phillip, W. A. *ACS Nano* **2014**, *8*, 12338-12345.

(26) Krasemann, L.; Tieke, B. *Langmuir* **2000**, *16*, 287-290.

(27) Abdu, S.; Sricharoen, K.; Wong, J. E.; Muljadi, E. S.; Melin, T.; Wessling, M. *ACS Appl. Mater. Interfaces* **2013**, *5*, 10445-10455.

(28) Cheng, C.; White, N.; Shi, H.; Robson, M.; Bruening, M. L. *Polymer* **2014**, *55*, 1397-1403.

(29) White, N.; Misovich, M.; Yaroshchuk, A.; Bruening, M. L. *ACS Appl. Mater. Interfaces* **2015**, *7*, 6620-6628.

(30) Jiang, S. P.; Tang, H. L. *Colloids Surf., A* **2012**, *407*, 49-57.

(31) Vanýsek, P. In *CRC Handbook of Chemistry and Physics*; 94 ed.; CRC Press: 2014, p 77.

(32) Sata, T.; Yamaguchi, T.; Matsusaki, K. *J. Phys. Chem.* **1995**, *99*, 12875-12882.

(33) Sata, T.; Mine, K.; Higa, M. *J. Membr. Sci.* **1998**, *141*, 137-144.

(34) Abdu, S.; Marti-Caatayud, M. C.; Wong, J. E.; Garcia-Gabaldon, M.; Wessling, M. *ACS Appl. Mater. Interfaces* **2014**, *6*, 1843-1854.

(35) Van der Bruggen, B.; Koninckx, A.; Vandecasteele, C. *Water Res.* **2004**, *38*, 1347-1353.

(36) Carrière, D.; Krastev, R.; Schönhoff, M. *Langmuir* **2004**, *20*, 11465-11472.

(37) Wong, J. E.; Rehfeldt, F.; Hänni, P.; Tanaka, M.; Klitzing, R. V. *Macromolecules* **2004**, *37*, 7285-7289.

(38) Kolthoff, I. M.; Elmquist, R. *J. Am. Chem. Soc.* **1931**, *53*, 1217-1225.

(39) Martell, A. E.; Smith, R. M.; *Critical Stability Constants Volume 3: Other Organic Ligands*; Plenum Press: New York, **1979**; Vol. 3.

(40) Adusumilli, M.; Bruening, M. L. *Langmuir* **2009**, *25*, 7478-7485.

(41) Skoog, D. A.; Holler, F. J.; Crouch, S. R.; *Principles of Instrumental Analysis*, 6th ed.; Thomson Brooks/Cole: Belmont, CA, **2007**.

(42) Krol, J. J.; Wessling, M.; Strathmann, H. *J. Membr. Sci.* **1999**, *162*, 145-154.

(43) Rubinstein, I.; Zaltzman, B. *Phys. Rev. E* **2000**, *62*, 2238-2251.

CHAPTER 4

Nanofiltration and electrically-driven removal of ions for water purification and desalination

4.1 Introduction

Nanofiltration (NF) is attractive for its unique filtration properties that are between the properties of RO and ultrafiltration. With pore sizes around 1 nm, NF membranes exhibit low monovalent ion rejections but effectively remove most small organic molecules.[1] Because of high rejections of small molecules and divalent ions along with a relatively low pressure drop compared to RO processes, NF finds many applications in water treatment,[2] removal of pharmaceutical compounds,[3] and food processing.[4] Moreover, recent studies demonstrate that NF removes organic dye molecules from wastewater solutions in the textile manufacturing industry.[5,6]

Several research groups used NF membranes to filter charged dyes from wastewater effluent streams. Chakraborty and coworkers removed reactive black and reactive red dyes with 400 Da molecular weight cutoff (MWCO) NF membranes in a crossflow cell. They achieved up to 94% rejection of both dyes, but rejection declined as transmembrane pressure increased. Although flux increases linearly with applied pressure, losses in rejection offset any gains from faster throughput.[7] Amini *et al.* modified polysulfone ultrafiltration membranes via acrylic acid grafting to achieve NF properties. These films rejected >86% of

several organic dyes, and rejection did not change appreciably upon increasing the transmembrane pressure from 1 to 4 bar. However, rejection declined ~20% in the presence of 100 mM Na_2SO_4, presumably because charge shielding reduced Donnan exclusion at high salt concentrations.[8] Hong and Miller used $(PSS/PAH)_4PSS$ films deposited on alumina membranes to remove dyes from water. Dye rejections >99.9% and a flux of 2 m^3 m^{-2} day^{-1} at a transmembrane pressure of 4.8 bar suggest that such NF films are promising for removing small molecules from salt solutions.[9] Numerous other studies focused on fouling issues[10,11] and specialized applications removing dyes from wastewater effluents in textile manufacturing with NF.[12-14] The first part of this chapter investigates PEMs deposited on ultrafiltration membranes as selective NF skins for removing charged dye molecules.

The second portion of this chapter examines the separation of charged species through ion concentration polarization (ICP). In this method, ion passage through electrically charged nanopores occurs selectively because the Debye length is non-negligible compared to the double-layer thickness in the pore.[15] Under an applied electric field across the pores, ions migrate toward the anode or cathode. If the nanoporous material, referred to as a nanojunction, is cation-selective, cations migrate through the junction while anions are rejected. The result is an ion-depleted region on the anode-side of the junction and an enrichment zone on the cathode-side. However, charge separation across the junction is unstable and requires high (>100V) potentials to sustain.[16]

Some studies aimed to harness ICP as a means for concentrating or removing ions in solution.[17] Using Nafion as a cation-selective nanochannel, Ko developed a single-channel nanofluidic device for preconcentrating proteins. They exploited ICP to prevent passage of charged dyes through a nanofluidic channel. As Figure 4.1a shows, the device consisted of a single channel overlaid on a cation-selective Nafion strip, obstructing only a small portion of the microchannel. Upon application of an electric field, cations pass through the Nafion strip but anions do not, and a depletion region forms in the vicinity of the Nafion while all ions accumulate just outside this region as a result of flow through the microchannel (Figure 4.1b). The protein concentration in the enrichment region increased with increasing voltage drop across the Nafion nanojunction.[18]

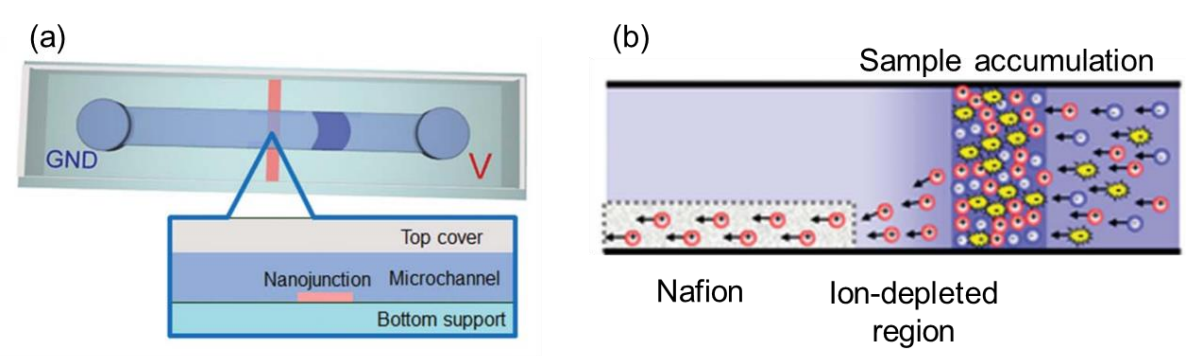

Figure 4.1. Schematic diagram of a single-channel preconcentration device (a) and formation of the ion-depletion region (b). (Reprinted with permission from *Lab Chip* 2012, *12*, 4472-4482)[18]

Choi *et al.* constructed a device with Nafion deposited on the walls of a capillary where marker dye concentrations increased ~2-fold in a 300 V applied electric field. Moreover, ICP occurs in the presence of electroosmotic or pressure-driven flow.[19] Kim and Han coupled pressure-driven flow with ICP for direct desalination of seawater (Figure 4.2). Ion-depletion near a Nafion nanojunction causes complete rejection of charged species, including biological macrostructures such as blood cells.[20] This chapter in part investigates ICP as a mechanism to remove ions from a solvent.

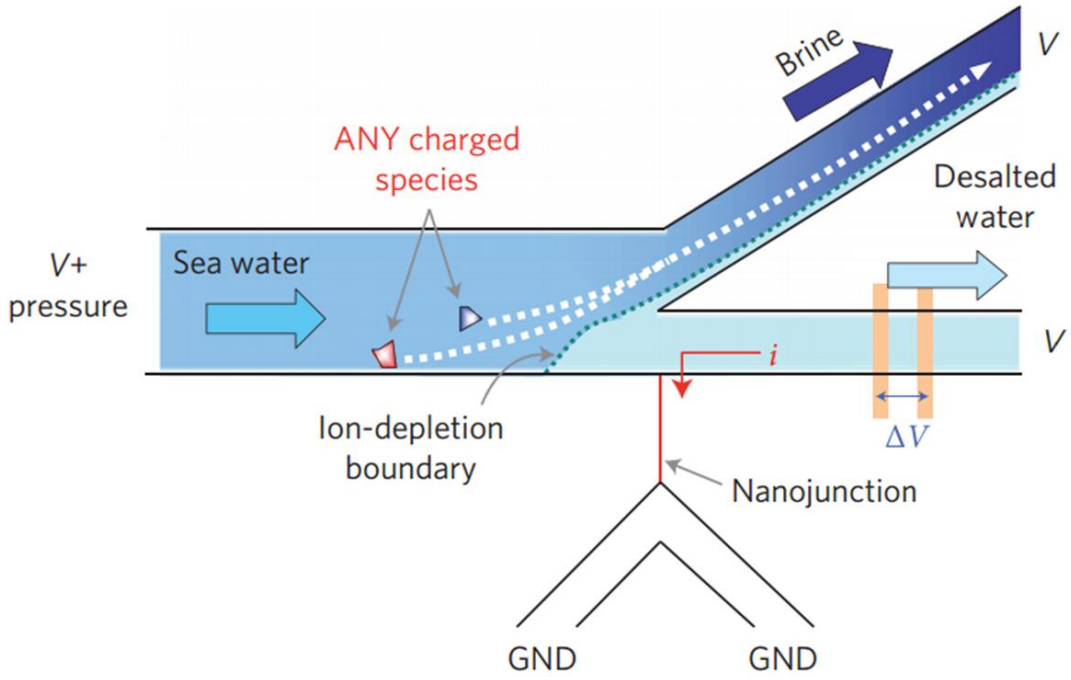

Figure 4.2. Schematic diagram of a microfluidic electrokinetic device for desalination by ion concentration polarization. (Reprinted with permission from *Nat. Nanotechnol.* 2010, *5*, 297-301)[20]

4.2 Experimental Section

4.2.1 Materials

PSS (MW = 70,000 Da), PAH (MW = 15,000 Da), PDADMAC (MW = 100,000-150,000 Da), fluorescein, reactive orange 16 dye, Nafion 117 solution, sodium chloride, potassium acetate (KOAc), manganese (II) chloride, and sodium bromide were purchased from Sigma-Aldrich and used without further purification. Polyethersulfone (PES) membranes (25,000 and 100,000 MWCO) were a gift from Pall Corporation (Port Washington, NY) and Whatman 30 nm polycarbonate track-etch (PCTE) membranes were purchased from GE Healthcare (Little Chalfont, UK). Silicon wafers for lithography were obtained from University Wafer (Boston, MA). SU-8 50 photoresist was purchased from Microchem Corporation (Newton, MA), and the polydimethyl siloxane (PDMS) elastomer and curing agent were obtained as a kit (Sylgard-184) from Dow Corning (Midland, MI). Piranha cleaning solution was prepared from 3 parts sulfuric acid (98%, Fisher) to 1 part hydrogen peroxide (30%, Fisher). *This solution must be handled with care and not stored in sealed containers*. The pH of the PAH, PSS, and PDADMAC solutions was adjusted to 2.3, 2.3, and 7.0, respectively, with dilute solutions of HCl or NaOH.

4.2.2 Film Deposition

PES ultrafiltration membranes were mounted in a home-built membrane holder that exposes only the feed side of the membrane to polyelectrolyte

solutions. The deposition solutions contained 0.02 M (with respect to the repeating unit) polyelectrolytes along with 0.5 M $MnCl_2$ for PSS and 0.5 M NaBr for PAH and PDADMAC. Defined pH levels determine the charge state for polyelectrolytes during deposition, and addition of supporting electrolytes to deposition solutions increases the surface charge density in PEMs.[21] Polyelectrolytes were adsorbed with alternating PSS and either PAH or PDADMAC layers according to a published procedure.[22] PEMs usually contained 4.5 polyelectrolyte bilayers (PSS served as the terminating layer to give a negatively charged film) to maintain high flux while ensuring that the underlying substrate was adequately covered.[23]

4.2.3 Nanofiltration

NF experiments were performed in the lab of Ismail Koyuncu of Istanbul Technical University. Figure 4.3 shows the apparatus used for NF experiments. Real or model dye solutions were placed in the feed tank and pumped via a centrifugal pump through a large microporous filter and a compartment containing pH, temperature, and conductivity probes. Following passage through the pump, solutions flowed across the surface of membranes placed in a SEPA crossflow cell (Sterlitech, Kent, WA). Spacers were used on the feed side to reduce concentration polarization and fouling by inducing turbulent flow across the surface. Permeate solutions passed through a second compartment containing pH, conductivity, and temperature probes before release into a permeate tank.

The tank was placed on a balance to continuously monitor flux across the membrane, and retentate was recirculated to the feed tank.

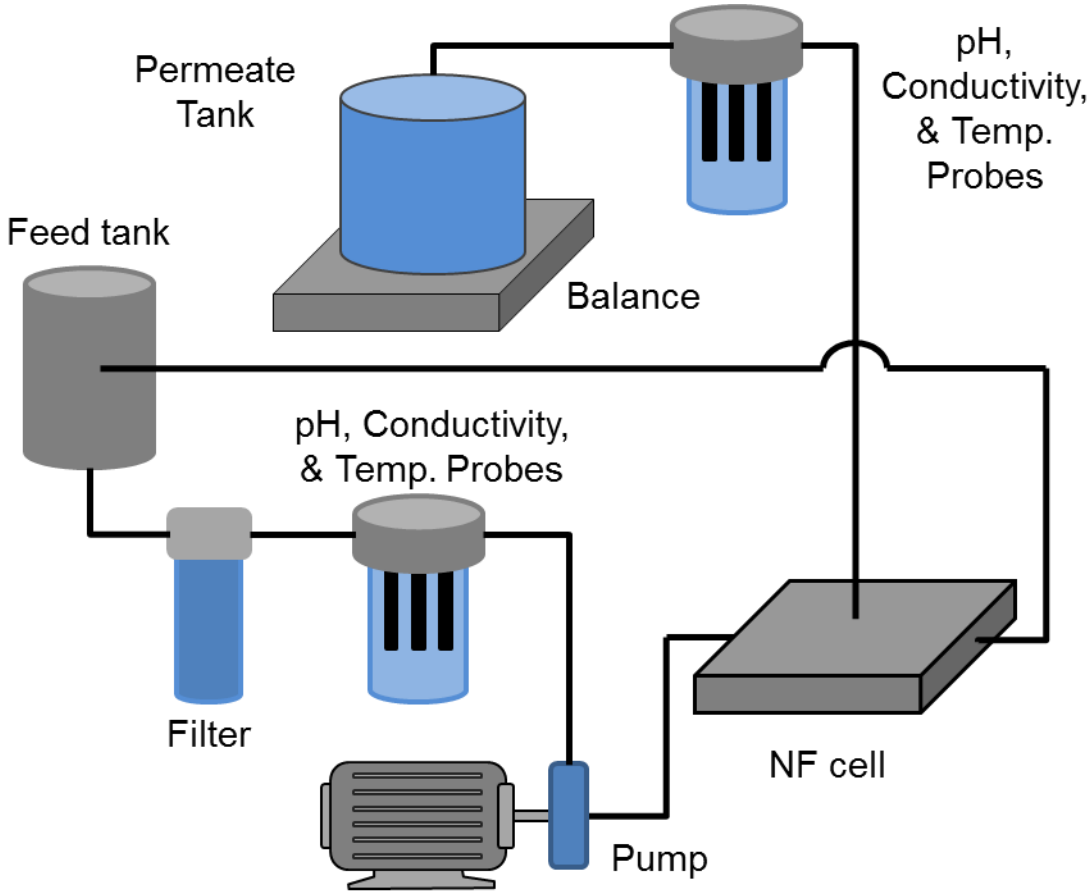

Figure 4.3. Schematic diagram of the cross-flow apparatus used for NF experiments with textile-manufacturing dye solutions. Wastewater retentate recirculates via the feed tank, and the membrane permeate collects in a secondary tank on a balance to monitor flux.

A model dye solution was prepared with 1 g/L of reactive orange 16 (structure shown in Figure 4.4) and 0.01 M NaCl to mimic dye solutions used in

the textile manufacturing industry. In NF experiments, 10 L of the solution was recirculated continuously through the crossflow cell for three hours at a pressure of 4.8 bar, and the permeate and feed concentrations were analyzed by UV-Vis spectroscopy to determine rejection. The exposed membrane area was approximately 150 cm^2. Other experiments aimed to remove dye molecules from wastewater effluent from a textile manufacturing facility in Istanbul, Turkey. Dye bath solutions were obtained from the immersion step during textile coloration, and dye wash solutions originated from the rinsing step afterward to remove loosely bound dye during textile modification.

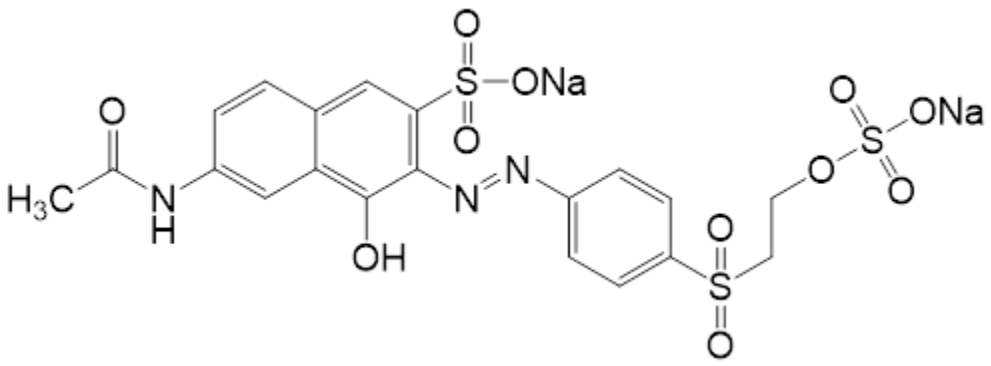

Figure 4.4. Structure of reactive orange 16 dye

4.2.4 Soft lithography and fabrication of a microfluidic device

Microfluidic devices require master templates that serve as molds for PDMS elastomers. Preparation of the template followed a literature procedure.[24] Initially, 100 mm silicon wafers were cleaned with piranha solution to remove any traces of

organic molecules. As Figure 4.5 shows, wafers were spin-coated with 1 mL SU-8 50 photoresist at 500 rpm for 15 s then at 1000 rpm for 30 s to produce a 100 µm photoresist film. A pre-bake step on a hot plate at 95°C for 15 min initiated curing of the polymer to facilitate handling. The coated wafer was then exposed, through a transparency printed with a single 300 µm x 4 cm channel, to ultraviolet light to induce cross-linking in the photoresist. Post-baking for 5 min at 95 °C ensured the exposed regions were fully cured. The master was developed in propylene glycol monoethyl ether acetate until the un-exposed photoresist dissolved. The resulting master was cured overnight in an oven at 75°C.[25]

PDMS fluidic devices were prepared according to established soft lithography techniques as Figure 4.5 shows.[26,27] PDMS was mixed with a cross-linking curing agent from the Sylgard-184 kit, degassed, and poured on the master. A 20:1 ratio of PDMS to cross-linker was used initially to facilitate thermocuring of the polymer to PCTE membranes and other PDMS components. After 13 min in an oven at 75°C, an additional PDMS layer with a 5:1 ratio was added for rigidity.[25] Following a second 13-min cure, the silicone was carefully removed. Holes were mechanically punched through the cured PDMS to create solvent wells. Coupled with a second 4 cm channel, a cross-channel device was assembled by layering the first channel, a 30 nm PCTE membrane (some modified with Nafion 117), and the inverted second channel at a 90-degree angle (see Figure 4.6 below).

Ion-depletion experiments with cross-channel devices employed a power supply (Bio-rad, Hercules, CA) to apply high potentials across the nanoporous membrane. The channels were filled with 10 mM sodium chloride and 10 mM fluorescein, and electrodes were placed at the ends of each channel. The extent of ion depletion was monitored with a fluorescence microscope equipped with a CCD detector. Some experiments incorporated flow (1μL min^{-1} in both channels) with each channel filled with 10 mM fluorescein and 10 mM NaCl or KOAc to evaluate ICP as a continuous method for desalination. K^+ cations have greater electrophoretic mobility than OAc^- which may increase ICP near cation-selective nanochannels, particularly compared to studies concerning NaCl where Cl^- is the more mobile ion.[28] Cation concentrations were determined in some cases using flame atomic absorption spectroscopy. Flow experiments utilized Nafion-modified 30 nm PCTE membranes prepared by flowing ~1 mL Nafion 117 solution (5% w/w in lower aliphatic alcohols and water) at 5 bar through PCTE membranes mounted in an Amicon cell (EMD Millipore, Billerica, MA). After modification, membranes were removed from the cell and air dried.

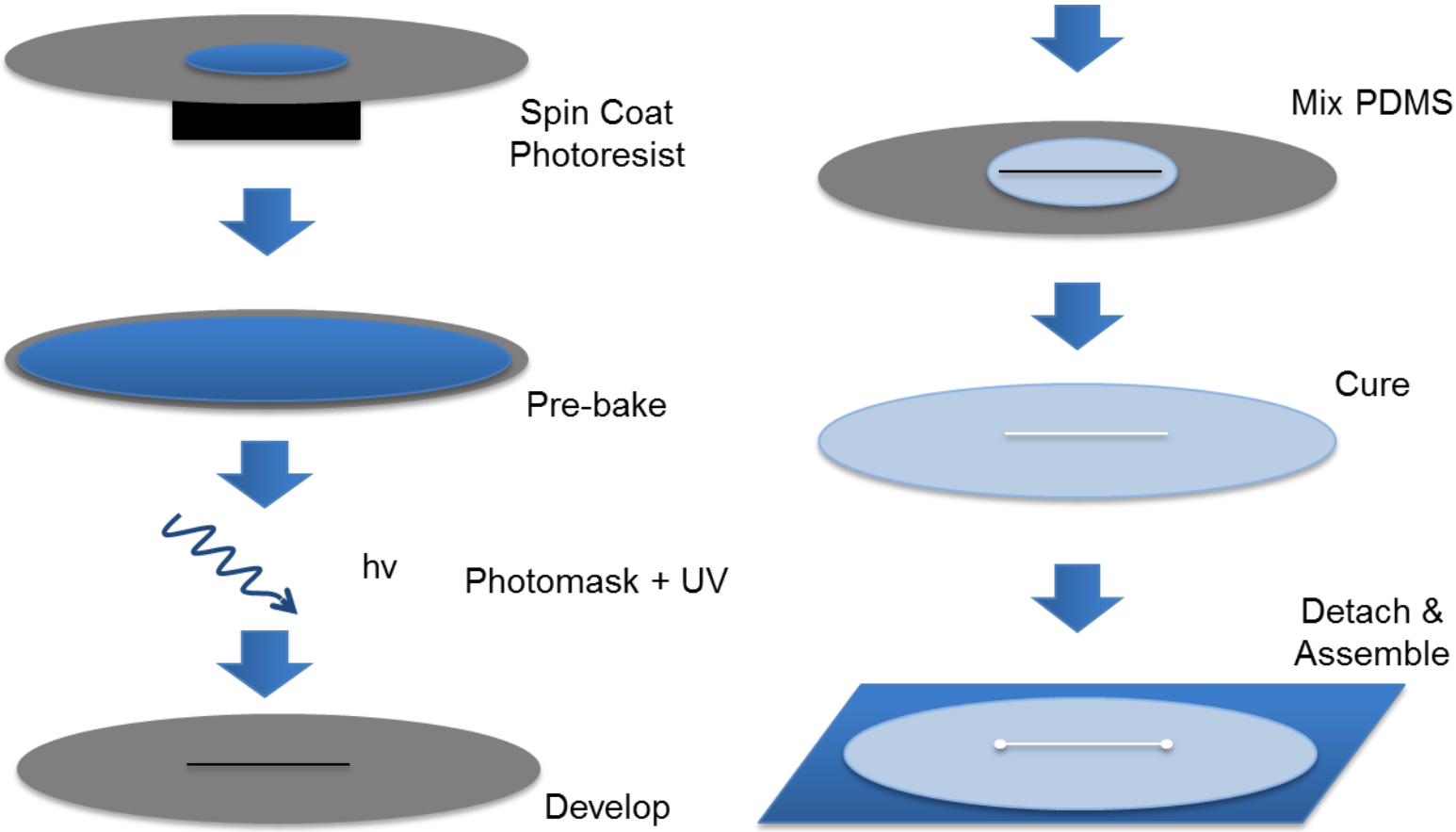

Figure 4.5. Master preparation and PDMS device fabrication with silicon wafers

4.3 Results and Discussion

4.3.1 Organic dye removal from industrial effluent

Table 4.1 shows the rejections of reactive orange 16 dyes from solutions filtered using the NF apparatus in Figure 4.3. Bare membranes show very low rejection after three hours of NF, presumably because the large pore sizes in the unmodified ultrafiltration membranes readily allow passage of small organic dye molecules. A small amount of rejection likely occurs with bare membranes because of electrostatic repulsion between the dye and the negatively charged membrane surface.[29]

All modified PES membranes show high rejections (>91%), but initial results show rejections >98% for 25,000 Da MWCO membranes during experiments with 3 h of continuous NF. Interestingly, while permeate flux through these membranes remains steady for bare (48.5 L m^{-2} h^{-1} bar^{-1}) and coated 100,000 Da MWCO membranes (10.4 L m^{-2} h^{-1} bar^{-1} and 5.2 L m^{-2} h^{-1} bar^{-1} for PSS/PAH and PSS/PDADMAC films, respectively), PSS/PDADMAC-coated 25,000 Da PES membranes show flux increases from ~1 L m^{-2} h^{-1} bar^{-1} to 3.1 L m^{-2} h^{-1} bar^{-1} over the course of the experiment, suggesting that the permeability increases. Similarly, flux through PSS/PAH films increases from ~1 L m^{-2} h^{-1} bar^{-1} to 1.5 L m^{-2} h^{-1} bar^{-1}. As expected, fluxes are large then a 100,000 rather than a 25,000 D MWCO membrane serves as the substrate for polyelectrolyte adsorption.

Table 4.1. Reactive Orange 16 dye rejections in NF[a] through PES membranes coated with PEMs.

Membrane	Modification	Rejection (%)
PES 25 kDa MWCO	$[PSS/PAH]_4PSS$	98.1
PES 25 kDa MWCO	$[PSS/PDADMAC]_4PSS$	99.6
PES 100 kDa MWCO	$[PSS/PAH]_4PSS$	95.9
PES 100 kDa MWCO	$[PSS/PDADMAC]_4PSS$	91.4
PES 100 kDa MWCO	Bare	20.7

[a]The feed solutions contained 1 g/L reactive orange 16 dye and 0.5 M NaCl

Some experiments examined NF with PEMs on PES ultrafiltration membranes to remove dyes from water used in textile manufacturing. Remarkably, all membranes tested showed rejections >99% for NF of the dye-bath solutions and near 100% for the dye-wash effluent (Table 4.2). For comparison, bare 100,000 Da MWCO PES rejects ~89% of the dye, likely higher than the model reactive orange 16 system because the textile dyes are more densely charged or significantly higher molecular weight than reactive orange 16. Moreover, dye-bath permeate flux through PSS/PDADMAC films is ~1 L m^{-2} h^{-1} bar^{-1} compared to 3-4 L m^{-2} h^{-1} bar^{-1} for PSS/PAH films. This suggests PSS/PDADMAC forms higher density or thicker PEMs on PES membranes. Nevertheless, these preliminary results indicate ultrafiltration membranes modified with PEMs are promising for removal of charged organic dyes from wastewater

effluents in the textile industry. However, the fluxes are only 1-4 L m^{-2} h^{-1} bar^{-1}, which is lower than the specific flux through some NF membranes.[30]

Table 4.2. Dye rejections in NF of textile solutions through PES membranes coated with PEMs.

Membrane	Modification	Dye Bath Rejection (%)	Dye Wash Rejection (%)
PES 25 kDa MWCO	$[PSS/PAH]_4PSS$	99.1	-
PES 25 kDa MWCO	$[PSS/PDADMAC]_4PSS$	99.7	100.0
PES 100 kDa MWCO	$[PSS/PAH]_4PSS$	99.8	100.0
PES 100 kDa MWCO	$[PSS/PDADMAC]_4PSS$	99.5	99.8
PES 100 kDa MWCO	Bare	89.1	-

4.3.2 Ion depletion in a microfluidic cross-channel device

Application of an electrical potential between two channels separated by a cation selective membrane should lead to accumulation of ions on the cathode side of the membrane and depletion of ions on the anode side (Figure 4.6). The depletion occurs because cations carry a larger fraction of the current in the track etch membrane than in the channels, due to a negative charge in the track-etch pores. Thus, electromigration carries more cations away from the membrane-anode channel interface than it brings to this interface. Similarly, electromigration

removes anions from this interface faster than they enter through the membrane, so depletion occurs for both cations and anions.

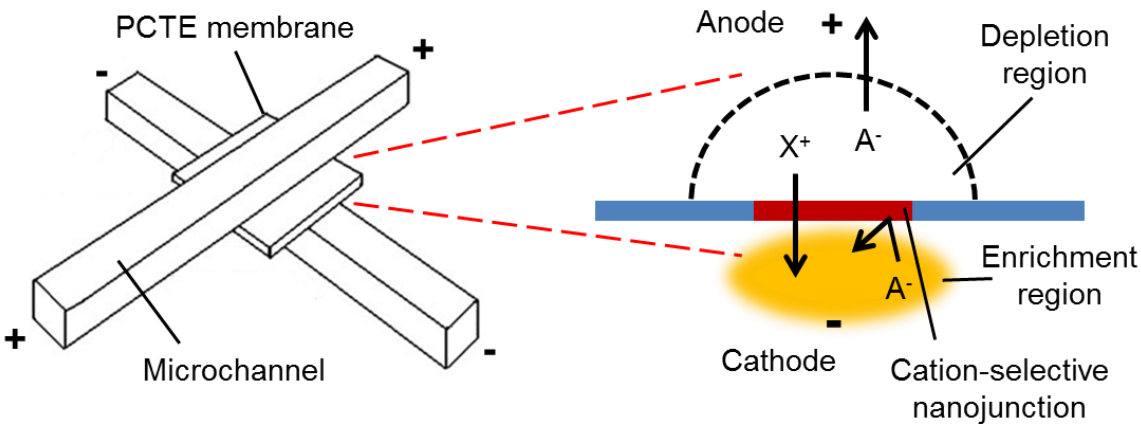

Figure 4.6. Schematic diagram and depletion region formation in a microfluidic cross-channel device with a cation-selective junction.

Figure 4.7 shows the progression of ion depletion and enrichment zones in a microfluidic cross-channel device. When the applied potential is +500 V in the anodic channel (vertical channel in the images) versus the cathode channel (horizontal in the images), ion-depletion zones form rapidly. After application of the potential for only 5 s (Figure 4.7b), the fluorescein concentration decreases on the anode-side of the PCTE membrane nanojunction and increases on the cathode-side (horizontal channel). Figure 4.7c shows formation of a large depletion region in the anodic (vertical) chamber and concurrent enrichment in the cathode (horizontal) chamber. Fluorescein molecules migrate toward the

nanojunction on the cathode-side because of electromigration and electrically balance the large influx of positively charged ions from the anode-channel. Figure 4.7d illustrates the near steady-state for ICP after 30 s of continuous ICP at 500 V. At higher applied potentials formation of electroconvective vortices brings additional ions to the bulk/depletion region interface and the extent of ICP decreases.[31]

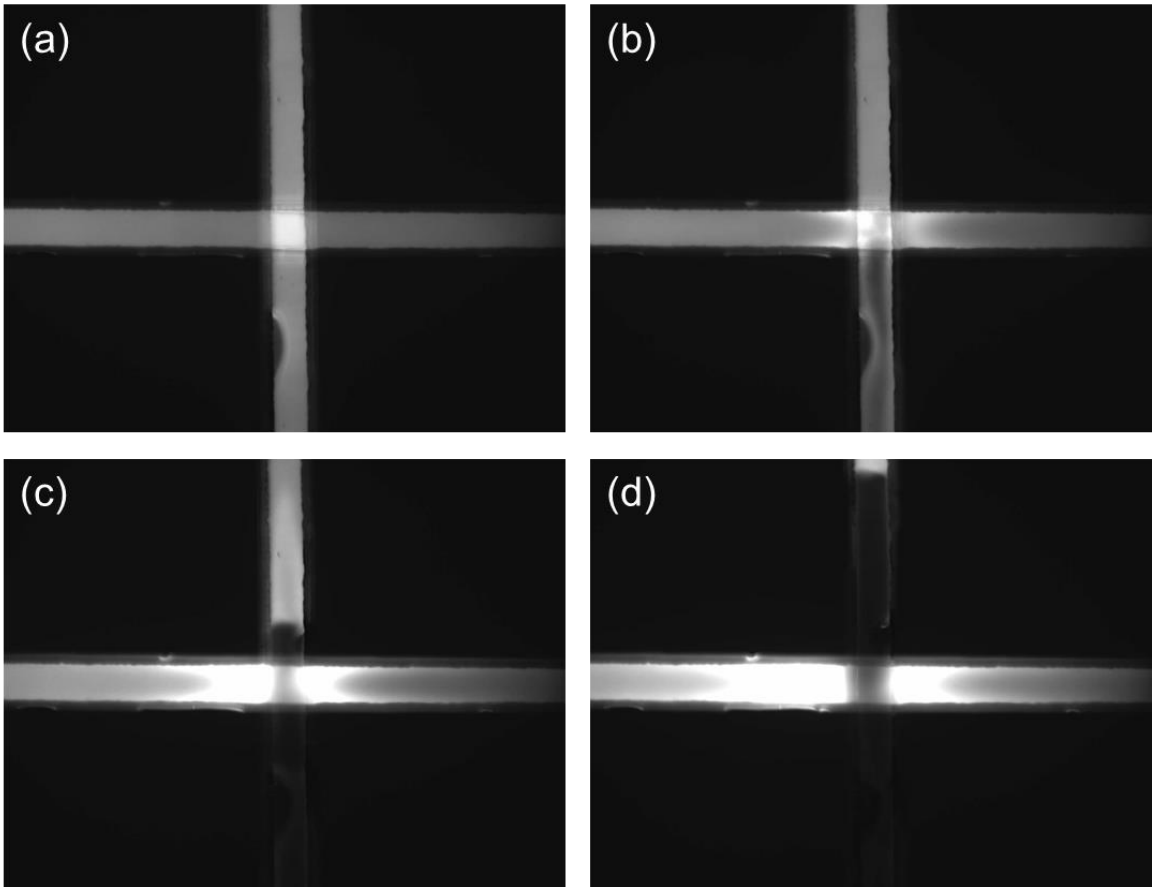

Figure 4.7. Ion depletion and enrichment in a microfluidic cross-channel device after (a) 0 s, (b) 5 s, (c) 10 s, and (d) 30 s. ICP occurred with no flow in either channel and +500 V in the anodic channel (vertical channel in images). The channels are separated with an unmodified PCTE membrane with 30 nm pores, and the solution initially contained 10 mM fluorescein and 10 mM NaCl.

Preliminary experiments with flow through the anode and cathode channels during ICP suggest that this technique may enable small-scale removal of salts from solution. Figure 4.8 shows the removal of fluorescein in an anodic (vertical)

flow channel using a 100 V potential between the anodes and cathodes where both channels contain 10 mM NaCl and 10 mM fluorescein. A cation-selective Nafion 117-modified 30 nm PCTE membrane separated the anodic and cathodic channels. Although the size of the ion depletion region (vertical channel, flow from top to bottom) exceeds the viewing area of the microscope, the absence of observable fluorescein in the channel indicates reduced ion concentrations in this region. In parallel, higher fluorescein levels in the downstream side of the cathode channel (flow left to right in image) indicate enrichment in this channel. Other experiments with 10 mM KOAc and 10 mM fluorescein and 1 μL min^{-1} flow in each channel confirm ion concentrations increase in the cathode channel ~50% while decreasing proportionally on the anode-side.

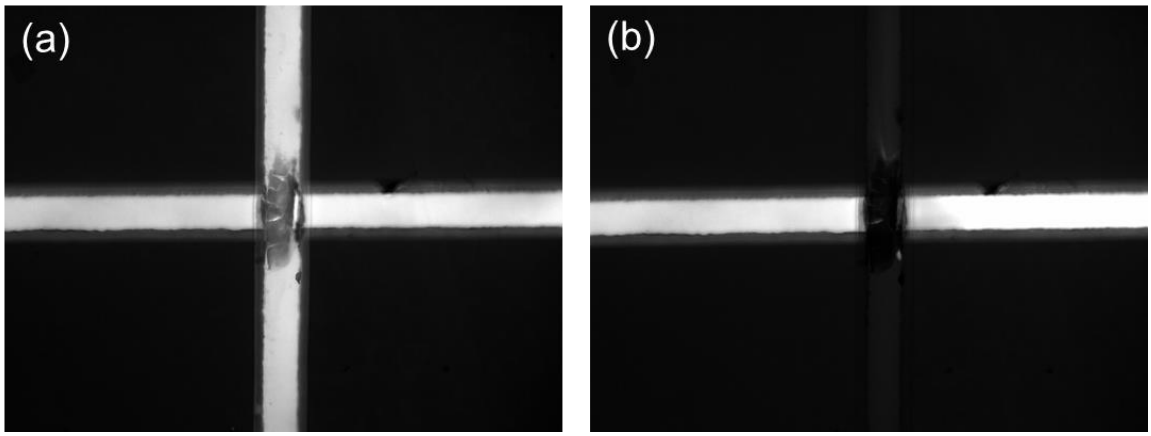

Figure 4.8. Ion depletion and enrichment in a microfluidic cross-channel device after (a) 0 s and (b) 10 s. ICP occurred with 1 μL min^{-1} flow in each channel and the anodic (vertical) channel at +100 V with respect to the cathodic (horizontal) channel. Solutions initially contained 10 mM KOAc and 10 mM fluorescein.

4.4 Conclusions

PEMs deposited on ultrafiltration membranes form selective barriers for removal of organic dyes from waste solutions generated in textile manufacturing. Early results show that membranes prepared from these films reject >99% of dyes from clothing manufacturing wastewater, and fluxes are comparable to those found through commercial NF membranes. In addition, ICP shows promise as a method to remove salts from solution, but the large currents required to maintain ion-enrichment and depletion zones in larger channels may limit its utility. Nevertheless, continuous ICP in microfluidic experiments with flow reduces ion concentrations ~50%, and this method may be suitable for specialized applications where small sample volumes reduce the feasibility of filtration techniques.

REFERENCES

REFERENCES

(1) Mohammad, A. W.; Teow, Y. H.; Ang, W. L.; Chung, Y. T.; Oatley-Radcliffe, D. L.; Hilal, N. *Desalination* **2015**, *356*, 226-254.

(2) Shahmansouri, A.; Bellona, C. *Water Sci. Technol.* **2015**, *71*, 309-319.

(3) Miralles-Cuevas, S.; Oller, I.; Perez, J. A. S.; Malato, S. *Water Res.* **2014**, *64*, 23-31.

(4) Salehi, F. *Food Bioprod. Process.* **2014**, *92*, 161-177.

(5) Aouni, A.; Fersi, C.; Cuartas-Uribe, B.; Bes-Pia, A.; Alcaina-Miranda, M. I.; Dhahbi, M. *Desalination* **2012**, *297*, 87-96.

(6) Chollom, M. N.; Rathilal, S.; Pillay, V. L.; Alfa, D. *Water SA* **2015**, *41*, 398-405.

(7) Chakraborty, S.; Purkait, M. K.; DasGupta, S.; De, S.; Basu, J. K. *Sep. Purif. Technol.* **2003**, *31*, 141-151.

(8) Amini, M.; Arami, M.; Mahmoodi, N. M.; Akbari, A. *Desalination* **2011**, *267*, 107-113.

(9) Hong, S. U.; Miller, M. D.; Bruening, M. L. *Ind. Eng. Chem. Res.* **2006**, *45*, 6284-6288.

(10) Van der Bruggen, B.; Cornelis, G.; Vandecasteele, C.; Devreese, I. *Desalination* **2005**, *175*, 111-119.

(11) Chidambaram, T.; Oren, Y.; Noel, M. *Chem. Eng. J. (Lausanne)* **2015**, *262*, 156-168.

(12) Koyuncu, I. *Desalination* **2002**, *143*, 243-253.

(13) Capar, G.; Yilmaz, L.; Yetis, U. *J. Membr. Sci.* **2006**, *281*, 560-569.

(14) Liang, C. Z.; Sun, S. P.; Li, F. Y.; Ong, Y. K.; Chung, T. S. *J. Membr. Sci.* **2014**, *469*, 306-315.

(15) Kim, S. J.; Wang, Y. C.; Lee, J. H.; Jang, H.; Han, J. *Phys. Rev. Lett.* **2007**, *99*.

(16) Kim, P.; Kim, S. J.; Han, J.; Suh, K. Y. *Nano Lett.* **2010**, *10*, 16-23.

(17) Kim, S. J.; Song, Y. A.; Han, J. *Chem. Soc. Rev.* **2010**, *39*, 912-922.

(18) Ko, S. H.; Song, Y. A.; Kim, S. J.; Kim, M.; Han, J.; Kang, K. H. *Lab Chip* **2012**, *12*, 4472-4482.

(19) Choi, D.; Choi, A.; Kim, D. S. *Int. J. Precis. Eng. Man.* **2015**, *16*, 1467-1471.

(20) Kim, S. J.; Ko, S. H.; Kang, K. H.; Han, J. *Nat. Nanotechnol.* **2010**, *5*, 297-301.

(21) Ouyang, L.; Malaisamy, R.; Bruening, M. L. *J. Membr. Sci.* **2008**, *310*, 76-84.

(22) Decher, G. *Science* **1997**, *277*, 1232-1237.

(23) Stanton, B. W.; Harris, J. J.; Miller, M. D.; Bruening, M. L. *Langmuir* **2003**, *19*, 7038-7042.

(24) Qin, D.; Xia, Y. N.; Whitesides, G. M. *Nat. Protoc.* **2010**, *5*, 491-502.

(25) Halpin, S. T.; Spence, D. M. *Anal. Chem.* **2010**, *82*, 7492-7497.

(26) McDonald, J. C.; Duffy, D. C.; Anderson, J. R.; Chiu, D. T.; Wu, H. K.; Schueller, O. J. A.; Whitesides, G. M. *Electrophoresis* **2000**, *21*, 27-40.

(27) Duffy, D. C.; McDonald, J. C.; Schueller, O. J. A.; Whitesides, G. M. *Anal. Chem.* **1998**, *70*, 4974-4984.

(28) Vanýsek, P. In *CRC Handbook of Chemistry and Physics*; 94 ed.; CRC Press: 2014, p 77.

(29) Susanto, H.; Ulbricht, M. *J. Membr. Sci.* **2009**, *327*, 125-135.

(30) Gopalakrishnan, A.; Mathew, M. L.; Chandran, J.; Winglee, J.; Badireddy, A. R.; Wiesner, M.; Aravindakumar, C. T.; Aravind, U. K. *ACS Appl. Mater. Interfaces* **2015**, *7*, 3699-3707.

(31) Kim, S. J.; Ko, S. H.; Kwak, R.; Posner, J. D.; Kang, K. H.; Han, J. *Nanoscale* **2012**, *4*, 7406-7410.

CHAPTER 5

Conclusions and future directions

This dissertation examines nanofiltration and electrically driven processes for ion separations. PEMs deposited on cation-exchange membranes form highly selective barriers for cation transport in electrodialysis, but selectivity decreases significantly at strongly overlimiting currents, showing the importance of understanding ion-transport mechanisms. Thus, chapter 1 introduces the utility and origins of ion separations, reviews specific methods for membrane-based ion separations including their mass transport mechanisms, and discusses applications and formation of thin polymer films.

Chapter 2 demonstrates that PEMs deposited on commercial cation-exchange membranes give rise to electrodialysis selectivities >1000 for monovalent over divalent cations. Moreover, these selectivities remain high at various source-phase concentrations. Membrane potential measurements during ED and the resulting current-voltage curves reveal complex electrochemical behavior at the PEM-membrane interface. The low permeability of the PEMs leads to extensive ion depletion with these films, and at sufficiently large current densities, high potential gradients causes water splitting near the interface of the PEM and the cation-exchange membrane.

Chapter 3 investigates whether the high K^+/Mg^{2+} selectivities reported in Chapter 2 extend to other pairs of monovalent and multivalent cations. Nafion membranes coated with PEMs show K^+/La^{3+} and Li^+/Co^{2+} selectivities >1000, but, curiously, the overall membrane resistance does not decline with fewer deposited

bilayers in the PEM. At overlimiting currents, protons and hydroxide from water splitting reduce current efficiency and cause precipitation of insoluble metal hydroxides on the membrane. Transference numbers approach 1.0 with 0.1 M source-phase cation concentrations because the diffusion-limited current exceeds the applied current. However, selectivity and transference numbers decline over time as PEM durability remains a significant challenge. Nevertheless, these extremely high selectivities are promising for high-value separations.

Chapter 4 explores other methods for removing ions in solution. Ultrafiltration membranes modified with PEMs effectively remove >91% of charged dyes in model systems, and these rejections increase to >98% in crossflow NF with wastewater effluent from textile manufacturing processes. This chapter also shows that ion concentration polarization in microfluidic channels connected by cation-selective membranes enriches the concentration of ions in one channel and depletes the ion concentrations in the other. However, the large potentials and localized nature of ICP (near the junction) will likely limit its utility to specialized applications.

5.1 Future work

Cation-exchange membranes coated with PEMs show extremely high selectivities for monovalent over multivalent cations. However, questions remain about the performance of these membranes in commercially viable situations or their durability for prolonged periods in electric fields. Furthermore, initial studies

suggest that scaling occurs at overlimiting current densities, but fouling through other processes has not been studied. Water splitting reduces efficiency in ED separations, so further studies should explore methods to avoid the production and transport of unwanted ions.

5.1.1 Increasing the stability of PEM-containing membranes

Electrostatic interactions between polycations and polyanions stabilize PEMs, and in many applications, this attraction is sufficient to assure the durability of the film. However, in the presence of strong electric fields, PEMs may delaminate because cationic and anionic polyelectrolytes migrate toward the cathode and anode, respectively.[1] One method to reduce this delamination is to crosslink individual layers through covalent linkages. Such and Caruso utilized "click" chemistry to produce robust films containing alternating layers of azide- and alkyne- functionalized PAA. With 4 bilayers, such films were 25 ± 6 nm thick, a value comparable to films studied in this dissertation.[2] Welsh *et al.* reported linear growth of branched-PEI/hexamethylene-1,6-di(aminocarboxysulfonate) (HDACS) mutilayers crosslinked with diisocyanate for films comprised of up to 18 bilayers.[3] Crosslinking may be the only method to ensure stability of the films in strong ED electric fields, and future work should focus on methods to incorporate crosslinking while preserving the high charge density of the films to maintain selectivity.

5.1.2 Reducing water splitting to enhance current efficiency

Low limiting currents and water splitting also pose a significant challenge for cation separations in ED. Much of the water splitting likely occurs at the PEM/Nafion interface on the feed side of the membrane, so elimination of this interface should greatly reduce water splitting. Future experiments should focus on ED with the PEM deposited only on the receiving side of the membrane. This configuration will continue to limit anion transport because of the cation-exchange substrate membrane and should also maintain some selectivity. Previous results showed that membranes coated only on the receiving side show greater selectivity than the membrane in its native state.[4] Increased limiting current densities would greatly improve the separation efficiency when the monovalent ion concentration is low.

5.1.3 Examining performance in membrane stacks

Practical separations will employ stacks of alternating cation- and anion-exchange membranes, so PEM-coated membranes should be tested in such a configuration. This will require preparation of a custom ED stack with an optimal geometry (short distances between membranes, larger areas, and efficient mixing). Figure 5.1 shows the configuration of a model ED stack that could be used to evaluate the performance of PEM-coated ion-exchange membranes. Isolation of the feed and permeate streams from hydroxide and proton production

at the cathode and anode, respectively, requires at least 4 membranes, and compartment dividers containing o-rings form individual compartments and seal each layer. Anode and cathode rinse and buffer solutions should contain high (at least 0.5 M) salt concentrations to minimize solution resistance in these cells. Ideally, platinized titanium or platinum mesh electrodes should span the entire exposed membrane area to maintain uniform current densities across the membranes. Small pumps will supply solutions to each compartment.

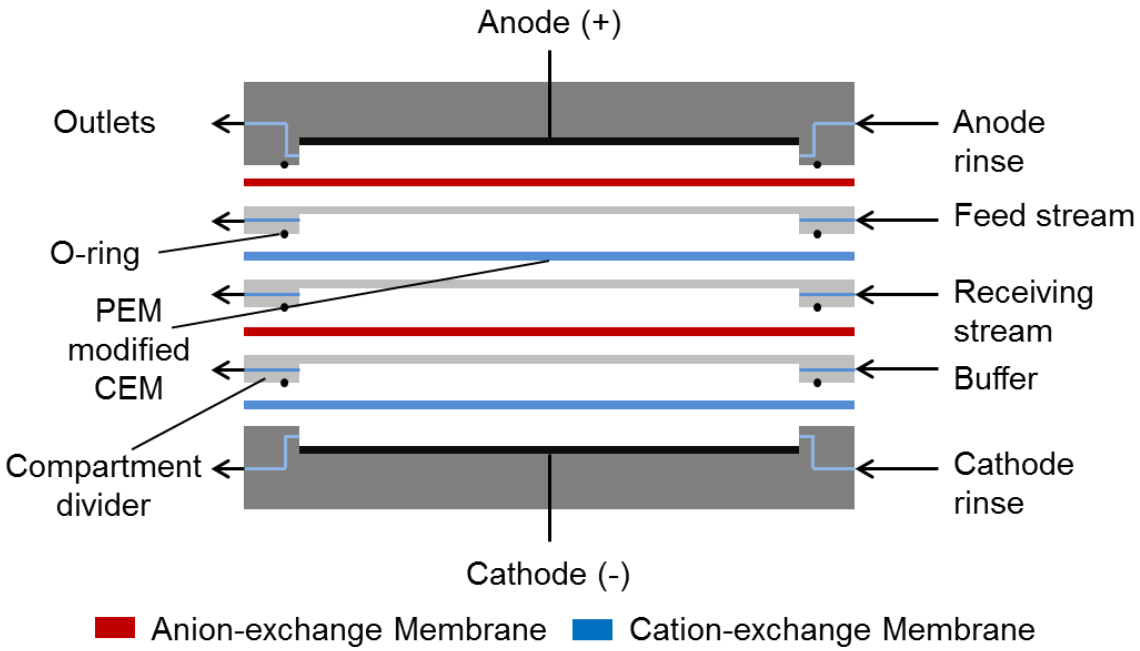

Figure 5.1. Schematic diagram of a cross-sectional view of an ED stack for testing PEM-modified cation-exchange membranes in continuous flow

Figure 5.2 shows a 3D rendering for a possible design of compartment dividers in the ED stack. The divider is 3 mm thick to minimize the distance between membranes and, therefore, the power consumption during ED. An o-ring channel surrounds the hollow center of the divider, and threaded inlets allow for simple connectivity to pumps via tubing. The exposed membrane area is 2 cm x 20 cm to maximize ED time without large membrane areas. In this design, multiple dividers can be stacked by alternating between the design shown in Figure 5.2 and a similar design in which the inlets are centered. This simple feature allows stacking of as many membrane compartments as necessary. The approximate residence time in the electric field is easily determined from the volume of the compartment and the flow rate through the compartment. This design mimics commercial ED stacks without using very large membrane areas. Demonstration of stable, highly selective membranes in practical ED separations using membrane stacks could lead to commercialization of these materials.

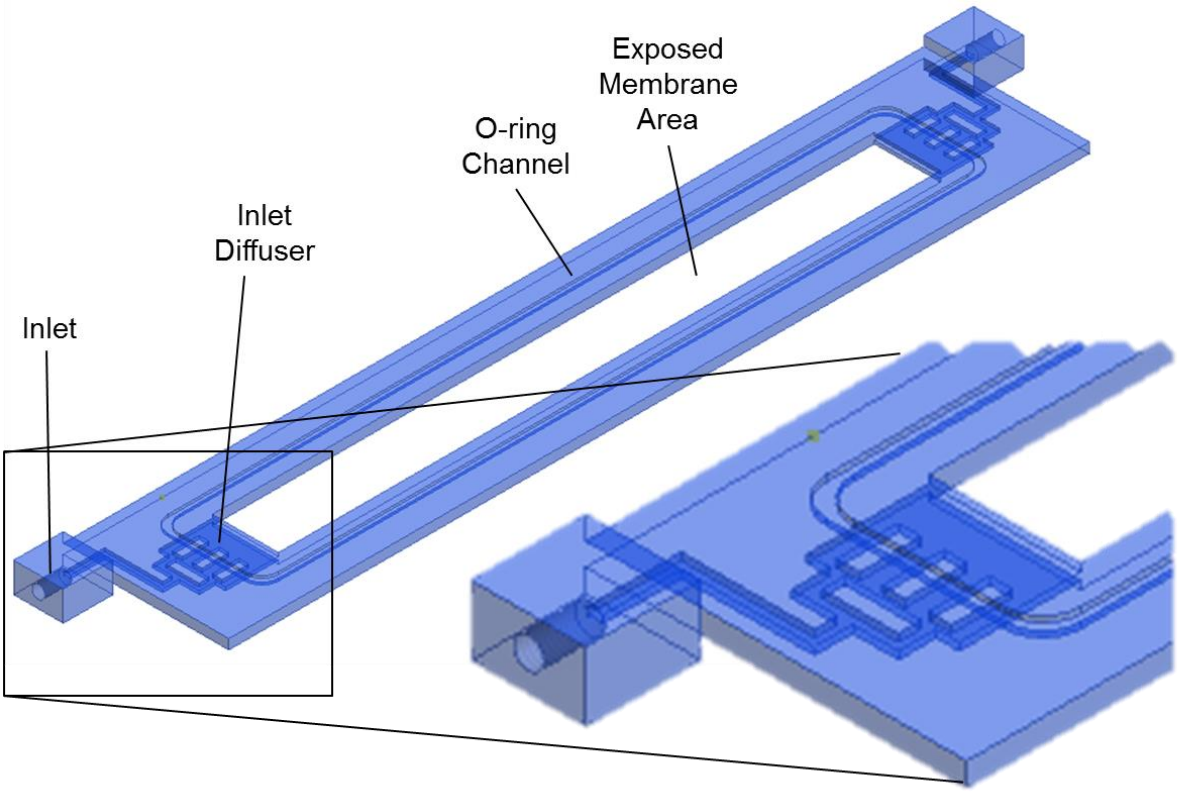

Figure 5.2. CAD drawing of compartment divider for an ED cell with multiple membranes.

REFERENCES

REFERENCES

(1) Sukhishvili, S. A.; Granick, S. *Macromolecules* **2002**, *35*, 301-310.

(2) Such, G. K.; Quinn, J. F.; Quinn, A.; Tjipto, E.; Caruso, F. *J. Am. Chem. Soc.* **2006**, *128*, 9318-9319.

(3) Welsh, E. R.; Schauer, C. L.; Santos, J. P.; Price, R. R. *Langmuir* **2004**, *20*, 1807-1811.

(4) White, N.; Misovich, M.; Yaroshchuk, A.; Bruening, M. L. *ACS Appl. Mater. Interfaces* **2015**, *7*, 6620-6628.